

A New Experiment Run Group Proposal Submitted to Jefferson Lab PAC44

A Search for Hybrid Baryons in Hall B with CLAS12

Volker Burkert (*Contact Person, Spokesperson*), Daniel S. Carman, Valery Kubarovsky,
Victor Mokeev (*Spokesperson*), Maurizio Ungaro, Veronique Ziegler
Thomas Jefferson National Accelerator Facility, Newport News, Virginia 23606, USA

Annalisa D'Angelo (*Spokesperson*), Lucilla Lanza, Alessandro Rizzo
Università di Roma Tor Vergata and INFN Roma Tor Vergata, 00133 Rome, Italy

Gleb Fedotov, Boris Ishkhanov, Evgeny Isupov, Evgeny Golovach (*Spokesperson*)
Skobeltsyn Institute of Physics, Moscow State University, 119234 Moscow, Russia

Ralf Gothe (*Spokesperson*), Iuliia Skorodumina
University of South Carolina, Columbia, South Carolina 29208, USA

Vincent Mathieu[†], Vladyslav Pauk, Alessandro Pilloni, Adam Szczepaniak[†]
Theory Center, Jefferson Laboratory, Newport News, Virginia 23606, USA
([†]*Joint with Indiana University, Bloomington, Indiana 47405, USA*)

Simon Capstick, Volker Crede
Florida State University, Tallahassee, Florida 32306, USA

Jan Ryckebushch
Ghent University, B-9000 Ghent, Belgium

Michael Döring
The George Washington University, Washington, DC 20052, USA

Philip Cole
Idaho State University, Pocatello, Idaho 83209, USA

Vincenzo Bellini, Francesco Mammoliti, Giuseppe Russo, Concetta Sutera, Francesco
Tortorici
INFN, Sezione di Catania, 95125 Catania, Italy

Ilaria Balossino, Luca Barion, Giuseppe Ciullo, Marco Contalbrigo, Paola Lenisa, Aram
Movsisyan, Luciano Pappalardo, Mateo Turisini
INFN, Sezione di Ferrara, 44100 Ferrara, Italy

Marco Battaglieri, Andrea Celentano, Raffaella De Vita, Erica Fanchini, Mikhail Osipenko,
Marco Ripani, Elena Santopinto, Mauro Taiuti
INFN, Sezione di Genova, 16146 Genova, Italy

Alessandra Filippi
INFN, Sezione di Torino, 10125 Torino, Italy

César Fernández-Ramírez
Universidad Nacional Autónoma de México, 04510 Mexico City, Mexico

Inna Aznauryan
Yerevan Physics Institute, 375036 Yerevan, Armenia
and the CLAS Collaboration

Abstract

This proposal aims to establish a program to search for new excited baryon states in the mass range from 1.8 GeV to 3 GeV, as well as to explore for the first time the behavior of resonance electrocouplings over the full spectrum of excited proton states at photon virtualities Q^2 approaching the photon point ($Q^2 < 0.2 \text{ GeV}^2$). This work focuses on measuring $K^+\Lambda$, $K^+\Sigma^0$, and $\pi^+\pi^-p$ exclusive final states in CLAS12 and detecting the scattered electrons in the angular range from 2.5° to 35° using the electron detection capabilities of the Forward Tagger and the CLAS12 detector. The experiment will use longitudinally polarized electron beams of 6.6 GeV and 8.8 GeV to cover the range of invariant mass W up to 3 GeV and Q^2 from 0.05 GeV^2 to 2 GeV^2 . The main aspects of the proposal are to:

- search for new hybrid baryon states with the glue as an extra constituent component beyond the three constituent quarks by focusing on measurements at $Q^2 < 1.0 \text{ GeV}^2$, where the expected magnitudes of the hybrid electroexcitation amplitudes are maximal;
- search for three-quark “missing” resonances in the electroproduction of different hadronic final states with the highest fluxes of virtual photons ever achieved in exclusive meson electroproduction experiments;
- study the structure of prominent nucleon resonances in the mass range up to 3 GeV in the regime of large meson-baryon cloud contributions and explore the N^* longitudinal electroexcitation approaching the photon point.

Exclusive events from KY and $\pi^+\pi^-p$ final states will be selected and the unpolarized differential cross sections will be obtained, complemented by measurements of the differential transverse-transverse and transverse-longitudinal interference cross sections. From these data the $\gamma_v p N^*$ electrocouplings will be determined for all possible new states with $I=1/2$ and $I=3/2$ and with all possible J^P quantum numbers, and the Q^2 evolution of their helicity amplitudes will then be determined in the low Q^2 range ($Q^2 < 2 \text{ GeV}^2$) for different reaction channels.

The hybrid baryons will be identified as additional states in the N^* -spectrum beyond the regular three-quark states. Since spin-parities of hybrid baryons are expected to be the same as those for regular three-quark states, the signature of the hybrid-baryon will emerge from the distinctively different low Q^2 -evolution of the hybrid-baryon electrocouplings, due to the additional gluonic component in their wave function.

This kinematic range also corresponds to the largest contributions from the meson-baryon cloud, allowing us to improve our knowledge on this component, which is relevant to understand the structure of all N^* states studied so far [2, 3], as well as to explore the longitudinal N^* electroexcitations as the photon virtuality goes to zero. This program adds an important new physics component to the existing CLAS12 N^* program at 11 GeV, which aims to measure the transition form factors for all prominent N^* states up to the highest photon virtualities ever probed in exclusive reactions $Q^2 < 12 \text{ GeV}^2$. The study of the spectrum and structure of excited nucleon states at distance scales from low to high Q^2 , encompassing the regime where low-energy meson-baryon degrees of freedom dominate to the regime where quark degrees of freedom dominate, creates new opportunities to better understand how the strong interaction of dressed quarks and gluons gives rise to the spectrum and structure of excited nucleon states and how these states emerge from QCD.

Contents

1	Introduction	5
2	Theoretical Studies of Hybrid Baryons	6
2.1	Model projections	6
2.2	Lattice QCD predictions	7
2.3	Hadronic couplings	8
2.4	Electromagnetic couplings	9
3	Strategies for identifying Hybrid- and three-quark new baryon states	10
3.1	Signature of the hybrid-baryon in the experimental data	14
3.2	Search for the three-quark new baryon states	15
3.3	Amplitude analyses of measured observables in a search for new baryon states.	17
3.4	Modeling the hybrid baryon contribution to exclusive KY and $\pi^+\pi^-p$ electroproduction off protons.	21
3.5	Search for the hybrid-baryon signal employing the moment expansion	23
4	The Experimental program	25
4.1	The CLAS12 detector	25
4.2	The Forward Tagger	26
4.3	Kinematical coverage of electron scattering in CLAS12	27
5	Simulations for the $ep \rightarrow ep\pi^+\pi^-$ final state	30
5.1	Event generator for $ep \rightarrow ep\pi^+\pi^-$	30
5.2	Acceptance estimates for $ep \rightarrow ep\pi^+\pi^-$	31
5.3	Resolution in hadronic mass reconstruction and background estimation for $ep \rightarrow ep\pi^+\pi^-$	33
5.4	Run conditions	35
6	Simulations for the $K\Lambda$ and $K\Sigma^0$ final states	36
6.1	Event generator for $ep \rightarrow eK\Lambda$ and $ep \rightarrow eK\Sigma^0$	36
6.2	Acceptances for $ep \rightarrow e'pK^+\Lambda$	37
6.3	Run conditions	43
6.4	Count rates from $K^+\Lambda$	46
6.5	Expected total event rates	47
7	Data Analysis and quasi data	48
7.1	Event selection	48
7.2	Event reconstruction	49
7.3	Extracting differential cross sections and normalized yields	51
7.4	Partial wave analysis	52
7.5	Analysis of quasi-data to determine CLAS12 sensitivity to minimum detectable resonance electrocoupling	53
7.6	Threshold values of statitically distinguishable hybrid baryon couplings in $\pi^+\pi^-p$ final state	53

7.7	Threshold values of statistically distinguishable hybrid baryons electrocouplings from $K\Lambda$ final state	55
7.8	Experimental sensitivity to hybrid resonance states in $\pi + \pi^- p$ and KY final states	60
8	Beamtime estimate	60
9	Summary	61
A	Appendix A - KY electroproduction	63
B	Appendix B - Hybrid Baryon excitation Amplitude	66

1 Introduction

The ongoing program at Jefferson Lab and several other laboratories to study excitations of nucleons in the so-called nucleon resonance region with real-photon and electron beams has been very successful. Although only a fraction of the data taken during the CLAS run groups g8, g9, g11, and g12 have been analyzed and published yet, the published data have allowed for very significant advances in light-quark baryon spectroscopy and have led to strong evidence for several new nucleon excitations as documented in the PDG review of 2014 [1]. These discoveries were possible due to the very high meson production rates recently obtained for energy-tagged photoproduction processes. Furthermore, the use of meson electroproduction has led to completely new insights into the nature of several prominent resonant baryons, such as the so-called Roper resonance $N(1440)_{\frac{1}{2}}^{+}$. This state defied for the longest time an explanation of its properties, as the mass, transition amplitudes, and transition form factors, within the constituent quark model (CQM). The analyses of the new electroproduction data were crucial in dissecting its complex structure and providing a qualitative and quantitative explanation of the space-time evolution of the state [4]. The Roper was also considered as a candidate for the lowest mass hybrid baryon [5] and It was only due to the meson electroproduction data that this possibility could be dismissed [2, 6].

The theory of the strong interaction, QCD, not only allows for the existence of baryons with dominant gluonic contributions (hybrid baryons), but Lattice QCD calculations have now also predicted several baryon states with a dominant gluonic admixture to the wave function, and with the lowest mass hybrids approximately 1.3 GeV above the nucleon ground state **got** in LQCD [7], i.e. in the range $W = 2.1 - 2.3$ GeV. In the meson sector, exotic states (hybrid mesons) are predicted with quantum numbers that cannot be obtained in a pure $q\bar{q}$ configuration. The selection of mesons with such exotic quantum numbers provides a convenient way to identify candidates for gluonic mesons. In contrast to the meson sector hybrid baryons have quantum numbers that are also populated by ordinary excited 3-quark states. Hybrid baryons hence mix with these 3-quark excited states or with dynamically generated states making the identification of gluonic baryons more difficult. An important question is therefore: How can we distinguish gluonic excitations of baryons from their ordinary quark excitations?

Mapping out the nucleon spectrum and the excitation strengths of individual resonances is a powerful way to answer a central question of hadron physics: "What are the effective degrees of freedom as the excited states are probed at different distance scales?". Previous analyses of meson electroproduction have shown to be most effective in providing answers in several cases of excited states: $\Delta(1232)_{\frac{3}{2}}^{+}$, $N(1440)_{\frac{1}{2}}^{+}$, $N(1520)_{\frac{3}{2}}^{-}$, $N(1535)_{\frac{1}{2}}^{-}$, $\Delta(1620)_{\frac{1}{2}}^{-}$, $N(1680)_{\frac{5}{2}}^{+}$ and $N(1675)_{\frac{5}{2}}^{-}$.

The experimental program outlined in this proposal is meant to vastly improve upon the available information and extend the reach of meson electroproduction to cover the nucleon resonance mass range up to 3 GeV and an extended low- Q^2 range from 0.05 GeV² to 2 GeV², using electron beam energies of 6.6 GeV and 8.8 GeV. The unpolarized differential cross sections will be measured for the KY and $\pi^+\pi^-p$ exclusive channels, complemented by measurements of the differential transverse-transverse and transverse-longitudinal interference cross sections and other polarizationdependent observables.

From these data the $\gamma_v p N^*$ electrocouplings will be determined employing the well known

unitary isobar models and dispersion relation approaches that have proven very effective for the study of two-body final states such as πN [2, 8] and KY [9], as well as the JLab-Moskov (JM) meson-baryon reaction model for $\pi^+\pi^-p$ electroproduction [3, 8], multi-channel partial wave techniques employing either the Bonn-Gatchina [10] or the GWU [11] approaches, and approaches starting from the Veneziano model and Regge phenomenology [12] that are applicable at higher energies, where many hadron channels open in the final state interactions.

The proposed experimental program will search for all possible new states with isospin $I=1/2$ and $I=3/2$ and all possible J^P quantum numbers. As new states are identified using the high event rates at very small Q^2 values (“quasi-real” photoproduction), the Q^2 dependence of their helicity amplitudes will be determined. The results at different values of Q^2 in the different exclusive channels will substantially enhance the discovery potential for new baryon states. Consistent results on resonance masses and $\gamma_v p N^*$ electrocouplings from the different exclusive decay channels, as well as Q^2 -independent partial hadronic decay widths over the full Q^2 range, will offer convincing evidence for the existence of new states and the reliable extraction of their parameters. This approach has been highly effective in determining the Q^2 dependence of the $A_{1/2}$, $A_{3/2}$, and $S_{1/2}$ helicity amplitudes for several of the lower mass baryons, such as the $\Delta(1232)3/2^+$, $N(1440)1/2^+$ and $N(1535)1/2^-$ excitation states [2, 3]. These and many other results are included in the review of the N^* and Δ^* states in the latest edition of the PDG [13].

The hybrid baryons will be identified as additional states in the N^* -spectrum beyond the regular three-quark states as it has been predicted in recent LQCD studies of the baryon spectrum [7]. Since spin-parities of hybrid baryons are expected to be the same as those for regular three-quark states, information on the $\gamma_v p N^*$ electrocoupling evolution with Q^2 becomes critical in the search for hybrid baryons. A distinctively different Q^2 evolution of the hybrid-baryon electrocouplings is expected considering the different color-multiplet assignments for the quark-core in a regular versus a hybrid baryon, i.e. a color singlet versus octet, which also calls for low photon virtualities as the preferential regime for studies of the hybrid-baryon electrocouplings.

In conjunction with experiment E12-09-003 [], which focusses on the highest Q^2 , as well as E12-06-108A [], which explores $K^+\Lambda$ production, the proposed experiment will complement the program of nucleon resonance electroexcitation.

2 Theoretical Studies of Hybrid Baryons

2.1 Model projections

In an extension of the MIT bag model, gluonic excitations of the nucleon, to states where a constituent gluon in the lowest energy transverse electric mode combines with three quarks in a color octet state to form a colorless state in the mass range of 1.600 ± 0.100 GeV, have been broadly discussed since 1983 [5].

The gluon flux-tube model applied to hybrid baryons [14, 15] came up with similar quantum numbers of the hybrid states, but predicted considerably higher masses than the bag model. For the lowest mass flux-tube hybrid baryon a mass of 1.870 ± 0.100 GeV was found. In all cases the lowest mass hybrid baryon was predicted as a $J^P = 1/2^+$ state, i.e. a nucleon or Roper-like state. Hybrid baryons were also discussed in the large

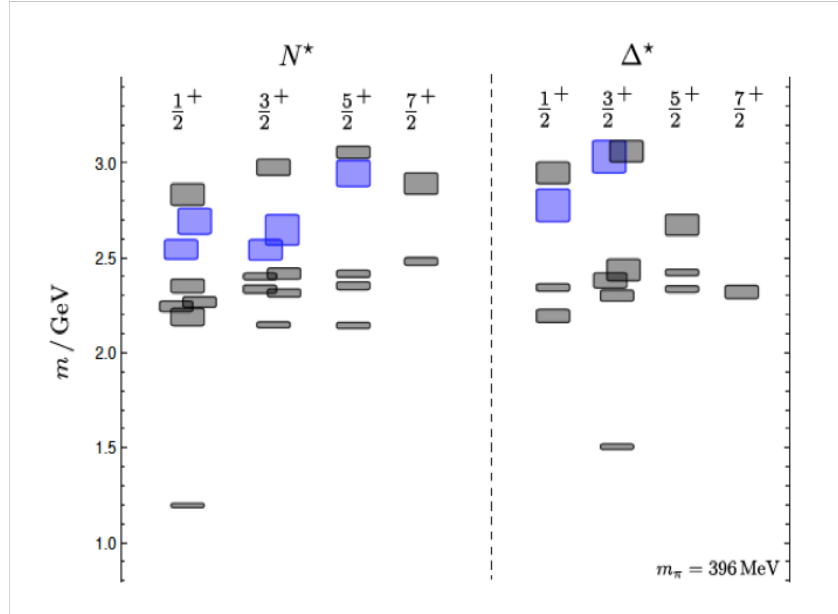


Figure 1: The light-quark baryon spectrum predicted in Lattice QCD at a pion mass of 396 MeV. The blue shaded boxes indicate states with dominant gluonic contributions. Note that both the mass of the nucleon ground state and of the $\Delta(1232)$ are shifted by nearly 300 MeV to higher masses.

N_c approximation of QCD for heavy quarks [16], which also led to the justification of the constituent glue picture used in the models. The high energy behavior of hybrid baryons was discussed in [17]. However, in contrast to hybrid meson production, which has received great attention both in theory and in experiments, the perceived difficulties of isolating hybrid baryon states from ordinary quark states led this part of the field to remain dormant for several years.

2.2 Lattice QCD predictions

The first quenched calculations on the lattice came in 2003 [18], when the lowest gluonic 3-quark hybrid system was projected at a mass of 1 GeV above the nucleon mass, placing the lowest hybrid baryon at a mass around 2 GeV. The first LQCD calculation of the full light-quark baryon spectrum with unquenched quarks that occurred in 2012 included the projections of the hybrid isospin $\frac{1}{2} N_G$ states and $\frac{3}{2} \Delta_G$ states [7]. Figure 1 shows the projected light quark baryon spectrum in the lower mass range.

At the pion mass of 396 MeV used in this projection, the prediction for the nucleon mass is shifted by nearly 300 MeV to higher masses. In the following we take this shift into account by subtracting 300 MeV from the masses of the excited states shown in Fig. 1. As stated in [7], the lowest hybrid baryons, shown in Fig. 1 in blue, were identified as states with leading gluonic contributions. If hybrid baryons are not too wide, we might expect the lowest hybrid baryon to occur at masses of about 1.3 GeV above the ground state, i.e. in a mass range of 2.2 to 2.5 GeV, and a few hundred MeV above the band of radially excited

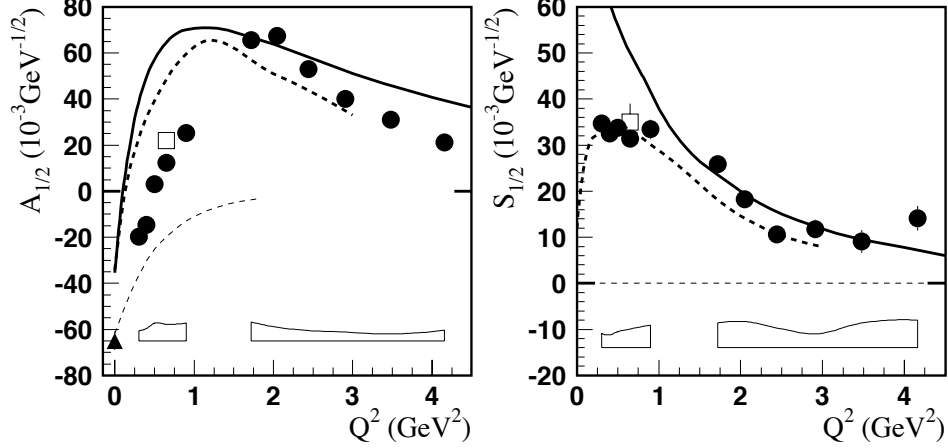


Figure 2: Electrocoupling amplitudes of the Roper resonance $N(1440)\frac{1}{2}^+$. The thin dashed lines are the constituent quark-gluon model predictions for the gluonic Roper [19]

$J^P = \frac{1}{2}^+$ 3-quark nucleon excitations of isospin 1/2 and thus possibly well separated from other states.

In this computation the lowest $J^P = \frac{3}{2}^+$ gluonic states are nearly mass degenerate with the corresponding $J^P = \frac{1}{2}^+$ gluonic states generating a glue-rich mass range of hybrid nucleons. If these projections hold up with LQCD calculations using near physical pion masses, one should expect a band of the lowest mass hybrid baryon states with spin-parity $\frac{1}{2}^+$ and $\frac{3}{2}^+$ to populate a relatively narrow mass band of 2.2 to 2.5 GeV. Note, that these states fall into a mass range where no 3-quark nucleon excitations are predicted to exist in these calculations. The corresponding negative parity hybrid states, which are expected to occur at much higher masses, are not included in this graph and are not further considered here; although they may be subject of analysis, should they appear within the kinematic range covered by this proposal.

2.3 Hadronic couplings

Very little is known about possible hadronic couplings of hybrid baryons but one might expect an important role for final states with significant gluonic admixture, e.g. $B_G \rightarrow N\eta'$ [19], or final states containing $s\bar{s}$ contributions due to the coupling $G \rightarrow s\bar{s}$, e.g. $B_G \rightarrow K^+\Lambda$, $B_G \rightarrow N^*(1535)\pi \rightarrow N\eta\pi$, $B_G \rightarrow N\pi\pi$, $B_G \rightarrow \phi(1020)N$, and $B_G \rightarrow K^*\Lambda$. Quark-model estimates of the hadronic couplings would be helpful in selecting the most promising final state for the experimental evaluation. As long as such estimates are not available we will use a range of assumptions on the hadronic couplings to estimate the sensitivity required for definitive measurements. Assuming hadronic couplings of a few percent in the less complex final states, e.g. $K^+\Lambda$, $K^*\Lambda$, or $N\pi\pi$, we should be able to identify these states and proceed to experimentally establish their electromagnetic couplings and Q^2 dependences. We focus in this proposal to on those decay channels that have already been successfully analysed and that will be further investigated with CLAS12, [2, 3], i.e. $K^+\Lambda$, $K^+\Sigma$ and $\pi^+\pi^-p$, but will not refrain from exploring other electroproduction channels such as $\phi(1020)N$ or $K^*\Lambda$.

2.4 Electromagnetic couplings

The studies of excited nucleon state electrocouplings in a wide range of photon virtualities is a proven effective tool in establishing the active degrees of freedom that contribute to the N^* structure at different distances [2, 3, 24–26]. The information on the $\gamma_v NN^*$ electrocoupling evolution with Q^2 becomes critical in the search for hybrid baryons. A distinctively different Q^2 evolution of the hybrid-baryon electrocouplings is expected considering the different color-multiplet assignments for the quark-core in a regular versus a hybrid baryon, i.e. color singlet versus octet.

Electromagnetic couplings have been studied within a non-relativistic constituent quark-gluon model, but only for two possible hybrid states, the Roper $N_G(1440)\frac{1}{2}^+$ and the $\Delta_G(1600)\frac{3}{2}^+$. In reference [20] the photoexcitation of the hybrid Roper resonance $N(1440)\frac{1}{2}^+$ was studied, and in reference [21] the electroproduction transition form factors of a hybrid Roper state were evaluated. The latter was essential in eliminating the Roper resonance as a candidate for a hybrid state, both due to Q^2 dependence of the transverse helicity amplitude and the prediction of $S_{1/2}(Q^2) = 0$ at all Q^2 , see Fig 2. It also showed that a hybrid Roper transition amplitude $A_{1/2}$ should behave like the $A_{1/2}$ of the ordinary $\Delta(1232)$. Clearly the $S_{1/2}$ behaves differently and an $A_{3/2}$ does not exist for the Roper. Both amplitudes exhibit a Q^2 dependence that is distinctively different from the hybrid baryon prediction. Especially the scalar amplitude $S_{1/2}(Q^2)$ was found to be large while it is predicted to be suppressed in leading order for the lowest mass $\frac{1}{2}^+$ hybrid state.

The aforementioned predictions should apply to each lowest mass hybrid state with $J^P = \frac{1}{2}^+$ and $\frac{3}{2}^+$. One may ask about the model-dependence of this prediction. The transverse amplitude has model sensitivity in its Q^2 dependence and it depends on the model ingredients, however, there are no ordinary 3-quark model predictions that would come even close to the predictions of the hybrid quark-gluon model. The radial excitation of the Roper resonance gives a qualitatively different prediction for $A_{1/2}(Q^2)$ compared to the hybrid excitation, where the 3-quark component remains in the ground state with only a spin-flip occurring (just as for the $N - \Delta(1232)$ transition). Even less model dependent is the suppression of the longitudinal coupling, which is a property of the $\gamma q G$ vertex and hence is largely independent of specific model assumptions.

The other state, $\Delta(1600)\frac{3}{2}^+$, was considered as a candidate for the lowest mass gluonic Δ_G . A result similar to the one for the hybrid Roper is found in [21] for a hybrid $\Delta_G(1600)\frac{3}{2}^+$, i.e. a fast falling $A_{1/2}(Q^2)$ and $S_{1/2}(Q^2) \approx 0$. The amplitudes at the photon point are not inconsistent with the ordinary 3-quark model calculation but are inconsistent with the hybrid baryon hypothesis. On the other hand this result is also in line with the expectation that the lowest mass hybrid states should have considerably higher masses than the first radially excited quark states. Note that there are currently no experimental results for the Q^2 dependence of the $A_{1/2}$ and $S_{1/2}$ amplitudes of this state.

Based on quark counting rules [?], we expect that the electrocouplings of hybrid baryons should decrease faster with increasing photon virtuality Q^2 than the regular 3-quark nucleon resonance because of the extra constituent. Therefore low photon virtualities are the preferential region to study hybrid-baryons and we are proposing to explore the $Q^2 < 2.0 \text{ GeV}^2$ range and a particular focus on the hybrid baryon search at $Q^2 < 1.0 \text{ GeV}^2$. In order to identify hybrid-baryons we are looking for their electrocoupling behavior, which should have

distinctively different features in comparison with already established CLAS results [3]. Electrocouplings of 3-quark resonances for $J^P = \frac{1}{2}^+$ shown in Figs 2,5 and for $J^P = \frac{3}{2}^+$ shown in Figs ??,??. If hybrid baryons will be established in the proposed experiment, further studies of their electrocouplings can be extended towards higher photon virtualities from the data of the approved CLAS12 experiments [].

3 Strategies for identifying Hybrid- and three-quark new baryon states

In this section we address the question if and how gluonic hybrid baryons are distinct from ordinary quark excitations. We will also elucidate the additional opportunities offered by the studies of exclusive electroproduction processes at different photon virtualities for the search of new baryon states both hybrid-baryons and regular three-quark so-called “missing” resonances.

Check for repetitions

Old version: In this section we address the question if and how gluonic hybrid baryons are distinct from ordinary quark excitations. As discussed in section 2.2 the lowest hybrid baryons should have isospin $I = \frac{1}{2}$ and $J^P = \frac{1}{2}^+$ or $J^P = \frac{3}{2}^+$, and their masses should be in the range of 2.20 to 2.50 GeV. This mass range must be verified once LQCD calculations with physical pion masses become available, as masses may shift with more realistic pion masses, likely to the lower mass range. Four states with $I = \frac{1}{2}$ and $J^P = \frac{1}{2}^+$ are predicted with dominant quark contributions and with masses below the mass of the lowest LQCD hybrid states. Of these four states two are the well known $N(1440)\frac{1}{2}^+$ and $N(1710)\frac{1}{2}^+$, and two are the less well established $N(1880)\frac{1}{2}^+$ and $N(2100)\frac{1}{2}^+$ with 2* and 1* ratings, respectively. Another state $N(2300)$ has a 2* rating, and falls right into the lowest hybrid mass band projected by LQCD. This state, if confirmed, could be a candidate for the predicted lowest LQCD hybrid state.

In order to address this question, it is necessary to confirm (or refute) the existence of the 2* state $N(1880)$ and of the 1* state $N(2100)$, and to measure the electromagnetic couplings of $N(2300)$ and their Q^2 dependence. Improved information on the lower mass states should become available in the next one or two years when the new high-statistics single- and double-polarization data from CLAS have been included into the multi-channel analysis frameworks such as the Bonn-Gatchina or Jülich/GWU approaches. Should these two states be confirmed, then any new nucleon state with $J^P = \frac{1}{2}^+$, which happens to be in the right mass range, could be a candidate for the lowest mass hybrid baryon. The $N(2300)\frac{1}{2}^+$ state has been seen at BES III only in the invariant mass $M(p\pi^0)$ of $\Psi(2S) \rightarrow p\bar{p}\pi^0$ events. In this case the production of $N(2300)$ occurs at very short distances as it emerges from heavy quark flavor $c\bar{c}$ decay. Hence the state may even be observable in single pion electroproduction $ep \rightarrow e'\pi^+n$ and $ep \rightarrow e'p'\pi^0$, if it couples to photons with sufficient strength to be measurable.

In the $J^P = \frac{3}{2}^+$ sector the situation is more involved. There are two hybrid states predicted in the mass range 2.2 to 2.4 GeV, with masses above five quark model states at same J^P . Of the five states, two are well known 4* and 3* states, the $N(1720)\frac{3}{2}^+$ and the $N(1900)\frac{3}{2}^+$, respectively, and one state, the $N(2040)\frac{3}{2}^+$, has a 1* rating. Here we will have

to confirm (or refute) the 1^* star state and find two or three (if $N(2040)$ does not exist) more quark model state with the same quantum numbers in the mass range 1.7 to 2.1 GeV. There is one candidate $\frac{3}{2}^+$ state with mass near 1.72 GeV seen in $p\pi^+\pi^-$ electroproduction [51], whose status we will be able to pin down with the expected very high statistics data.

Possible signatures of the lowest mass hybrid baryons are:

- Resonance masses in the range $2.0 \text{ GeV} \leq W \leq 2.5 \text{ GeV}$ with $I = 1/2$, and $J^P = \frac{1}{2}^+$ or $J^P = \frac{3}{2}^+$
- Q^2 dependence of the transverse helicity amplitude $A_{1/2}(Q^2)$ similar to the $\Delta(1232)\frac{3}{2}^+$ but dissimilar to radially excited states of same J^P , and
- a strongly suppressed helicity amplitude $S_{1/2}(Q^2) \approx 0$ in comparison to other ordinary 3-quark states or meson-baryon excitations.

This list of expected resonance properties may provide some initial guidance when examining new baryon states for signatures of large gluonic components, they are however not sufficient to firmly establish the hybrid nature of a state. To achieve this goal, improved modeling of other degrees-of-freedom such as meson-baryon contributions and direct calculations of electrocouplings from LQCD will be needed. The expected high statistics data will be used to identify any new or poorly known state, whether or not it is a candidate for a hybrid baryon state. This will aid in the identification of the effective degrees of freedom underlying the resonance excitation of all states that couple to virtual photons. ~~old:~~ **check for repetitions**

Besides the search for hybrid baryon states, there are many open issues in our knowledge of the structure of ordinary baryon excitations, that can be addressed with data taken in parallel from the same experiment. As an example we show in Fig. 3 the electrocouplings of the $N(1680)\frac{5}{2}^+$ resonance, the strongest state in the third nucleon resonance region. With the exception of the real photon point, the data are quite sparse for $Q^2 \leq 1.8 \text{ GeV}^2$ and the high statistics data expected from this project would remedy the lack of experimental information and address similar situations for other states as well. Note that the very high Q^2 part will be covered by the approved JLab experiment E12-09-003.

An even more compelling example is the $N(1675)\frac{5}{2}^-$ state, where data at $Q^2 > 1.8 \text{ GeV}^2$ have been published recently by the CLAS Collaboration [60]. Figure 4 shows the measured helicity amplitudes. Low Q^2 data are very important here, as for this state the quark transitions are strongly suppressed by the Moorhouse selection rule, and therefore, any non-zero value of the electrocoupling amplitudes will directly measure the strength of the meson-baryon contributions. The main data needed are single pion production $ep \rightarrow e'\pi^+n$ and $ep \rightarrow e'\pi^0p$. These processes can be accumulated with sufficiently high event rates, even with a pre-scale factor of 10 or more on the FT, should the overall event rate be too high in this 2-prong topology. As discussed in section 2.2, according to the LQCD evaluation [7] of the baryon spectrum from the QCD Lagrangian, the lowest hybrid baryons should have isospin $I = \frac{1}{2}$ and $J^P = \frac{1}{2}^+$ or $J^P = \frac{3}{2}^+$ (see Fig. 1). A difference between mass of the ground nucleon and LQCD expectation is $\approx 0.3 \text{ GeV}$ for the computation with pion mass 0.396 GeV. However, a difference between physical mass of $N(1440)\frac{1}{2}^+$ resonance and the LQCD expectation [7] is $\approx 0.7 \text{ GeV}$ suggesting that physics mass of the excited state can be push down by even more than 0.3 GeV, when the pion mass from LQCD is approaching

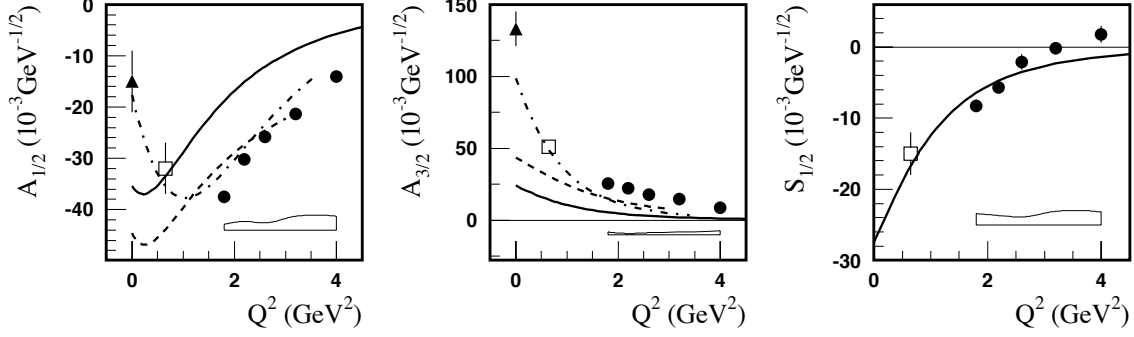


Figure 3: Electrocoupling amplitudes of the $N(1680)_{\frac{1}{2}}^{5+}$ resonance.

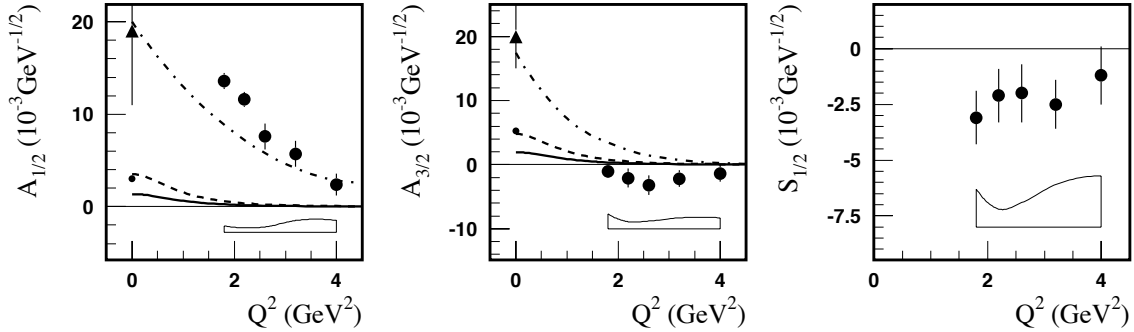


Figure 4: Electrocoupling amplitudes of the $N(1675)_{\frac{1}{2}}^{5-}$ resonance. Quark models predict the transverse amplitudes to be suppressed. The significant deviation of the $A_{1/2}$ amplitudes is consistent with meson-baryon contributions to the excitation strength (dashed-dotted lines).

the physics value. So, the masses of the lightest hybrids mass range should be in the range of 2.10 to 2.50 GeV. This mass range must be verified once LQCD calculations with physical pion masses become available. Three states with $I = \frac{1}{2}$ and $J^P = \frac{1}{2}^+$ are predicted with dominant quark contributions and with masses below the mass of the lowest LQCD hybrid states. Of these three states two are the well known $N(1440)_{\frac{1}{2}}^{1+}$ and $N(1710)_{\frac{1}{2}}^{1+}$, and less well established $N(1880)_{\frac{1}{2}}^{1+}$ with 2* rating. Other states $N(2100)_{\frac{1}{2}}^{1+}$ and $N(2300)$ have 1* and 2* ratings, respectively, and fall right into the lowest hybrid mass band projected by LQCD. The states $N(2100)_{\frac{1}{2}}^{1+}$ and $N(2300)$, if confirmed, could be the candidates for the predicted lowest LQCD hybrid state of $J^P = \frac{1}{2}^+$.

In the $J^P = \frac{3}{2}^+$ sector the situation is more involved. There are hybrid states predicted in the mass range 2.2 to 2.4 GeV, with masses above quark model states at same J^P . Of these states, two are well known 4* the $N(1720)_{\frac{3}{2}}^{3+}$ and the 3* state $N(1900)_{\frac{3}{2}}^{3+}$, and one state, the $N(2040)_{\frac{3}{2}}^{3+}$, has a 1* rating. Here we will have to confirm (or refute) the 1* star state and find (if $N(2040)$ does not exist) more quark model state(s) with the same quantum numbers in the mass range 2.1 to 2.5 GeV. Among the states of spin-parity $J^P = \frac{3}{2}^+$, there is one candidate $\frac{3}{2}^+$ state with mass near 1.72 GeV seen in $p\pi^+\pi^-$ electroproduction [51], whose status we will be able to pin down with the expected very high statistics data.

In the computation [7] the lowest $J^P = \frac{3}{2}^+$ gluonic states are nearly mass degenerate

with the corresponding $J^P = \frac{1}{2}^+$ gluonic states generating a glue-rich mass range of hybrid nucleons. If these projections hold up with LQCD calculations using near physical pion masses, one should expect a band of the lowest mass hybrid baryon states with spin-parity $\frac{1}{2}^+$ and $\frac{3}{2}^+$ to populate a relatively narrow mass band of 2.1 – 2.5 GeV. Note, that these states fall into a mass range where no 3-quark nucleon excitations are predicted to exist from these calculations. The corresponding negative parity hybrid states, which are expected to occur at much higher masses, are not included in the Fig. 1, and are not further considered here; although they may be subject of analysis, should they appear within the kinematic range covered by this Proposal.

Therefore, we propose to search for the extra states of spin-parity $J^P = \frac{1}{2}^+$, $J^P = \frac{3}{2}^+$, $I = \frac{1}{2}^+$, isospin in the excited nucleon spectrum in the mass range from 2.1 GeV to 2.5 GeV. In order to conclude on their hybrid nature further studies of their hadronic decays and electrocouplings are needed, since expected spin-parities and isospin of the lowest hybrid states are the same as for three-quark “missing” resonances.

Expected hadronic decays of hybrid baryons were discussed in the Section 2.3. Because of the coupling of the glue admixture to the $q\bar{q}$ pair, the hybrid baryons will manifest in the channels with strange mesons and baryons, as well as in the electroproduction of multi-meson final states with more than single mesons. We included into our Proposal those of the aforementioned channels which we already studied in details previously and included into the future N^* studies with the CLAS12 [2, 3], i.e. $K^+\Lambda$, $K^+\Sigma$ and $\pi^+\pi^-p$. Later on these studies may be extended by the exploration of other electroproduction channels such as $\phi(1020)N$, $K^*\Lambda$.

Studies of excited nucleon state electrocouplings in a wide range of photon virtualities is proven to be the effective tools in establishing the active degrees of freedom contributing to the N^* structure at different distances [2, 3, 24–26]. The information on the $\gamma_v NN^*$ electrocoupling evolution with Q^2 becomes critical in the search for hybrid baryons. The distinctively different Q^2 -evolution of the hybrid-baryon electrocouplings is expected considering the different color-multiplet assignments for the quark-core in a regular versus a hybrid baryon, i.e. a color singlet and octet, respectively.

The electroproduction transition form factors of a Roper state assuming the presence of glue (hybrid Roper) were evaluated in [21]. This studies demonstrated that for hybrid Roper longitudinal electrocouplings should be much smaller than transverse $A_{1/2}$ electrocouplings. Virtually $S_{1/2}$ electrocouplings should be comparable with zero at the scale of the transverse electrocouplings. It also showed that a hybrid Roper transition amplitude $A_{1/2}$ should behave like the $A_{1/2}$ of the ordinary $\Delta(1232)$. The aforementioned predictions should apply to each lowest mass hybrid state with $J^P = \frac{1}{2}^+$ and $J^P = \frac{3}{2}^+$. The suppression of the longitudinal coupling is a property of the $\gamma q G$ vertex and is largely independent of specific, which is purside of the current model assumptions.

Based on quark counting rules [?], we expect that electrocouplings of hybrid baryons should decrease with photon virtuality Q^2 more rapidly than for the regular three-quark nucleon resonance because of the extra- constituent. So, the low photon virtualities offer a preferential regime for the studies of hybrid-baryons. In our Proposal we are planning to explore the range of $Q^2 < 2.0 \text{ GeV}^2$ with particular focus for hybrid baryon search at $Q^2 < 1.0 \text{ GeV}^2$.

In a case of $J^P = \frac{3}{2}^+$ all three electrocouplings $A_{1/2}$, $S_{1/2}$ and $A_{3/2}$ contribute to the

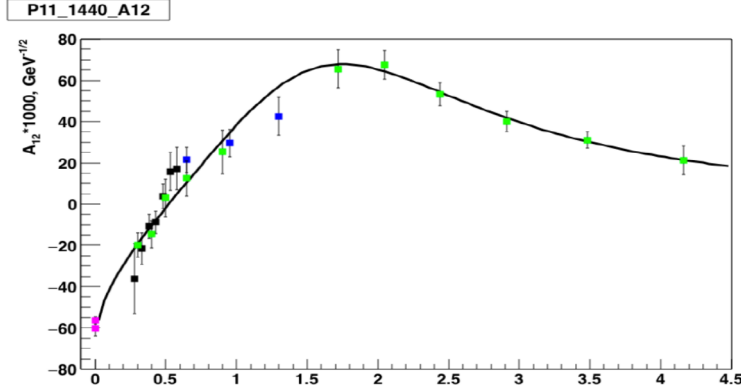


Figure 5: Interpolation of the $N(1440)1/2^+$ electrocouplings from the CLAS data on $N\pi$ (green circles) [6] and $\pi^+\pi^-p$ [26, 52] (black and blue squares) exclusive electroproduction off protons. The results at the photon point are taken from [1, 27]

state electroexcitations. The prediction on the relations between $A_{1/2}$, $A_{3/2}$, and $S_{1/2}$ hybrid electrocouplings exist only for the area large photon virtuality [17] which is outside of the current study scope. In the future the $A_{1/2}$, $S_{1/2}$ and $A_{3/2}$ hybrid electrocouplings will be evaluated within.... at $Q^2 < 2.0 \text{ GeV}^2$ as a part of the commitment of...

In order to identify hybrid-baryon we are looking for its electrocouplings behavior which should have distinctively different features in comparison with already established from the CLAS results [3] electrocouplings of three-quark resonances of $J^P = \frac{1}{2}^+$ shown in Fig 2 and of $J^P = \frac{3}{2}^+$ shown in Fig 7,8

3.1 Signature of the hybrid-baryon in the experimental data

We propose to search for the new baryon states in the exclusive $K^+\Lambda$ and $K^+\Sigma$ and $p\pi^+\pi^-$ electroproduction at the photon virtualities from 0.05 GeV^2 to 1.0 GeV^2 . Possible signatures of the lowest mass hybrid baryons are:

- Almost degenerated pairs of the states with isospin $I = 1/2$, and spin-parities $J^P = \frac{1}{2}^+$ or $J^P = \frac{3}{2}^+$ and the masses in the range $2.0 \text{ GeV} \leq W \leq 2.5 \text{ GeV}$. The hybrid-states of both spin-parities should belong to the two spin-parity bands with well established lowest $N(1440)1/2^+$ and $N(1720)3/2^+$ resonances and with the regular three-quark resonances of masses above and below the hybrid-baryon mass.
- particular features in Q^2 dependence of hybrid electrocouplings related to the color octet assignment for three constituent quarks including: dominance of the transverse over longitudinal amplitudes, similarity of the transverse helicity amplitudes $A_{1/2}(Q^2)$ for the hybrid-baryon and for the $\Delta(1232)\frac{3}{2}^+$ but dissimilar to the three-quark excited states of same J^P , and

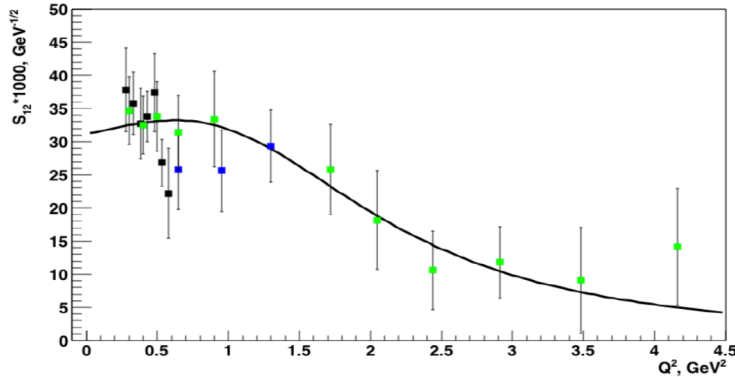


Figure 6: Interpolation of the $N(1710)1/2^+$ electrocouplings from the CLAS data on $N\pi$ (green circles) [28] exclusive electroproduction off protons. The results at the photon point are taken from [1, 27]

- a strongly suppressed helicity amplitude $S_{1/2}(Q^2) \approx 0$ in comparison to other ordinary 3-quark states.

3.2 Search for the three-quark new baryon states

Advanced studies of the data on exclusive meson photoproduction off protons carried out within the framework of the global multi-channel amplitude analysis developed by the Bonn-Gatchina group [30–32] revealed the signals from many new baryon states in the mass range from 1.7 GeV to 2.5 GeV. These states were included to the PDG [1] with the status from one to three star states. Notably, the most prominent signals from new states come from analyses of the CLAS [33–36], ELSA [37], MAMI [38] and GRAAL [39, 40] data on KY electroproduction. Studies of KY as well as $\pi^+\pi^-p$ exclusive electroproduction channels extend considerably our capability in establishing of the excited nucleon state spectrum, including both regular three-quark and exotic hybrid states.

The new baryon states, if they are excited in s-channel should be seen in exclusive reactions both with the real and virtual photons in the same final states. Furthermore, their masses, total decay widths, partial decay widths to different final states should be Q^2 -independent. The values of $\gamma_v p N^*$ electrocouplings obtained independently from analyses of different exclusive channels with completely different non-resonant contributions should be the same. Consistent results on resonance masses, $\gamma_v p N^*$ electrocouplings for all exclusive decay channels under study, and Q^2 -independent partial hadronic decay widths, over the full covered Q^2 -range, will offer convincing evidence for the existence of new states. These studies offer model independent way to prove not only the existence of new excited nucleon states but also their nature as the s-channel resonances eliminating the alternative interpretations for the structures observed in the kinematics dependencies of the observables as complex coupled channel effects, dynamical singularities for the non-resonant amplitudes,

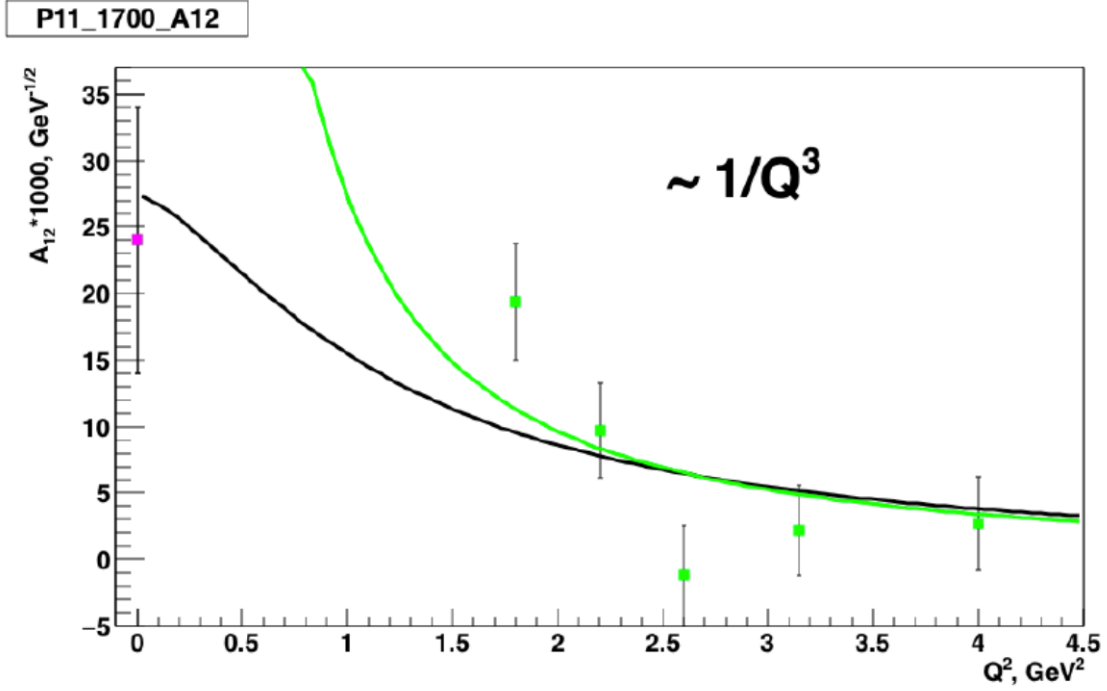


Figure 7: Interpolation of the $N(1720)3/2^+$ electrocouplings from the CLAS data on $\pi^+\pi^-p$ [29] exclusive electroproduction off protons [47]. The results at the photon point are taken from [27, 29]

kinematic reflections, etc.

This strategy was successfully employed in the recent analysis of the $\pi^+\pi^-p$ preliminary photo- and electroproduction cross sections [51] from the CLAS carried out combined within the framework of meson-baryon reaction model JM [29]. It was found that in order to describe both photo- and electroproduction data at W around 1.7 GeV keeping $\pi\Delta$ and ρp hadronic decay widths of all contributing resonances Q^2 -independent, new baryon state $N'(1720)3/2^+$ state is needed with almost the same mass, total widths and the same spin-parity as for the conventional $N(1720)3/2^+$ resonances, but with completely different branching fractions for the hadronic decay to the $\pi\Delta$ and ρp final state and Q^2 -evolution of its $\gamma_v p N^*$ electrocouplings.

The studies of exclusive KY , $\pi^+\pi^-p$ electroproduction channels at $Q^2 < 2.0$ GeV² with maximal virtual photon flux ever achieved in exclusive electroproduction will allow us to solidify the results on the spectrum of excited nucleon states, confirming or ruling out the signal of “missing” resonances observed in exclusive photoproduction. Furthermore, for the first time the information on $\gamma_v p N^*$ electrocouplings of new baryon states will become available offering an access to the structure of “missing” resonances elucidating their differences from the conventional resonances. Finally we want to note that the studies of two major exclusive $N\pi$ and $\pi^+\pi^-p$ electroproduction channels with CLAS revealed the relative growth of the resonant contributions with Q^2 in both channel. So, use of the high intensity virtual photon flux of the proposed experiment may be even preferential for new baryon state search

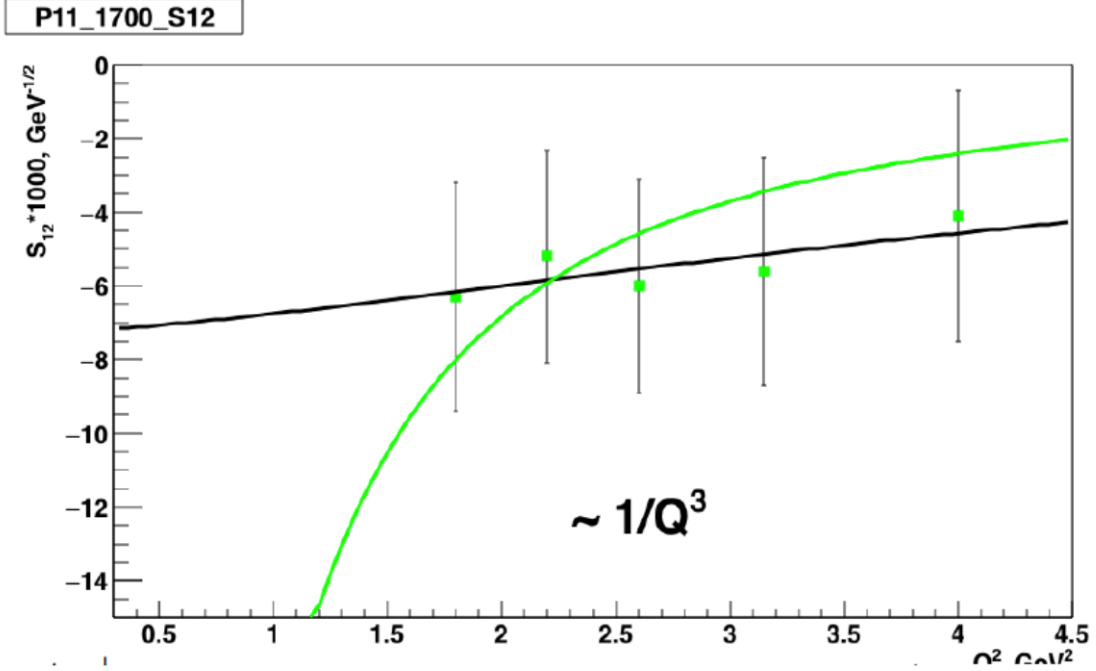


Figure 8: Interpolation of the $N'(1720)3/2^+$ electrocouplings from the CLAS data on $\pi^+\pi^-p$ [29] exclusive electroproduction off protons [47]. The results at the photon point are taken from [27, 29]

in comparison with the photoproduction. It still remain to be seen which range of photon virtualities is the most suitable for the discovery of new excited nucleon states.

3.3 Amplitude analyses of measured observables in a search for new baryon states.

In the analyses of the future experimental data we will apply the amplitude analyses methods for the resonance search and extraction of the resonance parameters. We will employ the global fit of all exclusive channels studied with the CLAS12 in the kinematics of out interest with a focus on new baryon state search within the framework of coupled channel approaches. We also planning to extract of the resonance parameters from the independent analyses of KY , $\pi^+\pi^-p$ exclusive electroproduction off protons carried our within the framework of the reaction models for description of these exclusive channels. Consistent results on the resonant parameters determined from independent analyses of different exclusive meson electroproduction channels and extracted from the global multi-channel fit of all available data will offer strong and almost the model independent evidences for the new state existence and reliable extraction of their parameters. Note, that in order to apply the coupled channel approaches to the analyses of KY , $\pi^+\pi^-p$ exclusive electroproduction data, the information

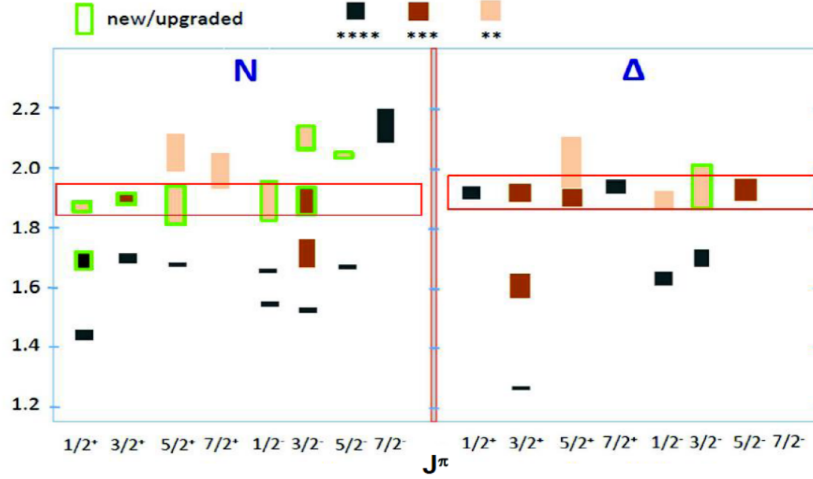


Figure 9: Recent results on the spectrum of excited nucleon states [1]. Signals from the states shown in green boxes were observed in global multi-channel analysis of exclusive meson electroproduction data carried out within the framework of Bonn-Gatchina approach[30–32].

on $N\pi$ electroproduction off protons is also needed. The $N\pi$ exclusive channels dominate at $W < 1.6$ GeV and remain have much bigger cross sections in comparison with the KY electroproduction in the entire kinematics area of our interest. The events from $N\pi$ exclusive channels will be collected simultaneously with the measurement of KY , $\pi^+\pi^-p$ exclusive electroproduction off protons offering the information on the $N\pi$ channel observables.

Advanced amplitude analysis approach for extraction of the nucleon resonance parameters from the global analysis of the photoproduction data, which include almost all relevant in resonance excitation region exclusive meson photoproduction channels off nucleons, has been developed by Bonn-Gatchina group [30–32]. In this approach production amplitudes are decomposed over the set of partial waves. The partial wave amplitudes are parameterized fully accounting for the restrictions imposed by the general unitarity and analyticity conditions, employing K - and D -matrix approaches for the final state interactions while for the photoproduction amplitudes the P -vector approach is used. In a case of pronounced t -channel contributions, Reggeized t -exchanges are incorporated to the photoproduction amplitudes. The hadronic final state interaction are treated employing phenomenological parameterisation, for the respective amplitudes. The resonance parameters were determined from the global fit of all available exclusive photoproduction data augmented by the fit of hadroproduction channels for the final states under studies. Application of the Bonn-Gatchina approach to the global analysis of the dominant part of exclusive meson photoproduction data measured with the CLAS and worldwide provided information on masses, widths, photocouplings and hadronic decay parameters for most excited nucleon states in the mass range up to 3.0 GeV. This analyses revealed the signal from around ten new baryon states, reported in the PDG [1] with the status from one- to three- stars and shown in Fig. 9.

Extension of this approach for description of exclusive electroproduction including KY channels represent the part of the commitment of the Bonn-Gatchina group reported in [41]. Bonn-Gatchina approach extended for analysis of the exclusive electroproduction will be used for extraction of resonance parameters and search for new baryon states in the proposed experiment. The aforementioned extension will be vital in order to check the signals from new baryon states observed in the exclusive meson photoproduction and shown in Fig. 9 independently in the exclusive electroproduction processes confirming or rejecting the candidate-states observed in the photoproduction. It is a critical part of effort in finalizing the long-term program on exploration of the spectrum of excited nucleon states and simultaneously the new avenue extending our knowledge on variety of hadrons in the Nature through the search for hybrid-baryons.

An advanced dynamical coupled-channel model (DCC) has been developed by the Argonne-Osaka collaboration for combined analysis of the world data for $\pi N, \gamma N \rightarrow \pi N, \eta N, K\Lambda, K\Sigma, N\pi\pi$ photo-electro and hadroproduction with a goal of extracting resonance parameters [42, 43]. The DCC approach incorporates three level diagrams derived from effective Lagrangian for the resonant and non-resonant contributions in the photo-/electroproduction as well as in the final state hadronic interactions. The amplitudes for all exclusive channels are fully consistent with the restrictions imposed by the general unitarity and analyticity conditions. This is the only coupled channel approach capable of describing the $N\pi\pi$ photo-/electro-/hadro- production in accord with a general unitarity condition. In order to fulfill the unitarity restrictions, the meson-baryon interactions from the non-resonant amplitudes of all included exclusive processes, the so-called meson-baryon cloud, are incorporated to the electromagnetic and hadronic vertices of nucleon resonances together with direct resonance decays to the $\gamma_{r,v}p$ and meson-baryon final states (bare vertices). Analysis of the observables within the framework of the DCC approach allows us not only to extract the full dressed resonance electromagnetic and hadronic decay amplitudes, but also to disentangle between the contributions from the meson-baryon cloud and bare vertices associated to the quark core part in the nucleon resonance structure. The DCC approach is capable of providing valuable insight to the structure of excited nucleon states. The DCC-model currently is the only available worldwide coupled channel approach that provides the results on $N \rightarrow \Delta(1232)3/2^+$ transition form factors at Q^2 up to 7. GeV² [3] and $N(1440)1/2^+$ electrocouplings at Q^2 up to 3 GeV² [44]. Argonne-Osaka DCC-model will be employed in analyses of the data of the proposed experiment with a goal to observe manifestation of new excited nucleon state and to extract $\gamma_v p N^*$ electrocouplings of the established and new baryon states. This model will allow us to fully account in extraction of $\gamma_v p N^*$ electrocouplings from KY channels for the impact of the final state interaction with the open channels for which the electroproduction cross sections are much larger, i.e. $N\pi$, and $N\pi\pi$. Furthermore, it is the only available worldwide approach capable to account for the complexity of the final state interactions in the $\pi^+\pi^-p$ final state in a way consistent with the unitarity.

So far, most of the results on $\gamma_v p N^*$ electrocouplings have been extracted from independent analyses of π^+n , π^0p , and $\pi^+\pi^-p$ exclusive electroproduction data off the protons.

The $N\pi$ data have been analyzed within the framework of two conceptually different approaches: a unitary isobar model (UIM) and dispersion relations (DR) [6, 28]. The UIM describes the $N\pi$ electroproduction amplitudes as a superposition of N^* electroexcitations in the s -channel, non-resonant Born terms and ρ - and ω - t -channel contributions. The

latter are reggeized, which allows for a better description of the data in the second- and third-resonance regions. The final-state interactions are treated as πN rescattering in the K-matrix approximation [6]. In the DR approach, dispersion relations relate the real to the imaginary parts of the invariant amplitudes that describe the $N\pi$ electroproduction. Both approaches provide good and consistent description of the $N\pi$ data in the range of $W < 1.7$ GeV and $Q^2 < 5.0$ GeV², resulting in $\chi^2/\text{d.p.} < 2.9$. In the proposed this approach will be used for evaluation of the $N\pi$ electroproduction amplitudes needed as the input for the aforementioned global multi-channel analyses of the KY and $\pi^+\pi^-p$ exclusive electroproduction data.

The $\pi^+\pi^-p$ electroproduction data from CLAS [47, 53] provide for the first time information on nine independent single-differential and fully-integrated cross sections binned in W and Q^2 in the mass range $W < 2.0$ GeV and at photon virtualities of $0.25 \text{ GeV}^2 < Q^2 < 1.5 \text{ GeV}^2$. The analysis of the data allowed us to develop the JM reaction model [8, 26, 52] with the goal of extracting resonance electrocouplings as well as $\pi\Delta$ and ρp hadronic decay widths. This model incorporates all relevant reaction mechanisms in the $\pi^+\pi^-p$ final-state channel that contribute significantly to the measured electroproduction cross sections off protons in the resonance region, including the $\pi^-\Delta^{++}$, $\pi^+\Delta^0$, $\rho^0 p$, $\pi^+N(1520)\frac{3}{2}^-$, $\pi^+N(1685)\frac{5}{2}^+$, and $\pi^-\Delta(1620)\frac{3}{2}^+$ meson-baryon channels as well as the direct production of the $\pi^+\pi^-p$ final state without formation of intermediate unstable hadrons. In collaboration with the JPAC [?] the special approach has been developed allowing us to remove the contributions from the s-channel resonances to the reggeized t-channel non-resonant terms in $\pi^-\Delta^{++}$, $\pi^+\Delta^0$, $\rho^0 p$ electroproduction amplitudes. The contributions from well established N^* states in the mass range up to 2.0 GeV were included into the amplitudes of $\pi\Delta$ and ρp meson-baryon channels by employing a unitarized version of the Breit-Wigner ansatz [52]. The JM model provides a good description of $\pi^+\pi^-p$ differential cross sections at $W < 1.8$ GeV and $0.2 \text{ GeV}^2 < Q^2 < 1.5 \text{ GeV}^2$ with $\chi^2/\text{d.p.} < 3.0$. The achieved quality of the CLAS data description suggest the unambiguous and credible separation between the resonant/non-resonant contributions achieved fitting the CLAS data [26]. The credible isolation of the resonant contributions makes it possible to determine the resonance electrocouplings and $\pi\Delta$, and ρN decay widths from the resonant contributions employing for their description the amplitudes of the unitarized Breit-Wigner ansatz [52] that fully accounts for the unitarity restrictions on the resonant amplitudes. This model will be used in the proposed experiment for analyses of exclusive $\pi^+\pi^-p$ electroproduction allowing us to determine electrocouplings of most excited nucleon since almost all nucleon resonances have substantial hadronic decays to the $N\pi\pi$ final states. Capability of the JM model to pin down new baryon states was demonstrated in the combined studies of exclusive $\pi^+\pi^-p$ photo- and electroproduction [29] which provided convincing evidence for new baryon state $N(1720)3/2^+$

The model for description of the KY exclusive photo- and electroproduction channels “regge-plus-resonance” (RPR) has been developed by the Ghent group [9, 58]. In this model full production amplitude is described by the superposition of eight resonances and the non-resonant contribution. The non-resonant amplitudes represent the sum of t -channel exchanges by K - and K^* -Regge trajectories. The model provided a good description of KY photoproduction data. It reproduces the gross features in Q^2 -evolution for the exclusive unpolarized structure functions. We are planning to use this model for extraction of the resonance electrocouplings from exclusive KY electroproduction data after the model upgrade

allowing improved description of the structure functions. The development in this direction was presented in [45].

3.4 Modeling the hybrid baryon contribution to exclusive KY and $\pi^+\pi^-p$ electroproduction off protons.

To prove the feasibility of observing hybrid baryons, we have studied the effect of implementing the contribution of the two lightest hybrid states of ≈ 2.2 GeV mass with spin-parities $J^P = \frac{1}{2}^+$ and $\frac{3}{2}^+$ into the reaction model of both $K\Lambda$ and $K\Sigma$ electroproduction.

For mass estimations of the hybrid baryon we have followed the considerations detailed in section 3 and we have modeled the hybrid baryons contributions considering spin-parities $J^P = \frac{1}{2}^+$ and $J^P = \frac{3}{2}^+$ in the mass range from 2.1 to 2.3 GeV. According to the RPP14 results [1] on the resonance parameters in the mass range around 2.0 GeV, we adopted for the total decay width of hybrid baryons a range from 250 to 300 MeV and for their branching fraction (BF) to the KY and $\pi^+\pi^-p$ final states the value of 3%.

The excitation of a single hybrid resonance in the helicity representation $\langle \lambda_f | T_r | \lambda_\gamma \lambda_p \rangle$ may be expressed using a relativistic Breit-Wigner (BW) ansatz:

$$M_{\lambda_\gamma}^{\lambda_p \lambda_f} = \langle \lambda_f | T_r | \lambda_\gamma \lambda_p \rangle = \frac{\langle \lambda_f | T_{dec} | \lambda_R \rangle \langle \lambda_R | T_{em} | \lambda_\gamma \lambda_p \rangle}{M_r^2 - W^2 - i\Gamma_r M_r}, \quad (1)$$

where M_r and Γ_r are the resonance mass and total width, respectively; we assumed both total and partial decay widths to be energy independent.

The matrix elements $\langle \lambda_R | T_{em} | \lambda_\gamma \lambda_p \rangle$ and $\langle \lambda_f | T_{dec} | \lambda_R \rangle$ are the electromagnetic production and hadronic decay amplitudes of the N^* with helicity $\lambda_R = \lambda_\gamma - \lambda_p$, in which λ_γ and λ_p stand for the helicities of the photon and proton in the initial state, and λ_f represents the helicity of final-state hadron in the N^* decays.

The explicit form of the $\langle \lambda_f | T_r | \lambda_\gamma \lambda_p \rangle$ amplitudes is reported in Appendix B. This contribution has been added to the most advanced reaction models of KY and $\pi^+\pi^-p$ exclusive electroproduction cross sections:

- in the case of the KY channel we considered as a reference the Regge plus resonance model (RPR-2011)[9, 22] in which reggeized non-resonant amplitudes and the contributions from the established N^* states have been used to describe both KY photo- and electro-production. The web-site [23] provides a full set of KY electroproduction observables off proton (KY Model A). The contribution of the new hybrid baryon state in the virtual-photon-proton s-channel, described by 25, has been coherently added to the PRP-2011 model at the amplitude level, and the resulting cross-section, including polarization terms, has been evaluated as a function of the hybrid resonance electro-coupling values (KY Model B).
- in the case of the $\pi^+\pi^-p$ channel we considered the effect of the coherent superposition of the hypothetical cross sections due to new hybrid baryon state to the most updated version of the JM model [8, 47–49]. We define as $\pi^+\pi^-p$ Model A as the updated JM model, while $\pi^+\pi^-p$ Model B is the one obtained after the inclusion of the hybrid baryon contribution.

In both cases the resulting cross sections have been used inside an event generator to study the experimental sensitivity to the hybrid baryon electrocouplings strength. The formalism used to determine the electroproduction cross section from the helicity amplitudes is described in Appendix A. We have varied the values of the hybrid baryon electrocouplings $A_{1/2}$, $S_{1/2}$ and $A_{3/2}$ to determine the minimum strength that would be observable in the proposed experiment.

It may be noted that, at the very high Q^2 regime, the following relations for the hybrid baryon electrocouplings $A_{1/2}$, $S_{1/2}$ and $A_{3/2}$ have been used in literature [17], to model the hybrid baryon signatures:

$$\begin{aligned} A_{1/2} &= A, \\ S_{1/2} &= AQ, \\ A_{3/2} &= A/Q^2, \end{aligned} \tag{2}$$

where $Q = \sqrt{Q^2}$ and A is a common term. However in the low Q^2 regime these relations are not valid and we have considered fixed independent values for all three electrocouplings. We have independently fixed the value for each electrocoupling strength $A_{1/2}$ and $S_{1/2}$ for the $\frac{1}{2}$ resonance and also the $A_{3/2}$ for the $\frac{3}{2}$ resonance, in the range $1 - 8010^{-3} GeV^{-2}$, setting the values of the other electrocouplings to zero.

For both KY and $\pi^+\pi - p$ final states the CMS angle distributions of the final mesons, simulated according to models A and B, with and without the contribution of the hybrid resonance, have been used to explore feasibility to observe the lightest hybrid baryons of minimal decay widths.

Two quantitative criteria have been used to determine the minimum detectable electrocoupling strength at different Q^2 values:

- the statistical significance of the difference between the event distributions, with and without the inclusion of the hybrid resonance, has been quantified introducing the $\chi^2/d.p.$ calculated as follows:

$$\chi^2/d.p. = \frac{1}{N_{d.p.}} \sum_{\theta_i, \phi_j, W_k} \frac{(d\sigma_{i,j,k}^A - d\sigma_{i,j,k}^B)^2}{\delta_{i,j,k}^2}, \tag{3}$$

where the $d\sigma_{i,j,k}^A$ and $d\sigma_{i,j,k}^B$ are the cross section determined for model A and model B, respectively, for each measurable kinematic defined by the CM energy W and the θ_i^* , ϕ_j^* final state meson angles. The uncertainty $\delta_{i,j,k}^2$ is the expected statistical error for the extraction of the cross section in the corresponding kinematical bin.

Previous experience in the analysis of the same final states in CLAS [3] suggest that a minimum value of $\chi^2/d.p. = 4$ is required for a set of experimental data to be sensitive to a resonance contribution. The dependence of the obtained $\chi^2/d.p.$ for increasing values of $A_{1/2}$, $S_{1/2}$ and $A_{3/2}$ has been studied, to determine the values of the electrocouplings required to reach the $\chi^2/d.p. = 4$ threshold at different Q^2 values.

- the sensitivity to the added hybrid resonance has been quantified by a $\chi^2/d.p.$ calculated as follows:

$$\chi^2/d.p. = \frac{1}{N_{d.p.}} \sum_{\theta_i, \phi_j, W_k} \frac{(d\sigma_{i,j,k}^B - d\sigma_{i,j,k}^R)^2}{\delta_{i,j,k}^2}, \tag{4}$$

where the $d\sigma_{i,j,k}^B$ and $d\sigma_{i,j,k}^R$ are the cross sections determined by model B for an hybrid baryon resonance of fixed mass and threshold electrocoupling values and for the same model B but with a different value of the resonance mass. The uncertainty $\delta_{i,j,k}^2$ is defined as in the previous case. Scanning the value of the resonance mass in evaluating $d\sigma_{i,j,k}^R$ and the corresponding $\chi^2/d.p$ value, for a fixed Q^2 value, one expects to find a minimum at the fixed hybrid resonance mass, which is more pronounced as the sensitivity to the contribution increases.

These criteria have been applied to both KY and $\pi^+\pi^-p$ event distributions to determine the minimum electrocoupling values that are detectable as a function of the integrated experiment luminosity. The results are reported in section 7.

3.5 Search for the hybrid-baryon signal employing the moment expansion

. The analysis using the Legendre moments proved to be a good way to distinguish signal from background. Legendre moments are defined as:

$$P_m = \frac{2m+1}{2} \int_{-1}^1 L_m d\sigma(x)_i dx \quad (5)$$

where

$$\begin{aligned} x &= \cos\theta_k^* \\ L_m(x) &= \sum_{j=0}^m a_{mj} x^j \\ a_{mj} &= (-1)^{(m-j)/2} \frac{1}{2^m} \frac{(m+j)!}{(\frac{m-j}{2})! (\frac{m+j}{2})! j!} \\ m-j &= \text{even} \end{aligned} \quad (6)$$

$d\sigma(x)_i$, with $i = T, L, TT$ and LT , represent the transverse, longitudinal and interference structure functions, which depend on the variables W , Q^2 and θ_k^* .

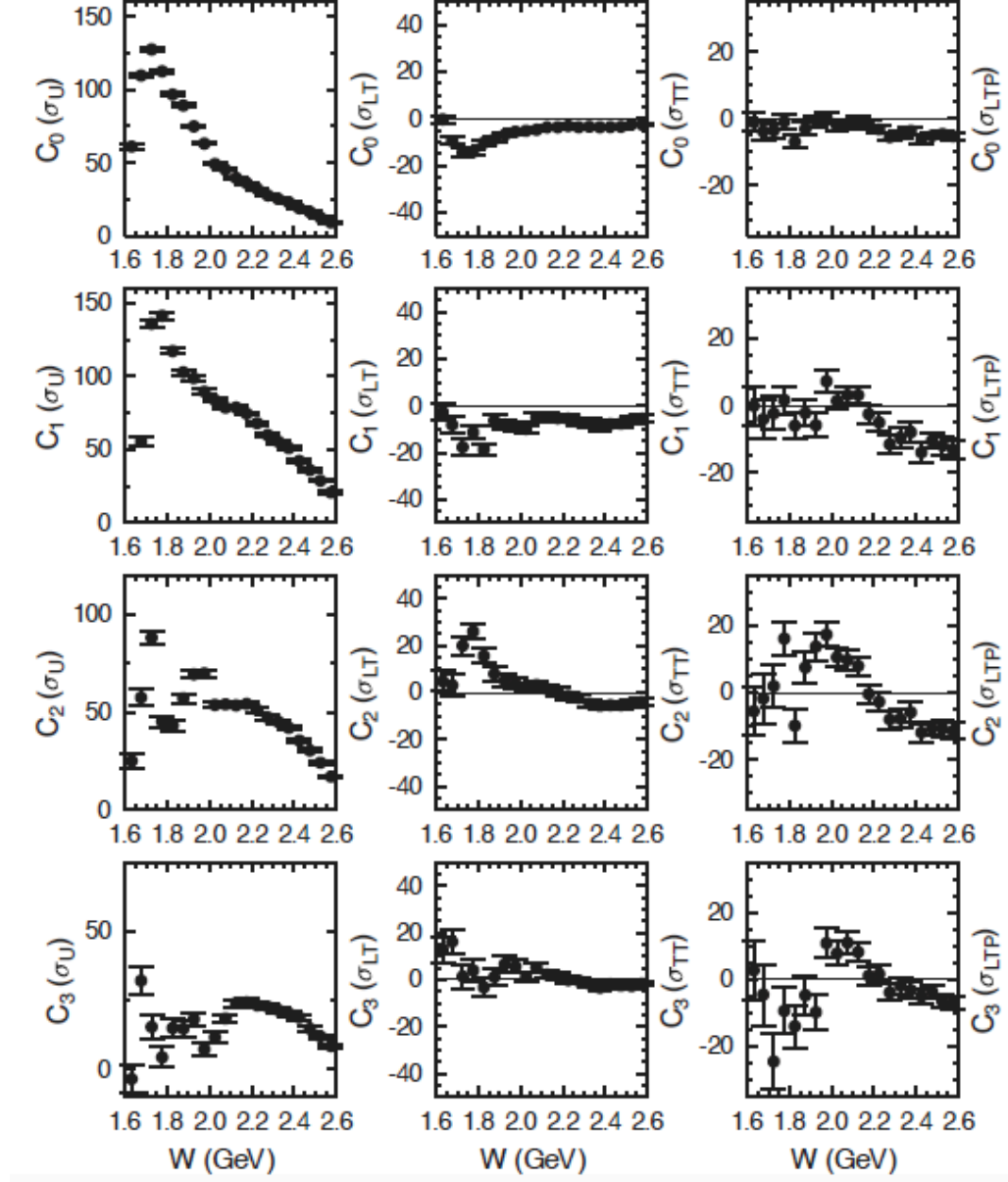


Figure 10: Legendre polynomial fit coefficients for $m = 0 \rightarrow 3$ as a function of W for the $d\sigma_U$, $d\sigma_T T$ and $d\sigma_L T$ structure functions for the $K\Lambda$ electroproduction at $Q^2 = 1.8 \text{ GeV}^2$ [46].

The Legendre moments may be used to expand the structure functions in terms of the orthogonal Legendre polynomials:

$$\sigma(x)_i = \sum_m P_m(Q^2, W) L_M(\cos\theta^* k) \quad (7)$$

where the first seven Legendre polynomial functions have the following form:

$$\begin{aligned} L_0 &= 1 \\ L_1 &= \cos\theta \\ L_2 &= \frac{1}{2}(3\cos\theta^2 - 1) \\ L_3 &= \frac{1}{2}(5\cos\theta^3 - 3\cos\theta) \\ L_4 &= \frac{1}{8}(35\cos\theta^4 - 30\cos\theta^2 + 3) \\ L_5 &= \frac{1}{8}(63\cos\theta^5 - 70\cos\theta^3 + 15\cos\theta) \\ L_6 &= \frac{1}{16}(231\cos\theta^6 - 315\cos\theta^4 + 105\cos\theta - 5). \end{aligned} \quad (8)$$

The expansion of the structure function in terms of Legendre moments is believed to be an alternative way to prove the sensitivity to the hybrid baryon contribution, since the appearance of a structure in a single Legendre moment at the same value of W for each Q^2 point is likely a signal from a resonance contribution.

Figure 10 reports the first four Legendre polynomial fits, measured by CLAS for the $K\Lambda$ electroproduction structure functions at $Q^2 = 1.8 \text{ GeV}^2$ [46]. They show the presence of a structure at $W = 1.7 \text{ GeV}$ for the C_0 in both the $d\sigma_U$ and $d\sigma_{LT}$ and a structure at $W = 1.9 \text{ GeV}$ in both C_2 and C_3 in $d\sigma_U$.

Of course only a full amplitude partial wave analysis will constitute a definite proof for the presence of a resonance, but the study of Legendre moments may provide the first hint of their appearance. A study of the first seven Legendre moments of the $d\sigma_U$, $d\sigma_{TT}$ and $d\sigma_{LT}$ structure functions has been performed for the models A and B of the $K\Lambda$ electroproduction, described in the previous section. The results are reported in section 7.

4 The Experimental program

4.1 The CLAS12 detector

The experimental program will use the CLAS12 detector, shown in Fig. 11, for the detection of the hadronic final state. CLAS12 consists of a Forward Detector (FD) and the Central Detector (CD). The Forward Detector is comprised of six symmetrically arranged sectors defined by the six coils of the toroidal superconducting magnet. Charged particle tracking is provided by a set of 18 drift chambers with a total of 36 layers in each sector. Additional tracking at $5^\circ - 35^\circ$ is achieved by a set of 6 layers of micromesh gas detectors (micromegas) immediately downstream of the target area and in front of the High-Threshold Cherenkov counter (HTCC). Particle identification is provided by time-of-flight information from two

layers of time-of-flight detectors (FTOF). Electron, photon, and neutron detection are provided by the triple layer electromagnetic calorimeter, PCAL, EC(inner), and EC(outer). The heavy gas Cherenkov Counter (LTCC) provides separation of high momentum pions from kaons and protons. The Central Detector consists of 6-8 layers of silicon strip detectors with stereo readout, 6 layers of micromegas, arranged as a barrel around the target, 48 scintillator bars to measure the particle flight time from the target (CTOF), and a central neutron detector. Further details on all CLAS12 components (magnets, detectors, data acquisition, software) may be obtained from Ref. [50].

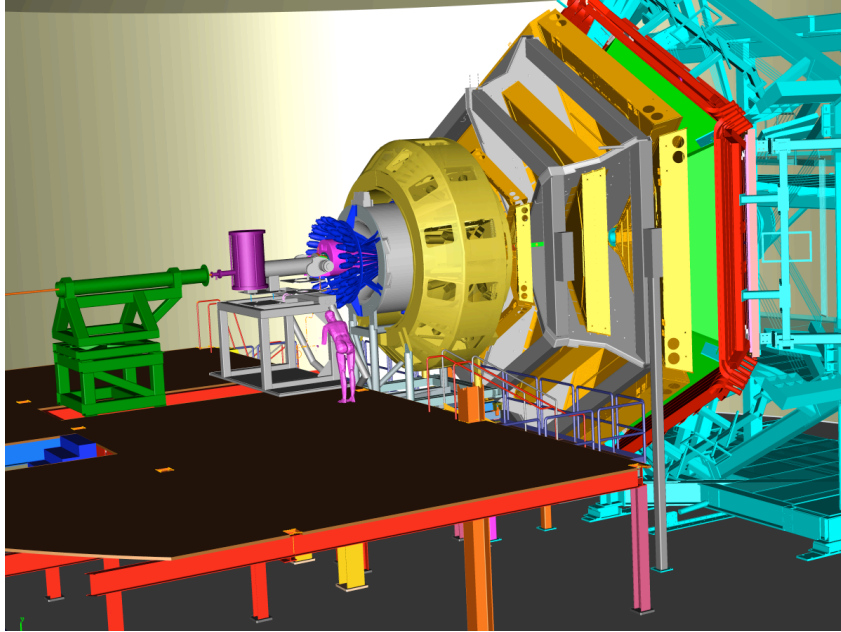


Figure 11: The CLAS12 detector has high hermeticity and high multiplicity reconstruction, can run at high luminosity ($L > 10^{35} \text{cm}^{-2} \text{s}^{-1}$), and is best suited to carry out the proposed experiment.

A polarized electron beam will be scattered off a liquid hydrogen target. The scattered electrons will be detected in the the Forward Detector of CLAS12 for scattering angles greater than about 6° and in Forward Tagger for angles from 2.5° to 4.5° , which allows us to cover the Q^2 range of interest between 0.05 and 2 GeV^2 . Charged hadrons will be measured in the full range from 6° to 130° . At an operating luminosity of $L = 10^{35} \text{ cm}^{-2} \text{s}^{-1}$ hadronic rates of $5 \times 10^6 \text{ s}^{-1}$ are expected.

4.2 The Forward Tagger

An essential component of the hadron spectroscopy program with CLAS12 is the Forward Tagger (FT) shown in Fig 12. The FT uses a high resolution crystal calorimeter composed of 324 lead-tungstate crystals to measure the scattered electrons in the polar angle range from 2.5° to 4.5° and with full coverage in azimuthal angle. The calorimeter measures electron

and photon energies with an energy resolution of $\sigma(E)/E \leq 0.02/\sqrt{E(\text{GeV})} + 0.01$. The fine granularity of the calorimeter also provides good polar angle resolution. A two-layer tiled scintillator hodoscope is located in front of the calorimeter for the discrimination of photons. An additional four-layer micromegas tracker, located in front of the hodoscope, will be used for precise electron tracking information. Electron detection in the FT will allow us to probe the crucial Q^2 range where hybrid baryons may be identified due to their fast dropping $A_{1/2}(Q^2)$ amplitude and the suppression of the scalar $S_{1/2}(Q^2)$ amplitude. Construction of

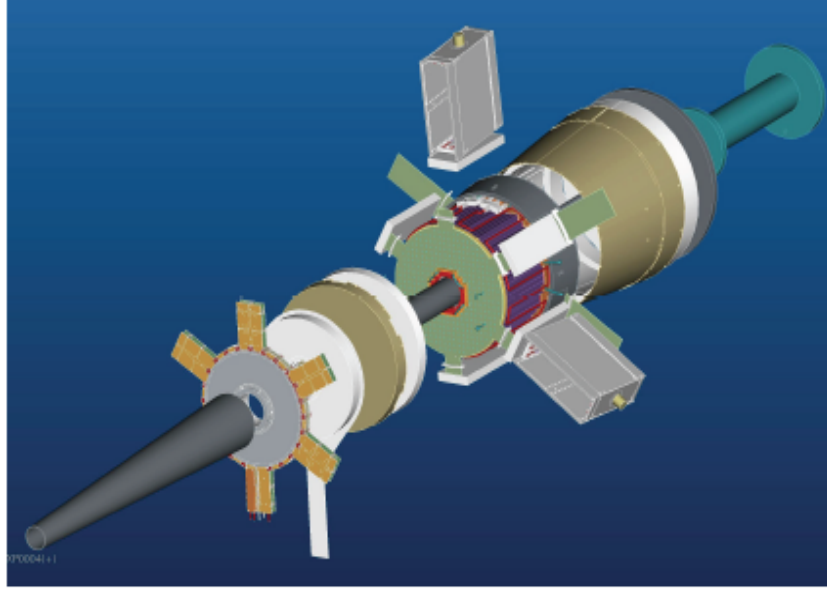


Figure 12: The Forward Tagger (FT) system. The FT provides electron and high energy photon detection in a range of polar angles $\theta_e = 2.5^\circ - 4.5^\circ$, and will be fully integrated into the operation of CLAS12.

the FT has been completed under the responsibility of INFN/Genova (Italy), CEA/Saclay (France), and the University of Edinburgh (UK). The FT has been shipped to Jefferson Lab, it has been assembled and it is now under calibration with cosmic rays. Installation into CLAS12 is expected in summer 2016.

4.3 Kinematical coverage of electron scattering in CLAS12

The CLAS12 detector acceptance to inclusive electron scattering events has been studied using a FAST Montecarlo, which is a simplified version of the CLAS12 reconstruction code. The event reconstruction takes into account the fiducial areas of the detector and provides smearing of the charged final particles momenta. The optimal beam energy conditions and torus current settings have been studied, to maximise the scattered electron acceptance in the W , Q^2 kinematical plane.

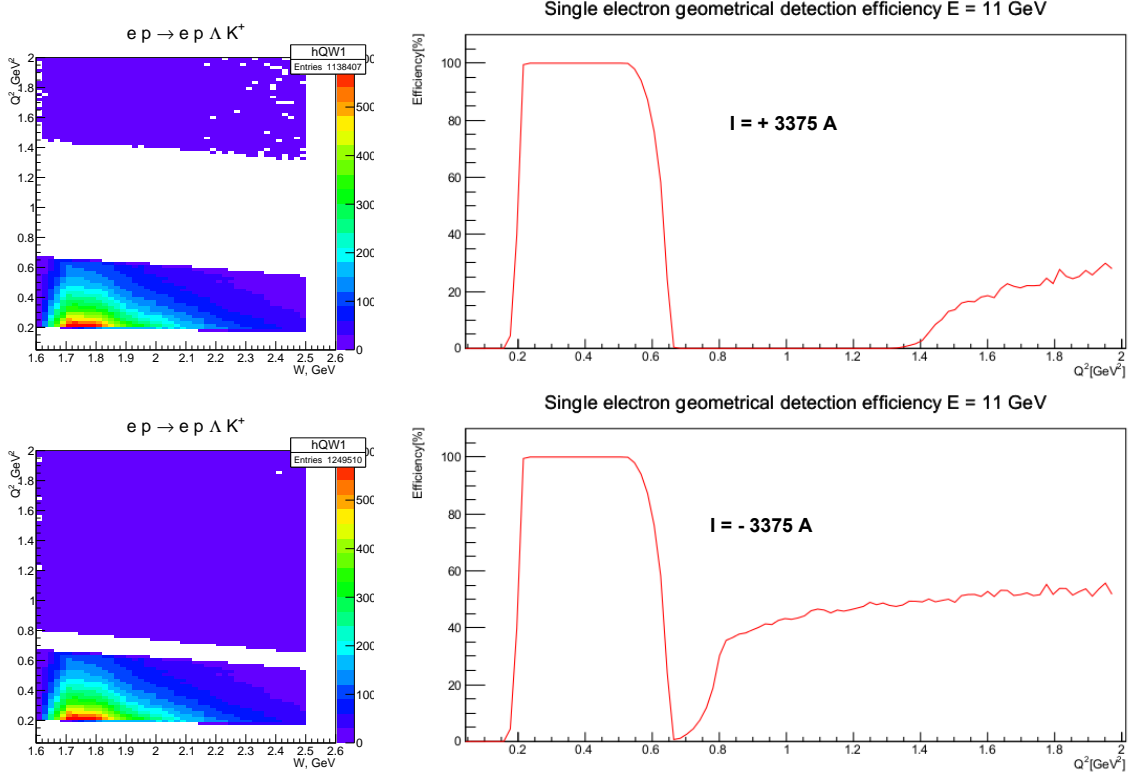


Figure 13: Left column shows the Q^2 vs W scatter plot of geometrically detected electrons in CLAS12 for $I = +3375$ A (top) and $I = -3375$ A (bottom) torus currents, for $E_e = 11$ GeV incoming electron beam energy. Right column shows the corresponding geometrical acceptances as a function of Q^2 , for the same torus current settings.

The virtuality of the emitted photon Q^2 is related to the scattered electron energy E'_e and polar angle θ_e through the relation $Q^2 = 4E_e E'_e \sin^2 \frac{\theta_e}{2}$, so reaching the lowest Q^2 range requires detecting the electrons emitted with the smallest scattering angle in the FT and using relatively low electron beam energies.

If a positive current in the torus is applied, the scattered electrons are forced to bend towards the beam axis and this causes an increase in the minimum detectable Q^2 value in CLAS12. On the contrary a negative current in the torus forces the scattered electrons to bend outwards, lowering the value of the minimum accessible Q^2 value. Figure 13 shows the scatter plot of Q^2 vs W values of the detected electrons in CLAS12 for operating torus currents $I = +3375$ A (top-left) and $I = -3375$ A (bottom-left), at the maximum electron beam energy available in HALL-B: $E_e = 11$ GeV. The empty region corresponds to the gap between the FT and the minimum polar angle accepted in CLAS12. The geometrical electron acceptance for the corresponding torus currents are shown in the right plots. The electrons that are detected in the FT, correspond to an accessible Q^2 range from 0.2 to 0.6 GeV²; electrons detected in CLAS12 have a lower geometrical efficiency, due to fiducial areas of the detector, and cover an higher Q^2 range that starts from 0.8 or 1.4 GeV² for the negative and positive torus currents, respectively.

Reaching the low- Q^2 region requires lowering the electron beam energy. Figure 14 shows

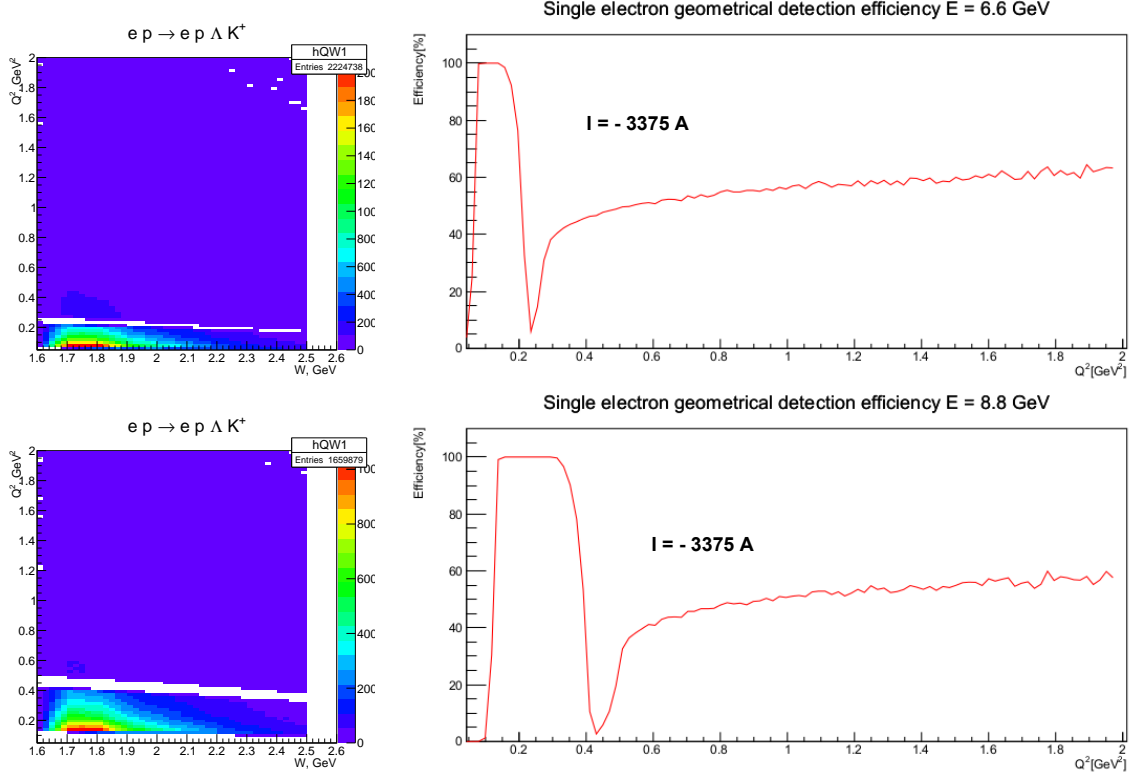


Figure 14: Left column shows the Q^2 vs W scatter plot of geometrically detected electrons in CLAS12 for $I = -3375$ A for electron beam energies $E_e = 6.6$ GeV (top) and $E_e = 6.6$ GeV (bottom). Right column shows the corresponding geometrical acceptances as a function of Q^2 , for the same electron beam energies.

the scatter plot of Q^2 vs W values of the detected electrons in CLAS12 for an operating torus current $I = -3375$ A at electron beam energies $E_e = 6.6$ GeV (top) and $E_e = 6.6$ GeV (bottom); the corresponding curves of geometrically accepted Q^2 ranges are shown in the right column. At $E_e = 6.6$ GeV electron energy the minimum Q^2 measurable value is as low as 0.05 GeV² and the accessible measurable range extends up to 2 GeV², with a gap between 0.15 GeV² and 0.3 GeV². This gap may be covered if an electron beam energy of $E_e = 8.8$ GeV is used, as shown in the bottom plots of Fig. 14. In this case the Q^2 threshold is 0.1 GeV² and the acceptance gap appears in the interval from 0.35 to 0.5 GeV², providing a nicely complementary range of measurable photon virtualities.

We conclude that the experimental optimal setting for the present proposal requires beamtime at both $E_e = 6.6$ GeV and $E_e = 8.8$ GeV electron beam energies, with negative operating torus current set at $I = -3375$ A. Detailed simulations of the $\pi^+\pi^-p$ and KY final states are reported in the next sections.

5 Simulations for the $ep \rightarrow ep\pi^+\pi^-$ final state

5.1 Event generator for $ep \rightarrow ep\pi^+\pi^-$

The previously existed 2π event generator was written in FORTRAN and had several limitations. It employed the $\pi^+\pi^-p$ differential cross sections from the older JM05 version of the JM model [47–49]. During the past several years the model was further developed [8] and significantly improved. Furthermore, the two-pion part of that event generator was only applicable up to 2 GeV in W and from 0.3 GeV² in Q^2 , and therefore excluded most of the region of interest (high W and low Q^2), where it used simple interpolations. A substantial need to develop new event generator emerged, and it was successfully developed for this proposal.

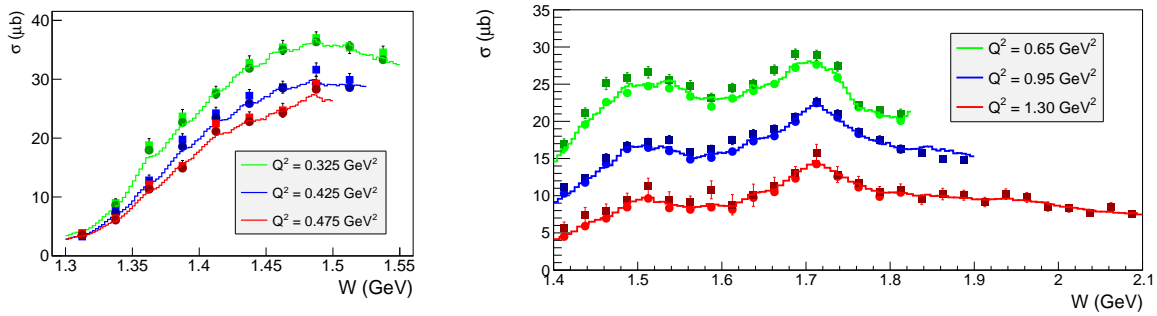


Figure 15: Comparison between the event distributions of the new two-pion event generator (curves) with the integrated cross sections from JM model (circles) and data (squares). Left plot shows the W dependence of the total cross section for three Q^2 bins in comparison with the model [52] and data [53] for the corresponding three Q^2 points at 0.325, 0.425, and 0.475 GeV². Right plot shows the W dependence of the total cross section for three Q^2 bins in comparison with the model [8] and data [51] for the corresponding three Q^2 points at 0.65, 0.95, and 1.3 GeV².

The new event generator employs the 5-fold differential cross sections from the recent version of the JM15 model fit to all results on charged double pion photo- and electroproduction cross sections from CLAS (both the published and preliminary [51–53, 56]). In the areas covered by CLAS data new event generator successfully reproduces the available integrated and single differential 2π cross sections. The quality of the description is illustrated in Fig. 15 for several Q^2 bins in comparison with the available electroproduction data [51–53].

In order to extend event generator to the area not covered by CLAS data, a special extrapolation procedure was applied, that included additional available world data on W dependencies of 2π photoproduction integrated cross sections [54, 55]. The new approach allows to generate 2π events at extremely low Q^2 (less than 0.1 GeV²) and high W (up to 3 GeV). On the left side of Fig. 16 the W dependence of integrated cross section for quasi-real Q^2 (0.0015 GeV²) is shown in comparison with data [54–56]. The right side of Fig. 16 illustrates a typical example of Q^2 dependence of the total cross section for one W bin in comparison with JM15 [8] for 8.8 GeV electron beam energy.

The new event generator has more advantages: it generates phase space distributions and applies multidimensional cross section as a weight for each event. This method enables to significantly speed up the generation process, especially in the areas with sharp cross

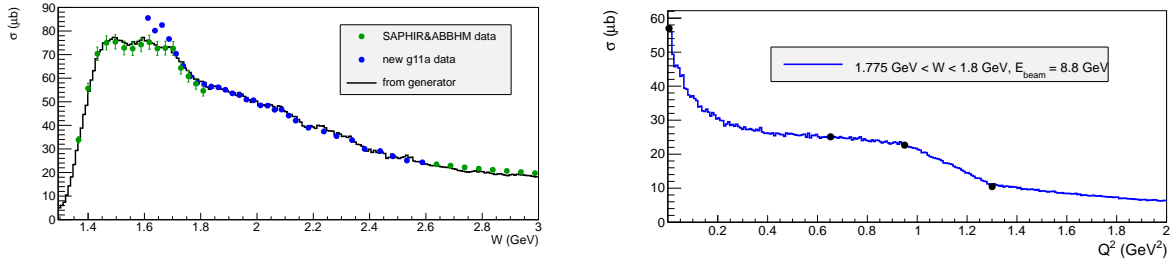


Figure 16: Left plot shows the W dependence of the integrated cross section for quasi-real Q^2 (0.0015 GeV^2) in comparison with data [54–56]. Right plot shows a typical example of Q^2 dependence of the total cross section for one W bin in comparison with JM15 [8] at $W = 1.7875 \text{ GeV}$ for 8.8 GeV electron beam energy.

section dependencies. It makes also possible to obtain absolute values of cross section from the generated distributions and this is helpful for various additional purposes, such as cross section predictions in areas not covered by experiment.

The new 2π event generator is written in C++, it includes inclusive radiative effects according to the approach described in [57] and produces an output compatible with the new CLAS12 reconstruction software.

Studies of the run conditions for this proposal were carried out with new 2π event generator described above. Exclusive events for $\pi^+\pi^-$ electroproduction off proton were generated in the range of invariant masses of the final hadron system W from the two-pion production threshold to 3 GeV and at photon virtualities Q^2 from 0.01 GeV^2 to 2.0 GeV^2 (see Fig. 17).

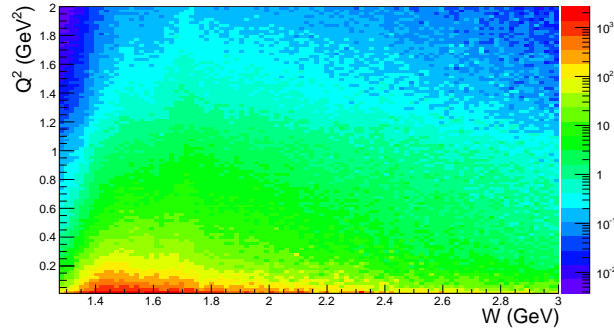


Figure 17: Q^2 versus W distribution for the generated $\pi^+\pi^-p$ events with an electron beam energy of 6.6 GeV .

5.2 Acceptance estimates for $ep \rightarrow ep\pi^+\pi^-$

For the event reconstruction a simplified version of the CLAS12 event reconstruction software, the so-called FASTMC routine, was employed to filter the generated events for acceptance. This routine accounts for the detector fiducial areas and provides smearing over the final particle angles and momenta. The accepted events are shown in Fig. 18 and are plotted in the Q^2 versus W plane. Left and right panels show the distributions for the reconstructed

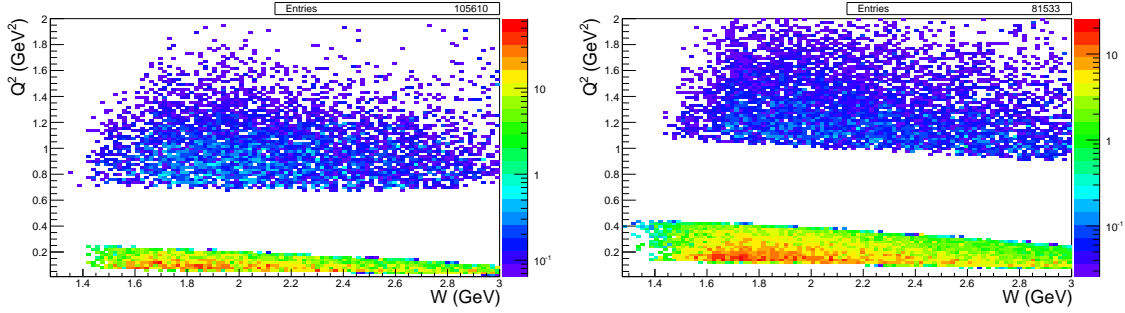


Figure 18: Q^2 versus W distributions for the reconstructed $\pi^+\pi^-p$ events (all particles in final state are registered). Left and right plots correspond to 6.6 GeV and 8.8 GeV beam energies, respectively. The torus current is set to + 3375 A.

$\pi^+\pi^-p$ events at two beam energies for the torus current set to +3375 A, which forces negatively charged particles to bend towards the beam line. Similarly to the results obtained in section 4.3, areas of zero acceptance can be seen in the plots, representing the gap between the Forward Tagger and the minimum polar angle accepted in CLAS12 for inbending particles. For the hybrid baryon search the area of small photon virtuality is of particular interest. The size of the gap depends on the torus current setting and the momentum of the scattered electrons. For a negative torus current, i.e. outbending electrons, the gap is simply given by the geometrical acceptance of CLAS12 and is largely independent of the particle momentum, while for inbending particles the acceptance depends on scattering angle, particle momentum, and magnetic field strength. The acceptance for electron scattering angles from 2.5° to 4.5° , which is covered by the FT, is independent of the torus current settings. A simulated $ep \rightarrow e'p\pi^+\pi^-$ event in CLAS12 is shown in Fig.21.

With a beam energy of 6.6 GeV, the influence of the magnetic field direction on the accessible kinematical coverage for $\pi^+\pi^-p$ electroproduction was further studied. The Q^2 versus W distributions for reconstructed $\pi^+\pi^-p$ events are shown in Fig. 19 for two opposite polarities of the torus current, +3375 A and -3375 A, which correspond to the maximum expected currents. A wide area of zero acceptance for the normal (+3375 A) direction of the magnetic field is clearly seen in Figure 19 (left). Reversing the magnetic field allows us to decrease substantially the inefficient area, as is shown in Fig. 19 (right). Therefore, as anticipated in section 4.3, the reversed magnetic field represents the best configuration for the proposed experiment, as well as for other experiments, for which the area of small photon virtualities is of particular interest.

We also examined the evolution of counting rates as a function of the magnetic field strength. The 2D Q^2 versus W distributions for the accepted $\pi^+\pi^-p$ events are shown in Fig. 20 for the torus currents, -3375 A (left) and -1500 A (right), that correspond to the full and less than half strength magnetic fields for the CLAS12 detector. Comparing the reconstructed event rates shown in Fig. 20, we expect the counting rate to increase by almost a factor of two at half strength of the magnetic field, because of the improved acceptance for the detection of all three $\pi^+\pi^-p$ particles in the final state and the scattered electron. From the other hand decreasing of the torus current will negatively affect particles momentum resolution so the maximum negative torus current will be used for this proposal.

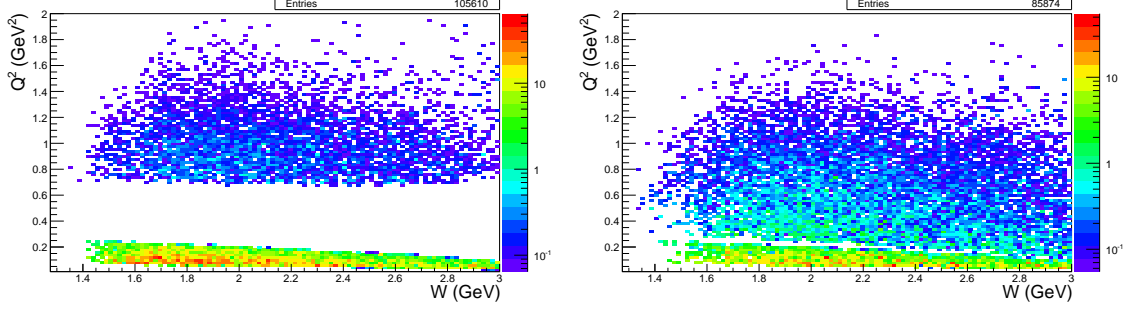


Figure 19: Q^2 versus W distributions for reconstructed $\pi^+\pi^-p$ events (all particles in final state are registered) for the torus currents +3375 A (left) and -3375 A (right) at 6.6 GeV² electron beam energy. The reversed magnetic field closes the gap between the Forward Tagger and CLAS12.

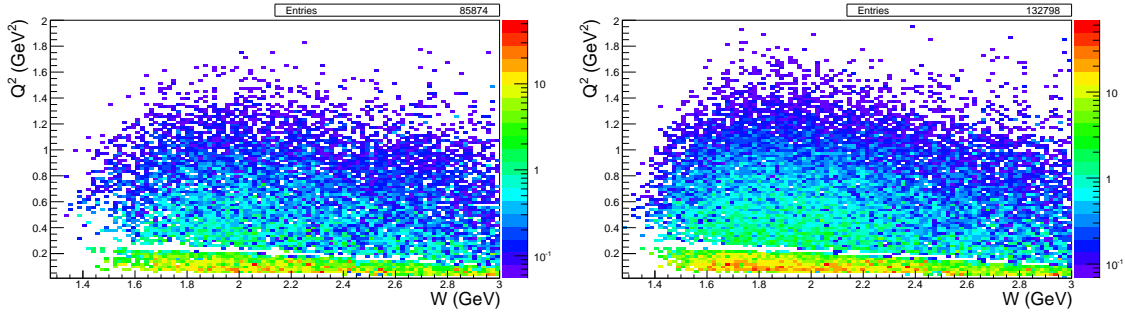


Figure 20: Q^2 versus W distributions for reconstructed $\pi^+\pi^-p$ events at 6.6 GeV beam energy (all final state particles are registered) with torus currents: -3375 A (left) and -1500 A (right). With lower torus current more events are reconstructed.

5.3 Resolution in hadronic mass reconstruction and background estimation for $ep \rightarrow ep\pi^+\pi^-$

The hadronic mass resolution is of particular importance in studies of excited nucleon states, since this quantity determines the ability to reliably extract the resonant contributions in exclusive cross sections. For a credible separation between the resonant and the non-resonant contributions the resolution over W should be much smaller than the N^* decay width. Typical values for the decay widths of nucleon resonances with masses > 2.0 GeV are in a range from 250 to 400 MeV. Hence a mass resolution of ≈ 30 MeV is sufficient for the reliable isolation of contributions from hybrid-baryons that are expected in the mass range from 2.0 to 3.0 GeV. The resolution in W for the reconstructed $\pi^+\pi^-p$ events was studied in the following way. For each reconstructed event we compute the difference between the exact W_{gen} and the reconstructed W_{rec} . We compare two different ways of determining the invariant mass of the final hadron system: a) from the difference between the four-momenta of the initial and the scattered electrons that is added to the four-momentum of the target proton (electron scattering kinematics) b) from the sum of the four-momenta of the final π^+ , π^- , and proton (hadron kinematics). The reconstructed $W_{gen} - W_{rec}$ event distributions provide the necessary information on the invariant mass resolution.

The aforementioned distributions for the electron scattering and hadron kinematics are shown in Fig. 22. The beam energy is set to 6.6 GeV and torus current to -3375 A. For

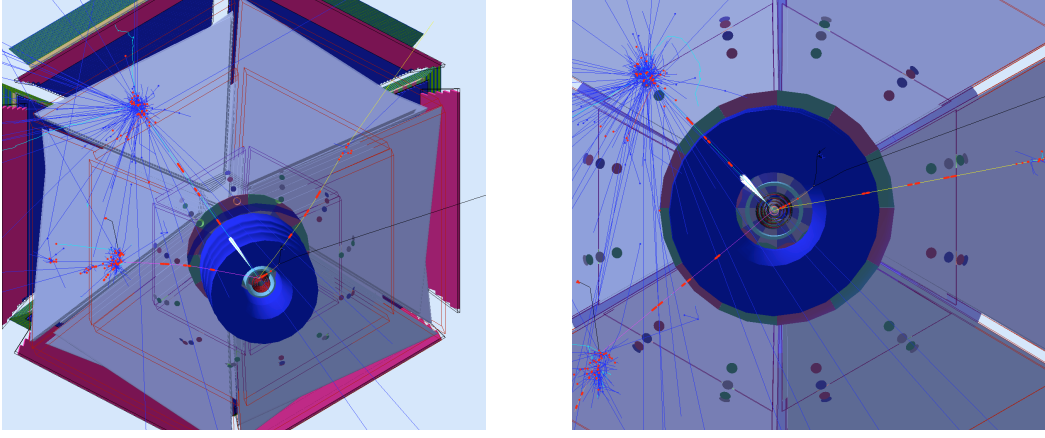


Figure 21: A Geant4 $ep \rightarrow ep\pi^+\pi^-$ event as seen in CLAS12. The left graph shows the scattered electron (cyan) generating Cherenkov light in the HTCC, leaving track segments in the 3 drift chamber regions, and hits in the FTOF planes and finally shower in the PCAL & EC calorimeters. The two pions π^+ (purple line) and π^- (yellow line) are tracked in the DCs, and leave hits in the FTOFs and calorimeters. The proton (short orange line) is tracked at large angles inside the solenoid magnet in the four SVT regions, and leaves hits in the CTOF. The right panel shows a close-up view of the same event from a different angle. The torus magnet is at 50% of full current.

both ways of determining the W_{rec} value, the resolution over the full W range is better than 30 MeV and sufficient for the separation of resonant/non-resonant contributions. If W_{rec} is computed from the hadron kinematics, the resolution is significantly better than in the case of electron scattering kinematics. However, the hadron kinematics requires the registration of all final hadrons with a detection efficiency lower than in the inclusive case where the value of W_{rec} is determined from the electron scattering kinematics.

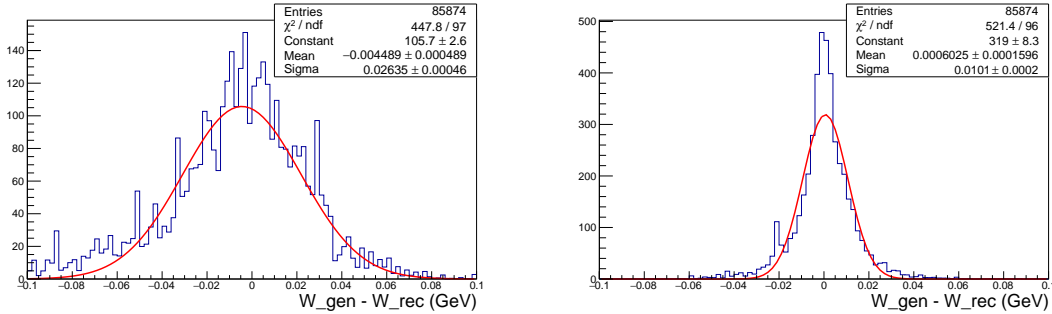


Figure 22: The $W_{gen} - W_{rec}$ distributions for $\pi^+\pi^-p$ events where W_{rec} is determined by electron scattering (left) and hadron (right) kinematics. See text for explanation of both kinematics.

The studies of charged double pion electroproduction with the CLAS detector [51, 53] demonstrated that the topology, where the final π^- is not detected and its four-momentum is reconstructed from energy-momentum conservation, provides the dominant part of the statistics. Hence topologies in which one of the final hadrons is not detected will provide the

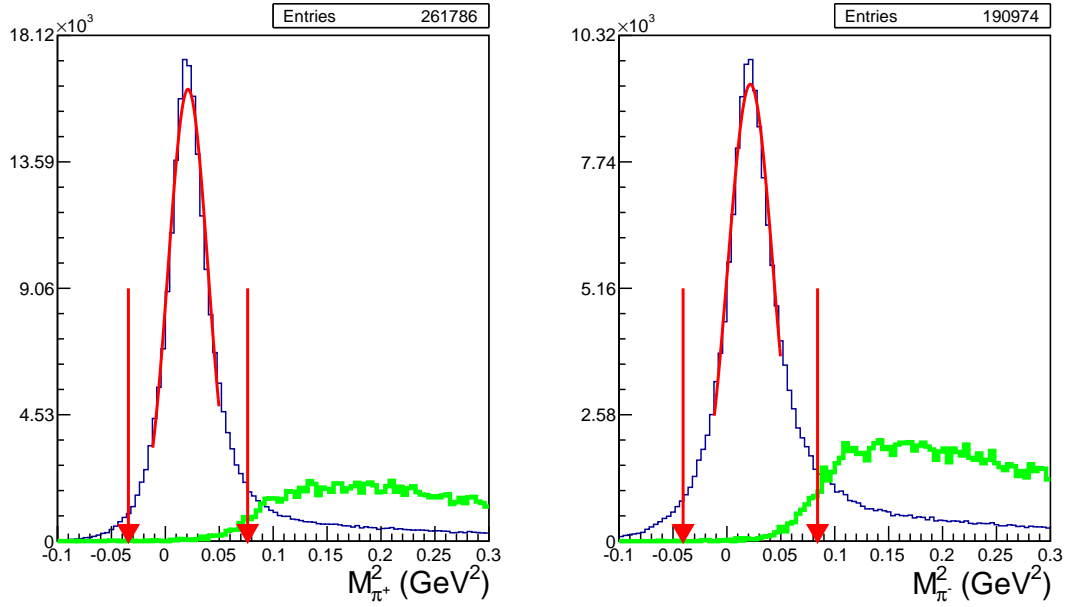


Figure 23: The reconstructed $\pi^+\pi^-p$ event distributions of the missing masses squared of π^+ (left) and π^- (right) for the generated $\pi^+\pi^-p$ events with an admixture of 3π events. The distributions were plotted for $W > 2$ GeV. Cross sections of 2π and 3π channels were assumed comparable in this kinematic region. The contributions from the $\pi^+\pi^-p$ and the $\pi^+\pi^-\pi^0p$ events are shown in blue and green, respectively. The red arrows indicate the applied exclusivity cuts.

dominant statistics also in the proposed experiment. We are planning to select the $\pi^+\pi^-p$ events by employing exclusivity cuts on the missing mass squared distributions of any of the final hadrons. The contribution from other exclusive channels (exclusive background) to the events within the exclusivity cuts was evaluated in the Monte-Carlo simulation. Most of the exclusive background events come from the $ep \rightarrow e'p'\pi^+\pi^-\pi^0$ channel. Both $\pi^+\pi^-p$ and $\pi^+\pi^-\pi^0p$ events were generated for $W > 2$ GeV. Cross sections of 2π and 3π channels were assumed comparable in this kinematic region. A phase space distribution is assumed for the 3π events. With this mixture of generated events we reconstructed the $\pi^+\pi^-p$ events and determined their distribution over the missing mass squared for π^+ and π^- . They are plotted in Fig. 23. The blue curves in Fig. 23 show the 2π event contributions and the green curves represent the 3π event contributions. The exclusivity cuts provide good isolation of the $\pi^+\pi^-p$ events with the following contributions from the 3π events: about 3% for π^+ missing topology and 4% for π^- missing topology.

5.4 Run conditions

The summary of the run conditions studied in the simulations described above is listed in Table 1. Bold rows correspond to the optimal set-up for the proposed experiment.

Whereas the summary of the kinematical coverage in terms of 2D plots of ϕ versus θ distributions for the final hadrons is shown in Fig. 24 for all final hadrons detected, a beam energy of 6.6 GeV, and torus current -3375 A. The vertical strips at $\theta = 40^\circ$ in all plots of Fig. 24 correspond to the detector gap between forward and central parts of CLAS12.

Energy (GeV)	Torus current (A)	Eff. all reg. (%)	Eff. π^+ miss (%)	Eff. π^- miss(%)	Eff. proton miss(%)	Q_{min}^2 (GeV ²)	$\sigma(W)$ (GeV)	$\sigma(\sqrt{s})$ (GeV)
8.8	+3375	8.2	9.8	10.3	8.6	0.13	35	11
8.8	-3375	8.3	12.7	10.6	12.1	0.13	33	10
8.8	+1500	11.5	12.9	11.9	11.6	0.13	35	11
8.8	-1500	12.8	16.8	13.5	16.0	0.13	36	11
6.6	+3375	10.6	13.0	14.1	11.4	0.05	27	11
6.6	-3375	8.7	13.8	11.5	13.1	0.05	26	10
6.6	+1500	15.0	17.3	16.3	15.7	0.05	25	11
6.6	-1500	13.4	18.4	14.8	17.7	0.05	29	10

Table 1: Comparison of run conditions for the $\pi^+\pi^-p$ channel. Bold rows represent the optimal run conditions for 6.6 and 8.8 GeV beam energy runs.

Since a reversed torus magnetic field was chosen, the low angle area is better populated for negatively charged particles (π^-).

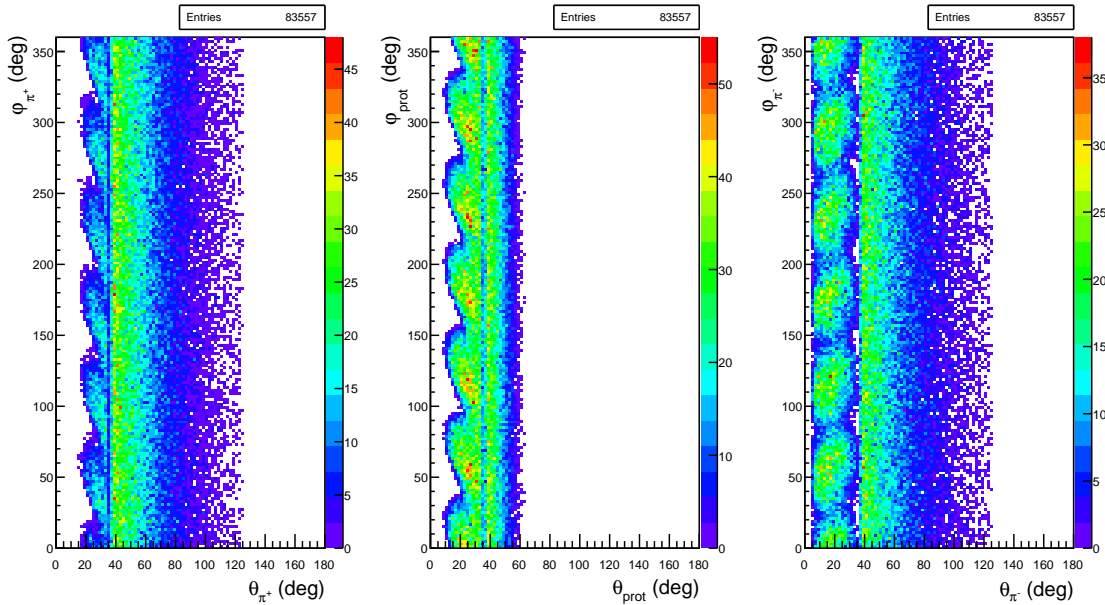


Figure 24: φ vs θ distributions for the final hadrons: π^+ (left), proton (middle), and π^- (right).

6 Simulations for the $K\Lambda$ and $K\Sigma^0$ final states

6.1 Event generator for $ep \rightarrow eK\Lambda$ and $ep \rightarrow eK\Sigma^0$

The $ep \rightarrow e'K^+\Lambda$ event generator is based on model cross section calculations. The models [9] for the $K^+\Lambda$ and [58] for the $K^+\Sigma^0$ channels describe KY electroproduction in the framework of a Regge-plus-resonance approach. Resonance contributions in the s-channel

are described with the help of the effective-Lagrangian approach and the background part of the amplitude is modeled in terms of t-channel Regge-trajectory exchange.

A comparison of the fully integrated model cross section with experimental CLAS data is shown in Fig. 25. The cross sections are presented as a function of Q^2 for a given bin in $W = 2.05$ GeV. Differential cross sections in certain bins of Q^2 and W are shown in Figs. 26 and 27. The model reproduces the experimental data for $0.65 \text{ GeV}^2 < Q^2 < 1.5 \text{ GeV}^2$, while it considerably underestimates the cross section for $Q^2 > 1.5 \text{ GeV}^2$. This underestimation is especially notable in the $K^+\Sigma^0$ channel for high Q^2 and low W , see plot corresponding to $Q^2 = 1.8 \text{ GeV}^2$ and $W = 1.73 \text{ GeV}$ in Fig. 27. It does not create any problems since our region of interest is at low Q^2 . We have to rely on the model cross section for $Q^2 < 0.65 \text{ GeV}^2$, as there are no experimental data to compare to. We can see in Figs. 26 and 27 that the model reproduces well the general features of the sharp cross section growth at large $\cos(\theta)$ for $Q^2 > 1.5 \text{ GeV}^2$ and $W > 2.0 \text{ GeV}$.

6.2 Acceptances for $ep \rightarrow e'pK^+\Lambda$

In Figs. 28 and 29 we compare the angular distributions of all final states particles for an electron beam of 6.6 GeV and for torus currents of **+3375 A** and the **-3375 A**. In Fig. 28 we see qualitatively the same behavior as for the $p\pi^+\pi^-$ final state: inbending electrons generated in a W interval from $K^+\Lambda$ threshold at 1.6 GeV to 3.5 GeV and scattering angles $\theta_e \geq 2^\circ$ are detected in CLAS12 starting at about 6.5° with the acceptance opening up towards larger scattering angles. The swirly pattern seen in the accepted protons and K^+ is due to the azimuthal motion of charged tracks in the strong solenoid field that generates a "kick" in azimuth that depends on the production angle and the particle momentum. It should be noted that the particles are not traversing the sectors in this pattern, as the plotted quantities are the values at the production vertex. The pattern for the π^- is different as they have on average much lower momenta and their migration in ϕ is larger and more diffuse.

For KY production off hydrogen, the recoil protons are kinematically limited to polar angles of $\leq 65^\circ$. Figure 29 shows the acceptances for out-bending electrons for which the polar angle gap between the FT and CLAS12 is strongly reduced and the azimuthal response is more uniform. As a result, the event acceptance for this configuration is almost a factor 2 larger than for the in-bending field configuration. We also note that for both configurations there exists a polar-angle band from 35° to 40° where the acceptance is depleted due to the partially blind transition region between the forward and central detectors.

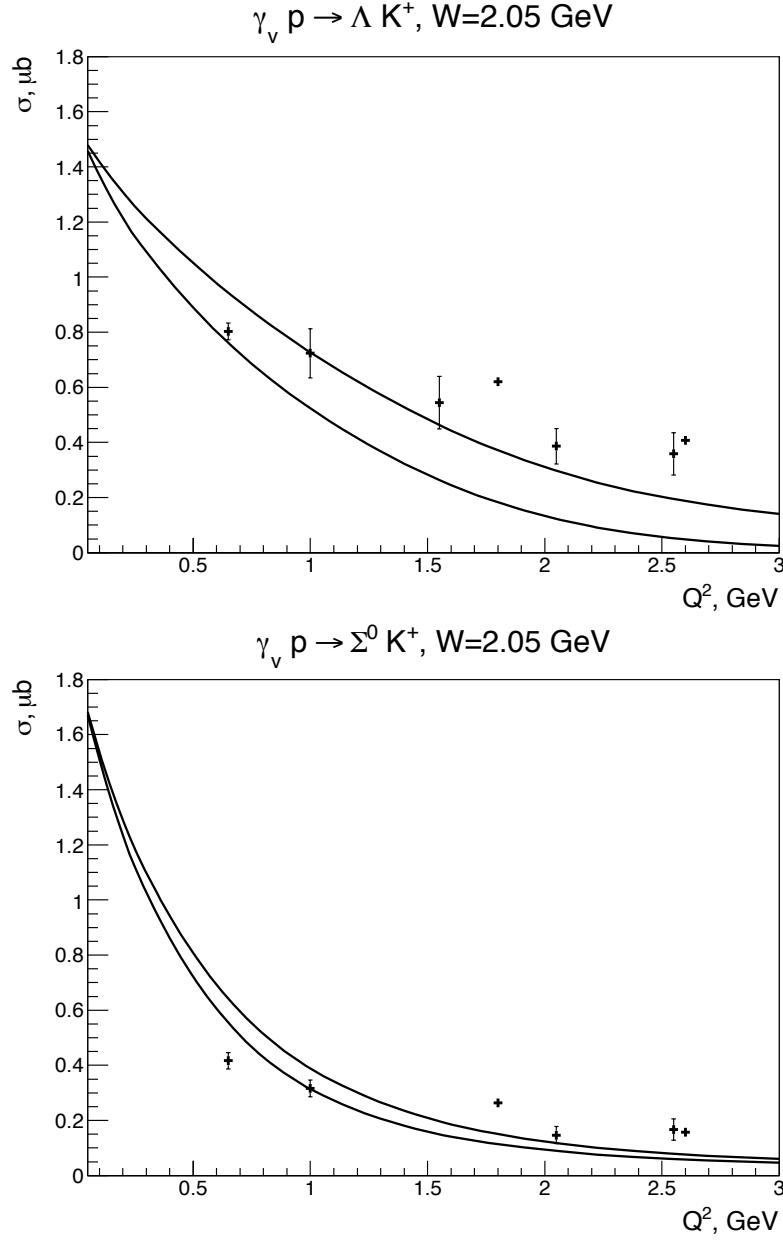


Figure 25: Integrated cross section for $K^+\Lambda$ (top) and $K^+\Sigma$ (bottom) as a function of Q^2 at $W = 2.05 \text{ GeV}$. Experimental cross sections at $Q^2 = 0.65 \text{ GeV}^2$ are measured at a beam energy of 2.567 GeV . Whereas cross sections at $Q^2 = 1.8 \text{ GeV}^2$ and 2.6 GeV^2 are measured at a beam energy of 5.5 GeV . All other Q^2 points correspond to a beam energy of 4.056 GeV . Model calculations are shown in two curves: upper curve is for a beam energy of 2.567 GeV and lower for 5.5 GeV .

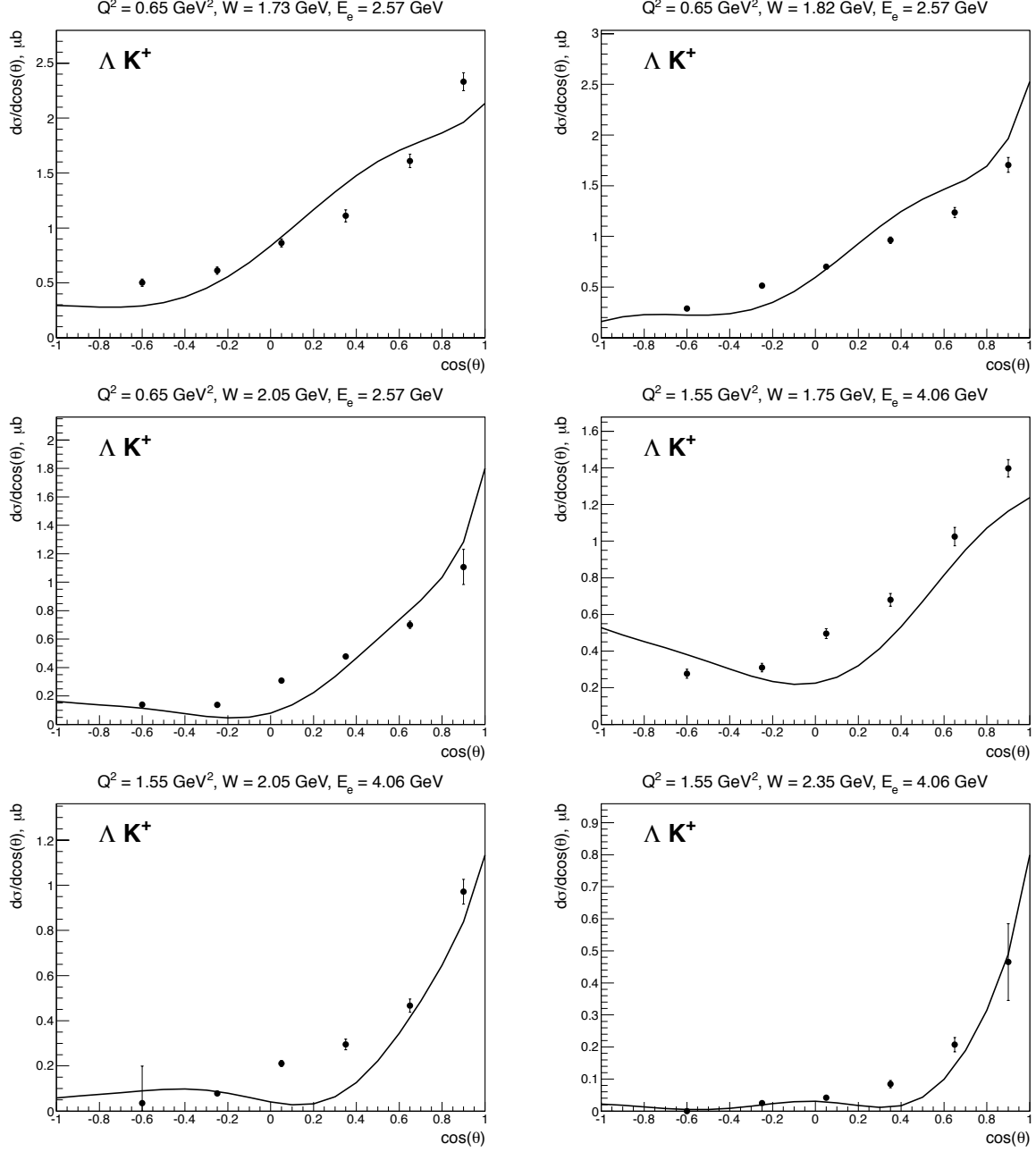


Figure 26: Differential cross sections for $K^+\Lambda$ channel in various Q^2 , W bins for two different beam energies. θ is the polar angle of the kaon in the CMS.

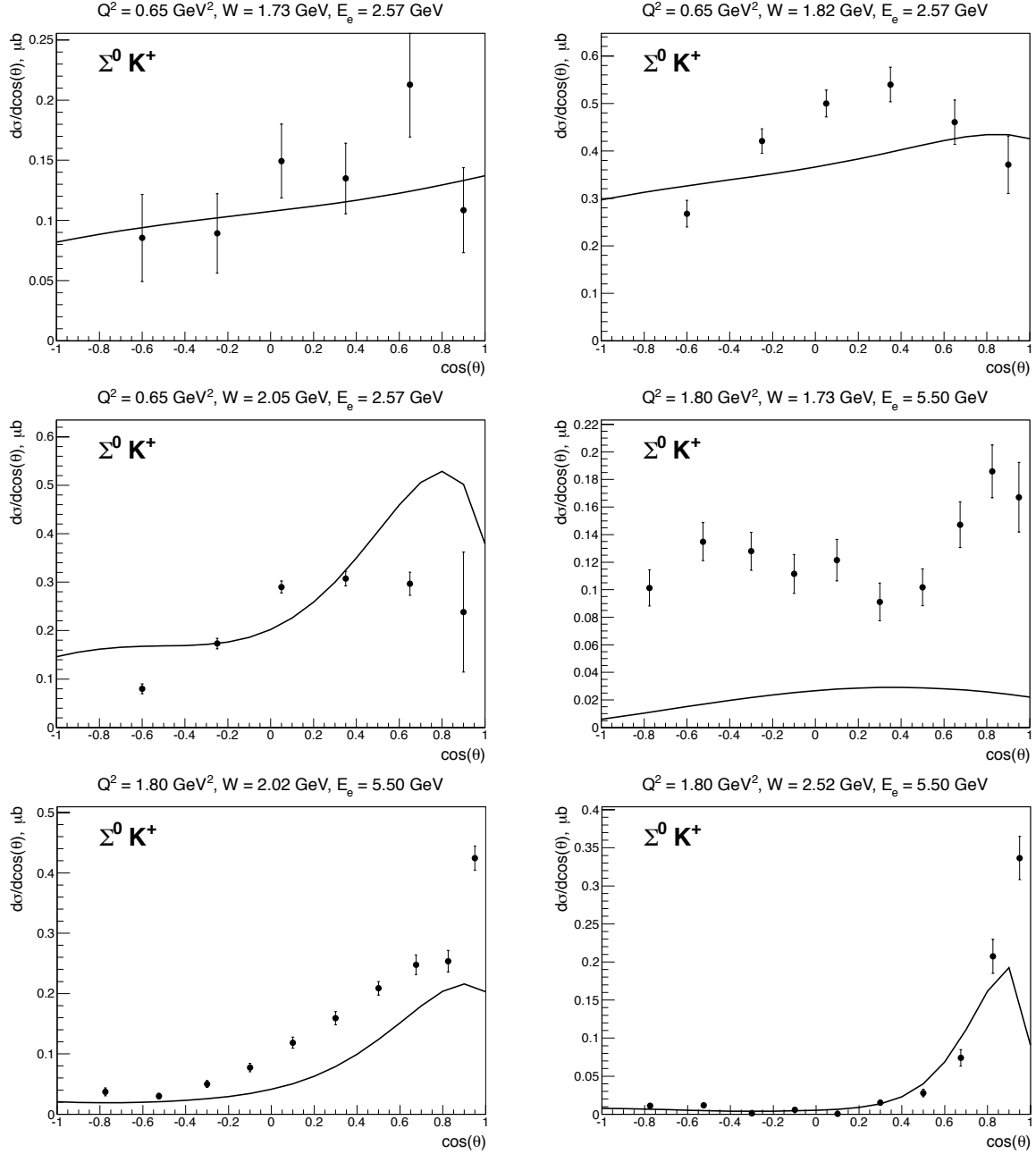


Figure 27: Differential cross sections for for $K^+\Sigma^0$ channel in various bins of Q^2 , W bins for some beam energies. θ is polar angle of the kaon in CMS.

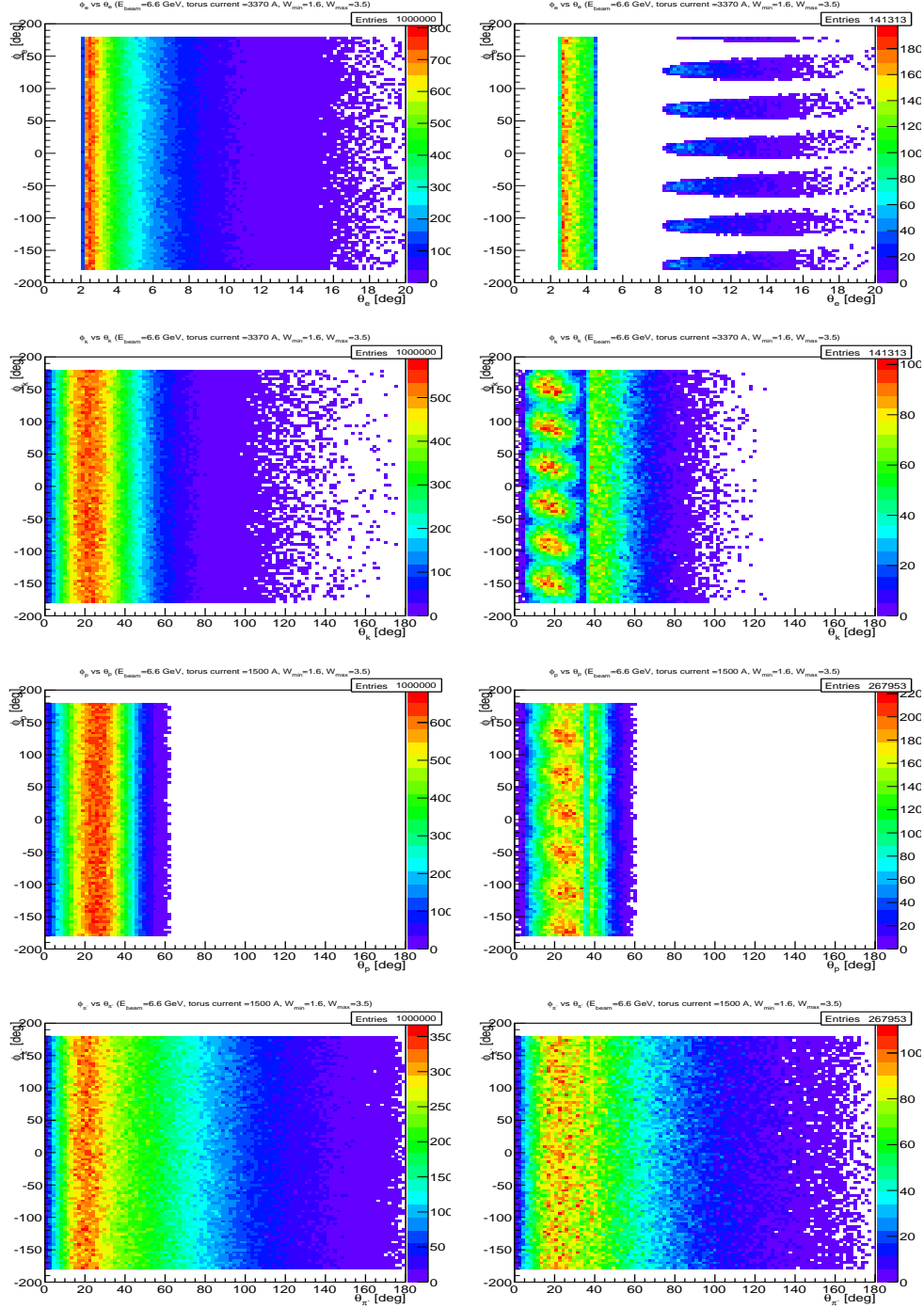


Figure 28: Azimuthal versus polar angle of generated (left) and accepted events (right) for electrons (top row), K^+ (2nd row), protons (third row), and π^- (bottom row). Events are generated for an electron beam energy of 6.6 GeV in a W range from 1.6 to 3.5 GeV. The torus current is set $I = +3375$ A, that bends negatively charged particles inward towards the beamline and reduces the acceptance for electrons within CLAS12.

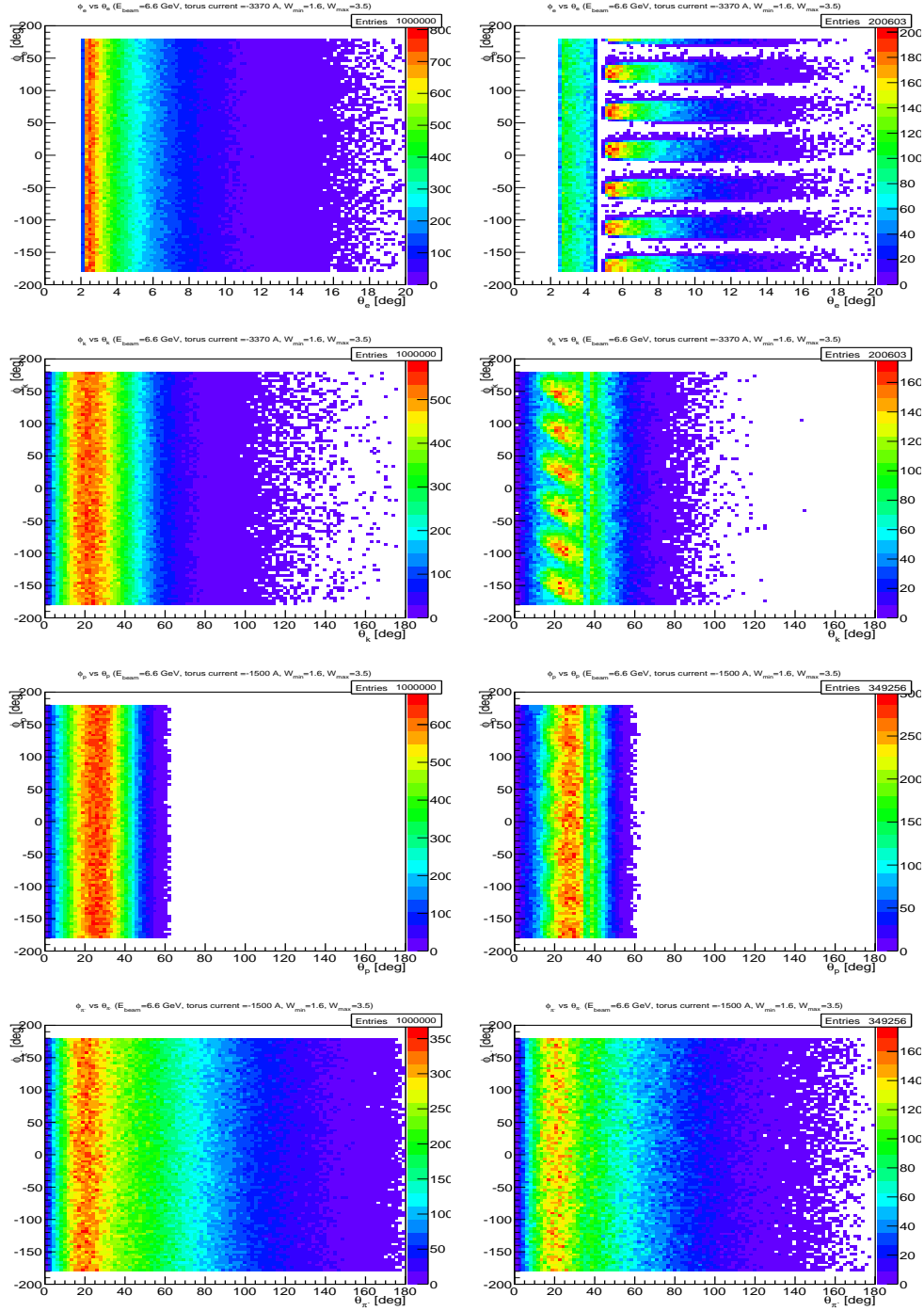


Figure 29: Azimuthal versus polar angle of generated (left) and accepted events (right) for electrons (top row), K^+ (2nd row), protons (third row), and π^- (bottom row). Events are generated for an electron beam energy of 6.6 GeV in a W range from 1.6 to 3.5 GeV. The torus current is set at $I = -3375$ A, that causes negatively charged particles to bend outwards.

6.3 Run conditions

We are planning to search for the hybrid states at low Q^2 and the accessible range of Q^2 depends on the beam energy and torus current. Another issue that affects the selection of the best run conditions is that we need good particle momentum resolution to be able to separate Λ and Σ^0 electroproduction channels and the best resolution is achieved with larger torus currents. The Λ and Σ^0 separation is based on using cuts on the reconstructed kaon missing mass. For this purpose the final kaon must be detected. Thus, we have to use the topologies where the final state electron, the kaon and at least one of the other hadrons (p or π^+) are detected.

The run condition studies were performed with a Fast Montecarlo. The results are shown in Figs. 30 and 31. and Table 2 summarizes the relevant information for different run conditions. As already mentioned in section 4.3, the best run conditions correspond to the large negative torus currents, as the maximal Λ and Σ^0 separation is achieved and the gap in the Q^2 coverage is small.

Table 2: Minimal achievable Q^2 (Q_{min}^2) and the percentage of the Λ and Σ^+ events that can be isolated from each other at different run conditions.

E_{beam} , GeV	Tor. current, A	Q_{min}^2 , GeV ²	Λ separation, %	Σ^0 separation, %
6.6	+1500	0.05	33	19
6.6	−1500	0.05	86	73
6.6	+3375	0.05	31	19
6.6	−3375	0.05	100	100
8.8	+1500	0.1	21	8
8.8	−1500	0.1	31	16
8.8	+3375	0.1	21	8
8.8	−3375	0.1	100	100

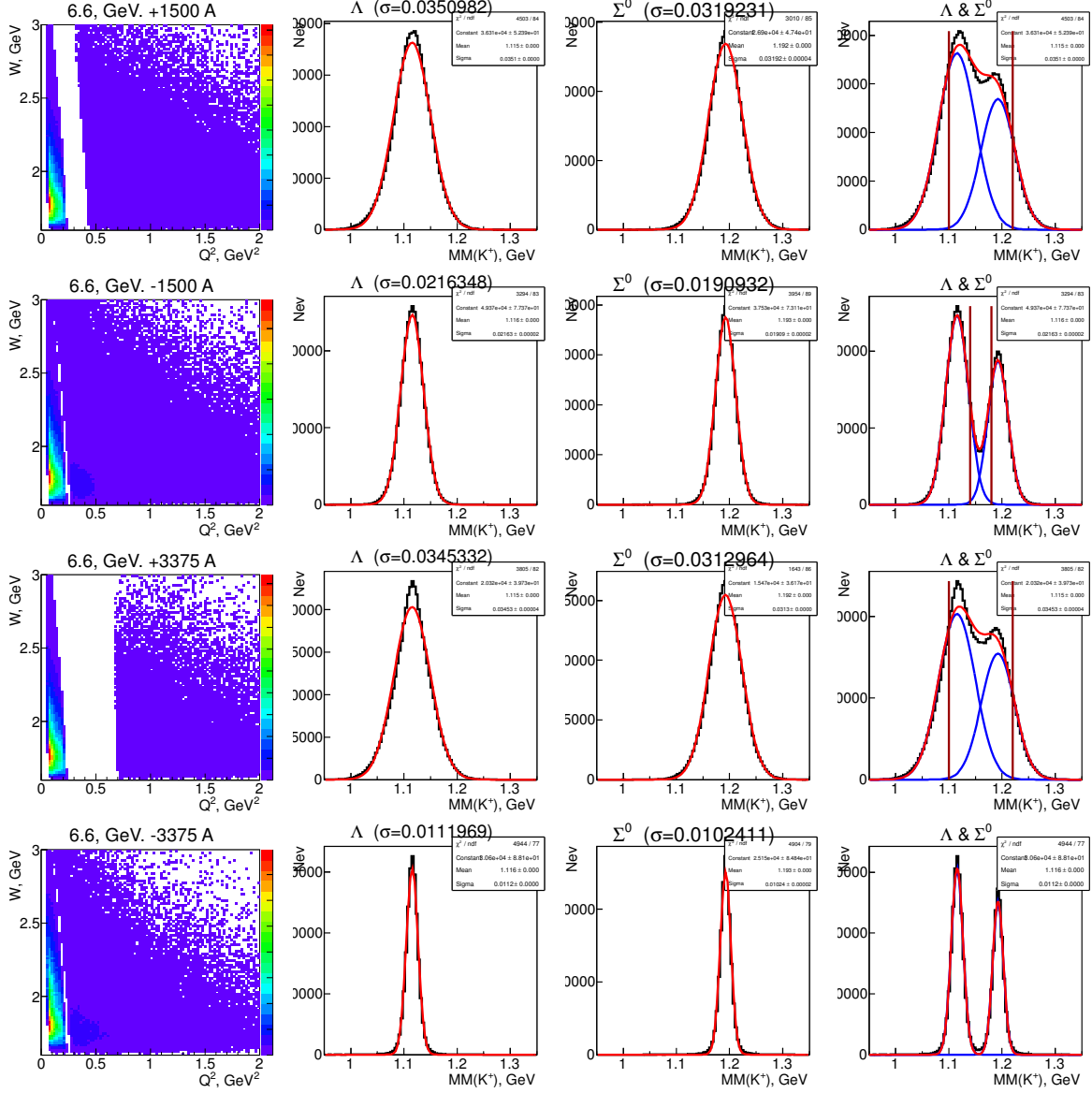


Figure 30: The left column shows the W versus Q^2 distributions at different torus currents for $Q^2 < 2 \text{ GeV}^2$ when the beam energy is 6.6 GeV. Next three columns show the distributions of the missing mass off K^+ for the corresponding torus current. The vertical lines indicate the cuts to be used to separate Λ or Σ^0 from its neighboring state. When no lines are drawn then Λ and Σ^0 are fully separated.

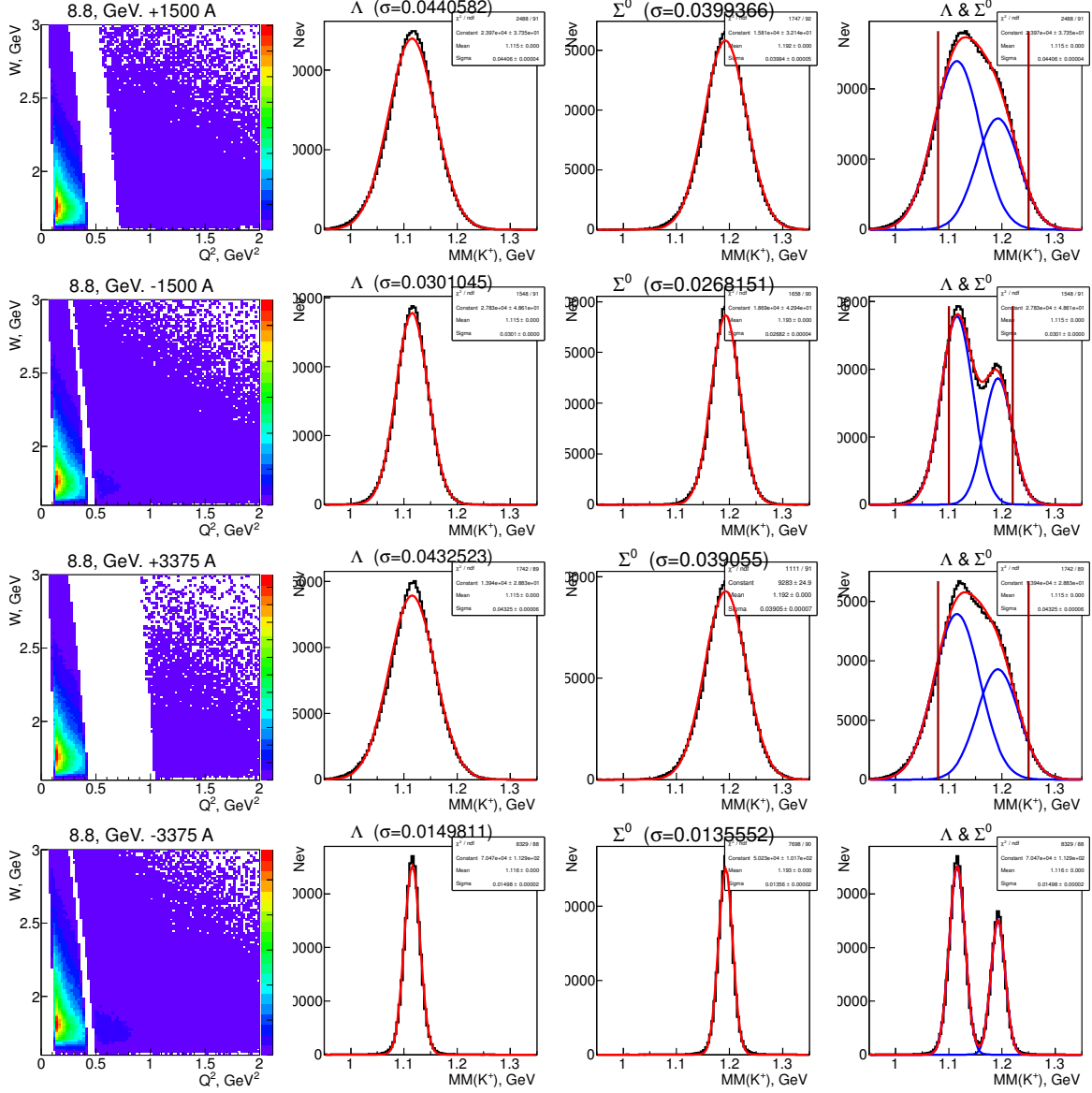


Figure 31: The left column shows the W versus Q^2 distributions at different torus currents for $Q^2 < 2 \text{ GeV}^2$ when the beam energy is 8.8 GeV. Next three columns show the distributions of the missing mass off K^+ for the corresponding torus current. The vertical lines indicate the cuts to be used to separate Λ or Σ^0 from its neighboring state. When no lines are drawn then Λ and Σ^0 are fully separated.

6.4 Count rates from $K^+\Lambda$

The expected total number of KY electroproduction events in the reaction $ep \rightarrow eK^+Y$ can be written as:

$$N = L \cdot t \cdot \int \frac{d^5\sigma}{dE_e d\Omega_e d\Omega_K^*} dE_e d\Omega_e d\Omega_K^*, \quad (9)$$

where

- $L = 1 \times 10^{35} \text{ cm}^{-2}\text{s}^{-1}$ is the expected CLAS12 operating luminosity
- t is the expected run time, and
- $\frac{d^5\sigma}{dE_e d\Omega_e d\Omega_K^*}$ is the cross section from (15) in detailed in Appendix A.

The event rate R is defined as $\frac{N}{t}$. The integration in (9) is performed over the whole kinematic space and it can be done numerically. We use the same model cross sections for $d^2\sigma/d\Omega_K^*$ as was used in the event generator (see section 6.1). The minimum achievable value of Q^2 in CLAS12 is determined by the forward hole, where high energy electrons cannot be detected. For all beam energies Q^2 is greater than 0.01 GeV^2 , so we can integrate equation (9) given that $Q^2 > 0.01 \text{ GeV}^2$. The calculated event production rates R_Λ and R_{Σ^0} are presented in Table 3.

Table 3: Estimated production rates for events with $Q^2 > 0.01 \text{ GeV}^2$.

$E_{beam}, \text{ GeV}$	$R_\Lambda, \text{ Hz}$	$R_{\Sigma^0}, \text{ Hz}$
6.6	1500	1200
8.8	1400	1100

To account for the acceptance of CLAS12 a detailed simulation is needed. As we need to generate events in the whole kinematic space with $Q^2 > 0.01 \text{ GeV}^2$, the ratio of reconstructed to generated events gives the averaged acceptance. Multiplying the event rates from Table 3 by that ratio we obtain the event rates which account for the acceptance.

An $ep \rightarrow e'K^+\Lambda \rightarrow e'K^+p\pi^-$ event is considered to be reconstructed if the electron and at least two hadrons have been detected. A trigger condition requiring at least two charged hadrons and an electron would select our channels of interest.

Accepted events rate calculations are presented in Table 4 for all possible beam energies and torus currents, taking into account a 64% rate reduction due to the $K\Lambda \rightarrow p\pi^-$ decay branching ratio. Currently FASTMC is used to estimate the acceptance. A full simulation and reconstruction will be carried out in the near future.

A rough estimate suggests that the KY exclusive channel contribution is about 1% with respect to the two and three pion production, which are expected to dominate the statistics of events that have an electron and at least two charged hadrons in the final state. The maximal total event rate is therefore expected to be $144 \times 100 / 0.64 = 24 \text{ kHz}$ for the trigger condition described above.

Table 4: Acceptance reduced event rates for the channel $ep \rightarrow eK^+\Lambda \rightarrow eK^+p\pi^-$. The scattered electron and two hadrons are required to be detected.

E_{beam} , GeV	Torr. cur, A	R_Λ , Hz
6.6	+1500	144
6.6	-1500	154
6.6	+3375	87 ?
6.6	-3375	72 ?
8.8	+1500	108
8.8	-1500	108
8.8	+3375	67 ?
8.8	-3375	52 ?

This estimate is compatible with the following considerations: suppose that the maximal inclusive event rate is 20 KHz, which is limited by the data acquisition. Then under the rough assumption that Λ event rate is about 1% with respect to the inclusive event rate, we can estimate the Λ event rate to be $\approx 200 \times 0.64 = 128$ Hz. This number is in a reasonable coincidence with the previously obtained value of 144 Hz.

Studies in the section 6.3 have shown that the preferable run conditions are achieved when using large negative torus currents, as Λ and Σ^0 can be fully separated.

The rate of the “separated” Λ or Σ^0 events when the beam energy is 6.6 GeV and the torus current is -1500 A is expected to be $144 \text{ Hz} \times 86\% \approx 124 \text{ Hz}$ (see section 6.3). When the beam energy is 6.6 GeV and the torus current is -3375 A the same rate is $72 \text{ Hz} \times 100\% \approx 70 \text{ Hz}$. However, we have to take into account: first the total event rate of 24 kHz may not be feasible due to the limitations of the data acquisition and secondly the momentum resolution may differ from what is predicted by fast MC, and in this case the percentage of the separated Λ or Σ^0 events may become smaller.

The obtained event rate should be reduced by 8%, as 8% of the events do not have reconstructed kaon. Assuming the Λ electroproduction rate at 6.6 (8.8) GeV electron energy is 70 Hz (50 Hz), we expect to collect in 30 days of the beam time $70 \text{ Hz} (50 \text{ Hz}) \times 92\% \times 30 \text{ days} \approx 1.7 \times 10^8 (1.2 \times 10^8)$ events.

6.5 Expected total event rates

At the very forward electron scattering angles, electron rates will be very high and may exceed the capabilities of the data acquisition system. Therefore additional constraints are needed to define an optimal trigger configuration which would enrich the sample with final state topologies as one might expect them from hybrid baryon candidates and reduce the total acquisition rate. For an initial program we therefore consider to trigger on hadronic final states with at least two charged particles. This will cover final states: $K^+\Lambda \rightarrow K^+p\pi^-$, $p\pi^+\pi^-$, $p\phi \rightarrow pK^+K^-$, $p\eta' \rightarrow p\pi^+\pi^-\eta$. For realistic rate estimates, projections of hadronic coupling strengths of hybrid baryons are needed, which are currently not available. In addition, a single charged hadron trigger will be incorporated with a pre-scaling factor for the FT, that will in parallel collect events with a single charged hadron in the final state,

i.e. π^+n , $p\pi^0$, $K^+\Lambda$, and $K^+\Lambda$, among others.

The operating luminosity of CLAS12 is estimated at $L = 10^{35} \text{ cm}^2\text{sec}^{-1}$. This corresponds to a production rate of 70 Hz (for $K^+\Lambda$) and about 50 Hz (for $K^+\Sigma^0$). For a 30 day run at that luminosity, the total number of $K^+\Lambda$ events is estimated to be 1.7×10^8 , and the number of $K^+\Sigma^0$ events to be 1.2×10^8 . The number of events in any histogram for certain smaller intervals of Q^2 and W can be found in the same way. The lowest event rate is expected for high Q^2 and high W . For the kinematics with lowest statistics, e.g. $2.0 \leq Q^2 \leq 2.5 \text{ GeV}^2$ and $2.675 \leq W \leq 2.700 \text{ GeV}$, a total number of 2.0×10^5 $K^+\Lambda$ events and 1.1×10^5 $K^+\Sigma^0$ events are expected.(to be checked)

While these rates seem very large, it should be kept in mind that the signals of hybrid baryons that we want to detect and quantify may be one or two orders of magnitude smaller than the signal from ordinary baryon states and will likely not simply be seen as a peak in the excitation spectrum, but rather as a broad region in W where specific quantum numbers, i.e. $I = \frac{1}{2}$ and $J^P = \frac{1}{2}^+$ or $J^P = \frac{3}{2}^+$, must be identified and the electromagnetic couplings must be measured versus Q^2 . This can be achieved in a partial-wave analysis that includes other channels in a multichannel fit, such as the Bonn-Gatchina or Jülich/GWU approaches. Other techniques may also be employed. Very high statistics is thus essential, and the transverse and longitudinal photon polarization that is inherent in electron scattering will provide amplitude interference and enhance the resonant signal.

7 Data Analysis and quasi data

7.1 Event selection

Electrons will be detected both in the Forward Tagger and in the CLAS12 Forward Detector (FD). Electrons measured in the FD can be identified at scattering angles above 6° in the High-Threshold Cherenkov counter (HTCC) and in the PCAL and EC calorimeters. Due to the higher Q^2 for electrons detected at larger scattering angles in CLAS12 compared to the FT region, the FD electron rate is comparatively much lower than the hadronic rate, which ensures good electron identification.

For electrons detected in the FT, the low Q^2 leads to a very high electron rate that completely dominates the event rate in the FT calorimeter and hodoscope. A direct electron identification at the trigger level is therefore not needed. However the complete event pattern may be checked for consistency with that hypothesis in the event reconstruction. Note that the full electron kinematics is measured in the FT calorimeter and the micromegas tracker and charged particle ID is provided by the two layer hodoscope in front of the calorimeter as well as with hits in the micromegas tracker.

Charged hadrons (π^\pm , K^\pm , and protons) will be tracked in the drift chambers and micromegas in the FD, and in the silicon tracker and barrel micromegas at large angles in the CD. At all angles, charged particle identification is provided in the CLAS12 time-of-flight detector systems. Photons and neutrons are detected at forward angles in the electromagnetic calorimeters (PCAL, EC, FT) and neutrons at large angles are detected in the Central Neutron Detector (CDN).

7.2 Event reconstruction

The event reconstruction software has been designed and developed to be deployed within the ClaRA framework, a Service Oriented Architecture framework for data processing. The reconstruction application consists of a chain of services which can be deployed within ClaRA. The services for each detector component are compiled as java archive (JAR) plugins which are included in the complete CLAS12 Software release package coatjava. The CLAS12 reconstruction software reconstructs, on an event-by-event basis, the raw data coming from either simulation or the detectors to provide physics analysis output such as track parameters and particle identification. The package provides scripts that can be launched on the farm to cook the data as well as a framework to do event analysis using the flexible scripting language Groovy. The documentation for the coatjava package can be available on the CLAS12 webpage: <http://clasweb.jlab.org/clas12offline/docs/software/html/>. For acceptance and efficiency studies, events are generated using the Geant-4 Monte Carlo simulation application GEMC. A detailed documentation of the detectors included in the simulation and of the various settings used to set the simulation parameters according to physics, backgrounds and magnetic field configurations is available from the gemc webpage: <https://gemc.jlab.org/gemc/Documentation/Documentation.html>. An example of a simulated event for the reaction $ep \rightarrow e'K\Lambda$ is shown in Fig. 32.

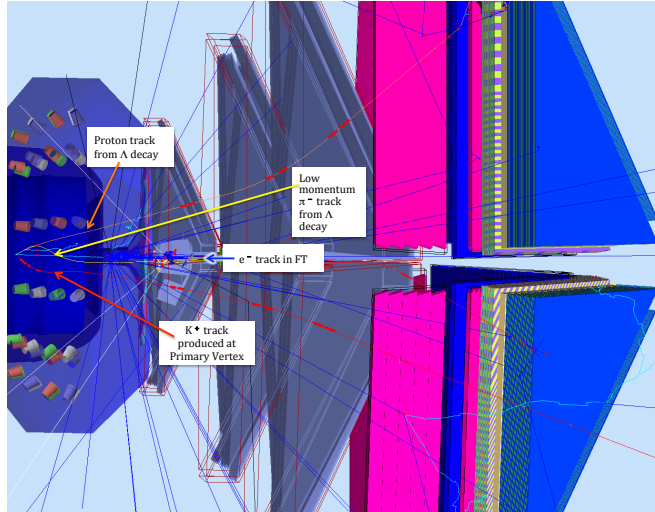
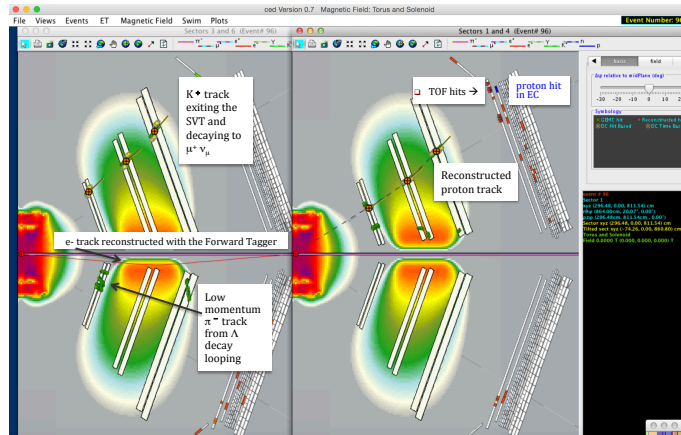


Figure 32: GEMC - Graphical User Interface Display of $ep \rightarrow eK^+\Lambda$ ($\Lambda \rightarrow p\pi^-$) event as seen in CLAS12 detectors.



The e- and proton tracks from the reaction $e p \rightarrow e' K^+ \Lambda$, $\Lambda \rightarrow p \pi^-$ reconstructed in the Forward Detectors

- The filled orange circles correspond to reconstructed 3-D points obtained from pattern recognition; the tangent to the reconstructed track at the 3-D point is represented by the line segment connected to the filled circle.
- The dashed line corresponds to tracks swam to $z = 0$ with the parameters extracted from the reconstruction algorithm

Figure 33: Event display for the reaction $ep \rightarrow e' K^+ \Lambda$.

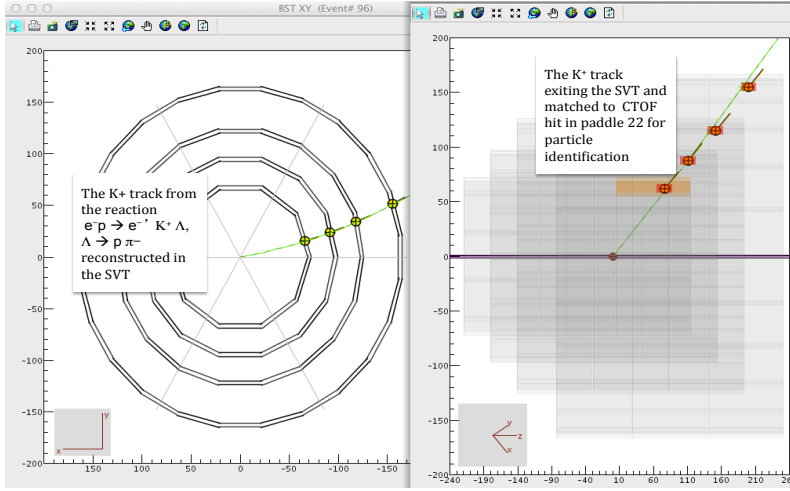


Figure 34: Event display for the reaction $ep \rightarrow e'K\Lambda$.

At present, the reconstruction software is still in development. The components that are available are the Silicon Vertex Tracker (SVT), the Central Time of Flight (CTOF), the High Threshold Cherenkov Counter (HTCC), the Drift Chambers (DC), the Forward Time-Of-Flight (FTOF), the Electromagnetic and Pre-shower Calorimeters (EC/PCAL), and the Forward Tagger Calorimeter and Hodoscope. A preliminary version for the Forward MicroMegas Tracker reconstruction is also available and is used to refit the track parameters coming from the DC.

An example of an event for the reaction $ep \rightarrow e'K\Lambda$ run through the reconstruction and displayed using the CLAS12 event display CED is shown in Figs. 33 and 34. An overall Event Builder takes the track momentum and flight path information obtained from Central and Forward tracking and links the track to the outer detector to obtain the responses and determine the PID. The electron is mostly identified by the Forward Tagger for the kinematics of the Hybrid Baryon Proposal.

The studies for this letter of intent were done using FastMC. For the Proposal these studies will be repeated by generating events with the event generators described in section IV, tracking all particles through CLAS12 with GEMC and subsequently reconstructing these events with coatjava and obtaining the analysis selection criteria using the kinematic fitter available with the package.

An example of a reconstructed Λ mass spectrum obtained from the missing mass against the eK^+ in the reaction $ep \rightarrow e'K^+\Lambda$ generated with GEMC is shown in Fig. 35. The reconstruction uses only the electron detected in the Forward Tagger calorimeter and the produced K^+ . Improved mass resolution is obtained when the Λ is reconstructed from the invariant mass of the proton and the π^- .

7.3 Extracting differential cross sections and normalized yields

After the raw data have been subjected to the CLAS12 event reconstruction software package CLARA, we intend to extract differential cross section for all processes with two-body final

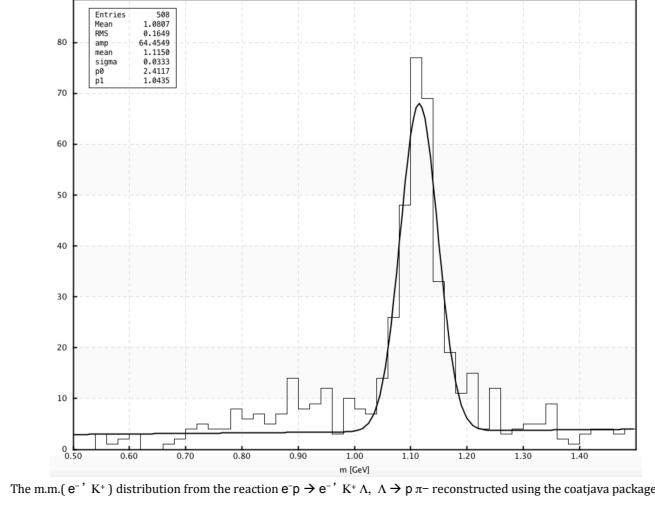


Figure 35: Reconstructed Λ mass distribution obtained from the recoil mass against the e' and K^+ for the reaction $ep \rightarrow e'K^+\Lambda$ at a beam energy of 6.6 GeV. This figure is obtained using the coatjava plotting package (under development).

states, e.g. KY , $N\pi$, $p\eta$, $p\eta'$, and $p\phi$ using simulations of large amounts of Monte Carlo events to fully understand the acceptances for these processes at the accuracy level required for the partial wave analysis. As for all electroproduction data, the raw cross sections will be subjected to radiative corrections in order to extract the fully corrected differential cross sections. The radiative correction procedure for exclusive processes is well established, and it has been used for correcting single π^+n and $p\pi^0$ production as well as $K^+\Lambda$ and $K^+\Sigma$ electroproduction employing the exact procedure developed in Ref. [59]. As it has been recently demonstrated [60], radiative corrections are very important for the analysis of exclusive processes in terms of resonance excitations as they affect both the polar and azimuthal angular dependencies, and consequently the partial wave analyses based on these processes.

For three-body final states, such as $p\pi^+\pi^-$ and $p\eta\pi^0$, in addition to extracting differential and integrated cross section, we also we consider event-based analysis techniques, where acceptances will be assigned to each event, and acceptance weighted events will be subjected to a maximum-likelihood fitting procedure. This procedures preserves the full correlations among the final state particles. **more on how to separate the different cross sections components: σ_U , σ_{LT} and σ_{TT}**

7.4 Partial wave analysis

Using modern partial wave analysis tools several new excited N^* and Δ^* states have been identified or have been significantly improved in their evidence and their star rating in the 2014 edition of the Review of Particle Properties (RPP) of the Particle Data Group [1]. The use of high statistics photoproduction data from CLAS of a number of final states, e.g. $K^+\Lambda$, $K^+\Sigma$, π^+n , $p\pi^0$, including polarization observables, was essential in establishing this

new evidence. This success has also shown the importance of high statistics data sets in the search for new excited states, and has helped to re-vitalize the field of hadron spectroscopy. In the analysis of the data to be taken with the program discussed in this letter-of-intent, we will make full use of these advanced tools of amplitude and partial wave analysis. Significant progress has also been made in the analysis of electroproduction data where transition form factors have been extracted from several excited states using the high statistics data from CLAS [2, 6, 60]. We expect that these data analysis packages will be well-honed by the time the proposed data will be taken, including the extension of the photoproduction analysis to include the existing and planned electroproduction data sets.

7.5 Analysis of quasi-data to determine CLAS12 sensitivity to minimum detectable resonance elctrocoupling

...

7.6 Threshold values of statitically distinguishable hybrid baryon couplings in $\pi^+\pi^-p$ final state

To estimate threshold values of hybrid state couplings that are distinguishable in data analysis, a phenomenological JM15 [8] model was used. A resonance state with mass 2.2 GeV, width 200 MeV, and $J=\frac{1}{2}$ was introduced into the model, in addition to the preliminary established contributions from known resonant states as well as non-resonant mechanisms, in the region of W from 2.1 to 2.3 GeV and for three Q^2 points (quasi real $Q^2 \approx 0, 0.65, 1.3 \text{ GeV}^2$).

The statistical significance of hybrid signal was studied at different values of $A_{1/2}$ electrocoupling using a χ^2 criterion. The χ^2 was determined by the following formula (10).

$$\chi^2 = \frac{1}{N_{d.p.}} \sum_{W_i} \sum_{\substack{X=m_{\pi^+\pi^-}, m_{\pi^+p}, \\ \theta_{\pi^-}, \alpha_{\pi^-}}} \left(\frac{\left(\frac{d\sigma_{nohyb}}{dX} - \frac{d\sigma_{hyb}}{dX} \right)^2}{\left(\varepsilon_{nohyb} \frac{d\sigma_{nohyb}}{dX} \right)^2 + \left(\varepsilon_{hyb} \frac{d\sigma_{hyb}}{dX} \right)^2} \right) \quad (10)$$

where $m_{\pi^+\pi^-}$, m_{π^+p} , θ_{π^-} and α_{π^-} are the variables that describe the final hadron state. $\frac{d\sigma_{nohyb}}{dX}$ is the single-fold differential cross section with hybrid $A_{1/2} = 0$. $\frac{d\sigma_{nohyb}}{dX}$ is the same cross section with $A_{1/2}$ equal to a certain variable value. ε_{nohyb} and ε_{hyb} are the relative statistical uncertainties of single-fold differential cross sections for the cases when hybrid signal is switched off and on, respectively. The sums run over all points (from 1 to $N_{d.p.}$) of single-fold differential cross sections for all W bins from 2.1 to 2.3 GeV.

The statistical uncertainty of single-fold differential cross section with hybrid state was chosen to be the following: 3% at $Q^2 = 1.3 \text{ GeV}^2$, 2% at $Q^2 = 0.65 \text{ GeV}^2$, 1% at $Q^2 = 0 \text{ GeV}^2$. This choice was made, based on the expected reaction yield, roughly estimated in comparison with previous CLAS experiment [51]. Taking into account that the expected DAQ rate in CLAS12 experiments is going to be about ten times higher than in CLAS experiments, run duration is planned to be about two times longer, while the 2π efficiency is expected to be larger by one order of magnitude.

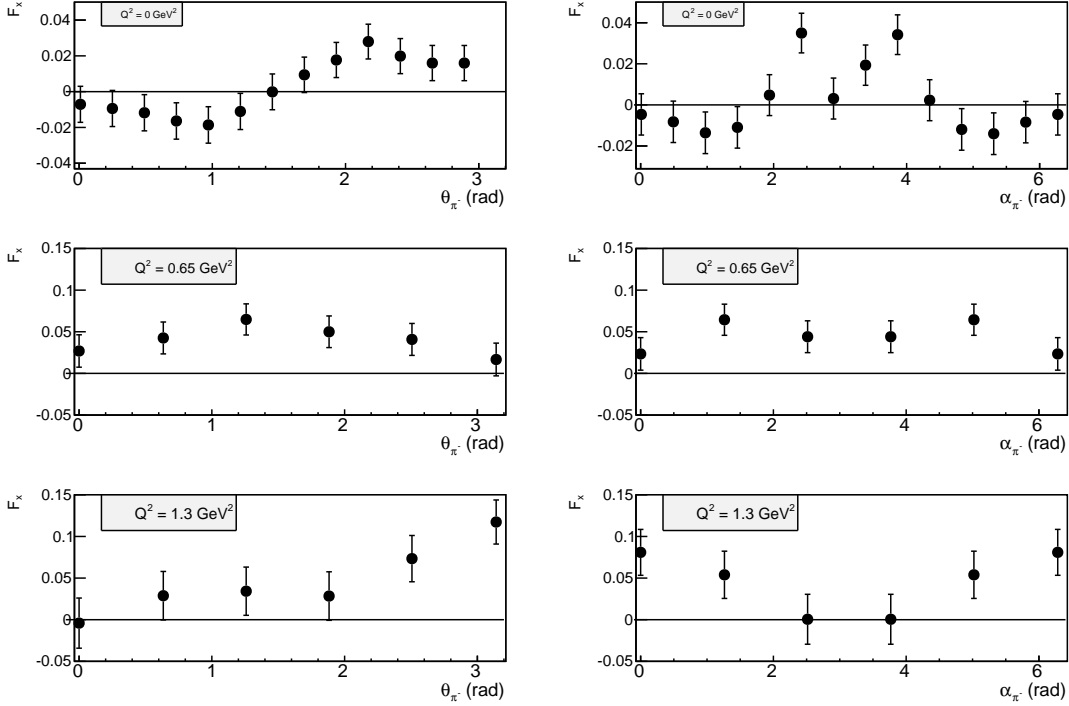


Figure 36: Relative difference between 2π cross sections with and without hybrid state as a function of angles of final hadrons, for three Q^2 points.

Q^2 (GeV)	0.	0.65	1.3
$A_{1/2} \times 10^{-3}$ (GeV $^{-1/2}$)	45	37	19

Table 5: Threshold values of $A_{1/2}$ couplings for statistically distinguishable hybrid state signal.

It needs to be mentioned that the aforementioned uncertainty estimation is rather conservative, in the sense that it assumes that just electron trigger will be used. If two or three charged particles trigger will be used a significant increase of 2π events rate is expected and making the statistical uncertainties negligible. Since the KY channel cross section is only few percent of the 2π cross section, run conditions and trigger choice needs to be determined according to KY channel needs.

The statistical uncertainty for the single-fold differential cross section without hybrid state (ε_{nohyb}) was assumed to be zero, since in model analysis of real data only experimental data points have errors, while the model cross section is fitted to the data.

The hybrid signal was considered to be statistically significant if $\chi^2 > 4$. Threshold values of $A_{1/2}$ electrocoupling for statistically significant hybrid state signal are summarized in the Tabl. 5. Obtained threshold values of $A_{1/2}$ electrocoupling for hybrid state do not exceed the electrocouplings values of most of the known resonances in this kinematical region, that makes our estimation very encouraging for the search of new states. If we assume that two or three charged particles trigger is in use, the threshold values of electrocouplings are going to be even lower.

The hybrid signal manifests itself mostly in the cross section angular distributions. In

Fig. 36 the relative difference of 2π cross section with and without hybrid state are plotted as functions of θ_{π^-} and α_{π^-} angles for three Q^2 bins. Distributions in Fig. 36 are produced for the threshold values of $A_{1/2}$ electrocouplings listed in Tabl. 5. As it is seen from the plots in Fig. 36, this difference grows as Q^2 increases, that corresponds to the fact that relative contribution of resonant part to the total 2π cross section increases with Q^2 .

7.7 Threshold values of statistically distinguishable hybrid baryons electrocouplings from $K\Lambda$ final state

In order to quantify the statistical significance of the difference between the exclusive KY event distributions over the θ_K , ϕ_K CMS angles, simulated according to the models A and B, as described in paragraph 3.4, the following χ^2 definition has been used:

$$\chi^2 = \frac{1}{N_{d.p.}} \sum_{W, \cos(\theta_K), \phi_K} \frac{\left(\frac{d^2\sigma_A}{d\Omega_K} - \frac{d^2\sigma_B}{d\Omega_K} \right)^2}{\delta^2}, \quad (11)$$

where $\frac{d^2\sigma_A}{d\Omega_K}$ and $\frac{d^2\sigma_B}{d\Omega_K}$ are the cross sections simulated in the models A and B, respectively.

The χ^2 is evaluated in each Q^2 bin independently and we choose a 0.1 GeV² bin width in Q^2 . The sum over W in (11) runs from $M_R - \Gamma_R/2$ to $M_R + \Gamma_R/2$ and the bin width in W is 20 MeV. We used 24 bins in $\cos(\theta_K)$ and ϕ_K . Assuming that the statistical uncertainties dominate, the uncertainties for the differences $\left(\frac{d^2\sigma_A}{d\Omega_K} - \frac{d^2\sigma_B}{d\Omega_K} \right)$ between the event distributions simulated in the models B and A, respectively, can be evaluated as:

$$\delta^2 = \left(\frac{\frac{d^2\sigma_A}{d\Omega_K}}{\sqrt{N_A}} \right)^2 + \left(\frac{\frac{d^2\sigma_B}{d\Omega_K}}{\sqrt{N_B}} \right)^2, \quad (12)$$

where N_A and N_B are the number of events in three dimensional bins in W and Ω_K for the two models.

The number of events in the mentioned above three dimensional bins for a given Q^2 bin can be calculated knowing the expected total number of events in the whole covered kinematic space. The number of events in each multidimensional bin is proportional to the cross section in that bin, taking acceptance into account. The cross section $\frac{d^2\sigma}{d\Omega_K}$ are obtained by integrating over the other kinematic variables: final state electron azimuthal angle ϕ_e and spherical angles of one of the Λ decay product particles, say proton, θ_p , ϕ_p , assuming that the cross section $\frac{d^5\sigma}{d\Omega_K d\phi_e d\theta_p d\phi_p}$ does not depend on ϕ_e , θ_p and ϕ_p . Then the number of events (N) in every four dimensional bin is

$$N(Q^2, W, \theta_K, \phi_K) = C \int_{\phi_e, \theta_p, \phi_p} a \times \frac{d^5\sigma}{d\theta_K d\phi_K d\phi_e d\theta_p d\phi_p} = C \int_{\phi_e, \theta_p, \phi_p} a \times \frac{d^2\sigma}{d\Omega_K} \approx C \sum_{\phi_e, \theta_p, \phi_p} a \times \frac{d^2\sigma}{d\Omega_K}, \quad (13)$$

where a is the CLAS12 acceptance, which depends on all kinematic variables and C is a constant. Set the sum of all $N(Q^2, W, \theta_K, \phi_K)$ equal to the expected total number of events in the whole kinematic covered space we find the constant C .

The number of evens in each multidifferential bin was calculated assuming the total number of $K\Lambda$ events to be collected in the experiment is 2×10^8 (see section 6.4).

The typical number of events in one bin of the single differential distribution $\frac{d\sigma}{d\cos(\theta_K)}$ is about few thousands and the statistical errors are negligible, while in two fold differential distribution $\frac{d^2\sigma}{d\Omega_K}$ statistical errors are meaning. This can be seen in Figs. 37 through 40

We define the the minimal value of the photocoupling such as it is the minimal value of the photocoupling when the χ^2 from (11) characterizing the difference between two cross sections is more than 4. The minimal values of A_{12} , A_{32} and S_{12} found in this way are presented in Tables 6 and 7. The mass of the hybrid state was 2.2 GeV and the total width was 0.250 GeV. The Q^2 bin width was 0.1 GeV².

Table 6: The minimal values of the photocouplings for the beam energy 6.6 GeV and the torus current -2950 A for the resonances with the spin (J_R) 1/2 and 3/2. A_{12} , A_{32} and S_{12} are in the units of $10^{-3} \times \text{GeV}^{-1/2}$. When determining the minimal value of A_{12} we varied only A_{12} setting the other photocouplings to zero. The minimal values of A_{32} and S_{12} were obtained in the same way.

Q^2 , GeV ²	$J_R=1/2$		$J_R=3/2$		
	A_{12}	S_{12}	A_{12}	A_{32}	S_{12}
0.1	12	12	16	11	10
0.5	17	19	18	19	12
1.0	16	21	16	18	10

Table 7: The minimal values of the photocouplings for the beam energy 8.8 GeV and the torus current -2950 A for the resonances with the spin (J_R) 1/2 and 3/2. A_{12} , A_{32} and S_{12} are in the units of $10^{-3} \times \text{GeV}^{-1/2}$. When determining the minimal value of A_{12} we varied only A_{12} setting the other photocouplings to zero. The minimal values of A_{32} and S_{12} were obtained in the same way.

Q^2 , GeV ²	$J_R=1/2$		$J_R=3/2$		
	A_{12}	S_{12}	A_{12}	A_{32}	S_{12}
0.3	12	12	14	12	9
0.5	19	20	19	21	12
1.0	16	21	16	18	9

It was found that the minimal photocoupling values are weakly dependent on the run conditions and Q^2 . The weak dependence on Q^2 can be explained. The resonance manifestation is more pronounced at small Q^2 , as the non-resonant background is smaller, on the other hand statistical errors are larger (the same Q^2 bin width (0.1 GeV²) is used at all

Q^2) and the sensitivity to the resonance gets smaller. These two factor works in opposite direction and the χ^2 does not change significantly.

Figs. 37 through 40 present examples of the comparison of the model to the model plus resonance one- and two fold differential cross sections. The model plus resonance cross section was calculated when the photocoupling was set to its minimal value from the Table 7.

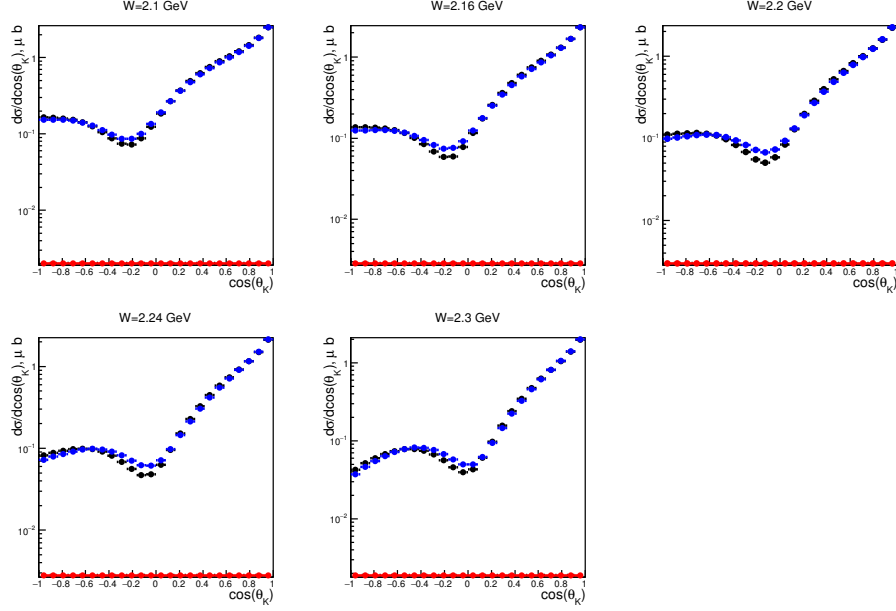


Figure 37: Comparison of the model cross section $d\sigma/d\cos(\theta_K)$ (black points) with the model plus resonance cross section (blue points) for the beam energy 8.8 GeV and the torus current -2950 A at $Q^2=0.3$ GeV² and at few values of W . The cross section of the resonance contribution is shown in red. The spin of the resonance is 1/2 and the A_{12} is $12 \times 10^{-3} \text{ GeV}^{-1/2}$, it corresponds to the minimal A_{12} from the table 7. Statistical errors are negligible.

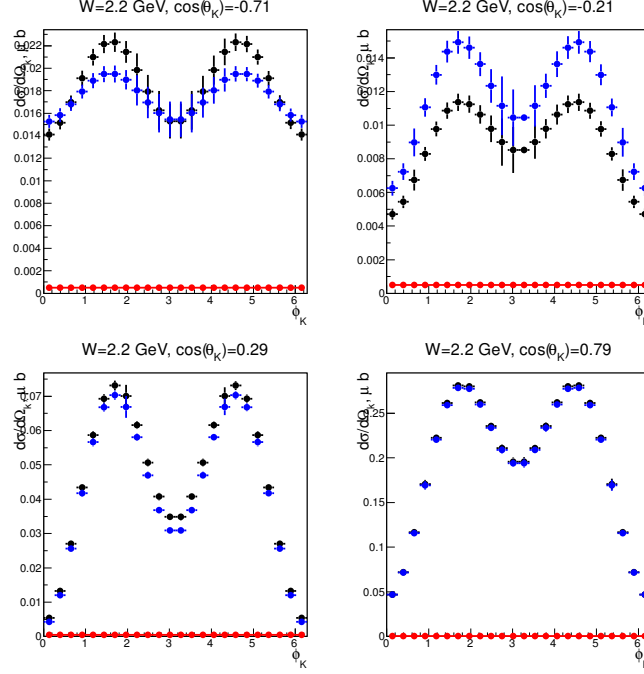


Figure 38: Comparison of the model cross section $d\sigma/d\Omega(\theta_K)$ with the model plus resonance cross section at $W = M_R$ and few values of $\cos(\theta_K)$. The same conditions run condition and Q^2 as in Fig. 37. The errors are statistical only.

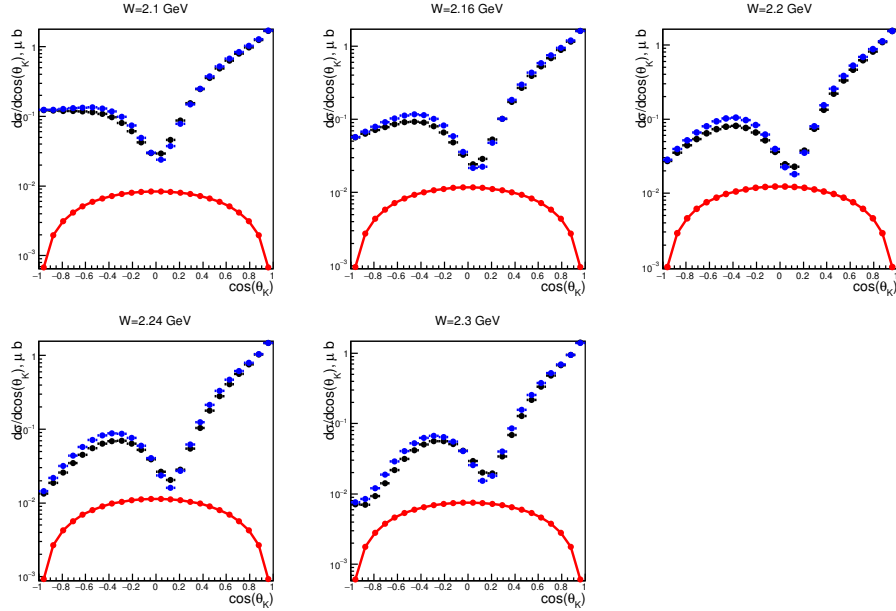


Figure 39: Comparison of the model cross section $d\sigma/d\cos(\theta_K)$ (black points) with the model plus resonance cross section (blue points) for the beam energy 8.8 GeV and the torus current -2950 A at $Q^2=0.3 \text{ GeV}^2$ and at few values of W . The cross section of the resonance contribution is shown in red. The spin of the resonance is $3/2$ and the A_{32} is $18 \times 10^{-3} \text{ GeV}^{-1/2}$, it corresponds to the minimal A_{32} from the table 7. Statistical errors are negligible.

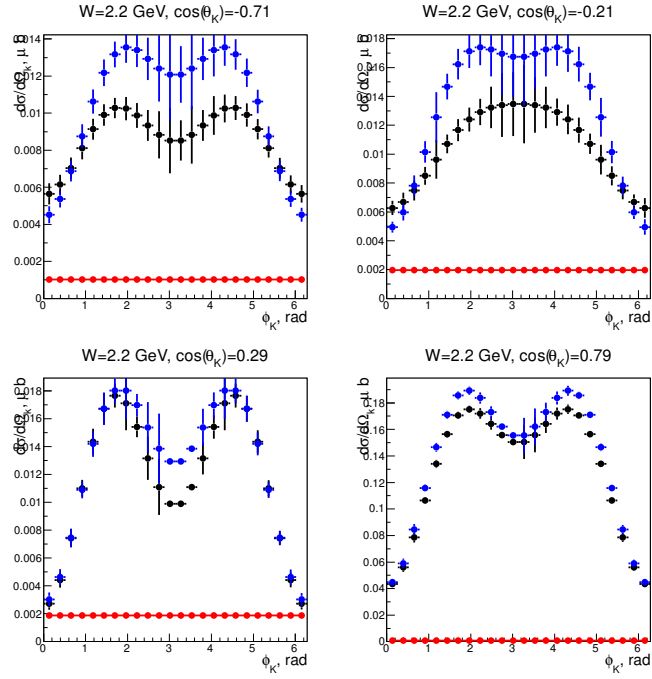


Figure 40: Comparison of the model cross section $d\sigma/d\Omega(\theta_K)$ with the model plus resonance cross section at $W = M_R$ and few values of $\cos(\theta_K)$. The same conditions run condition and Q^2 as in Fig. 39. The errors are statistical.

7.8 Experimental sensitivity to hybrid resonance states in $\pi + \pi^- p$ and KY final states

The ability of JM model to distinguish hybrid state signal is also illustrated in Fig. 41, where the χ^2 value is plotted as a function of the resonance mass for Q^2 points. The dip in χ^2 dependences is clearly seen on the W_h value corresponding to the expected mass of the hybrid state.

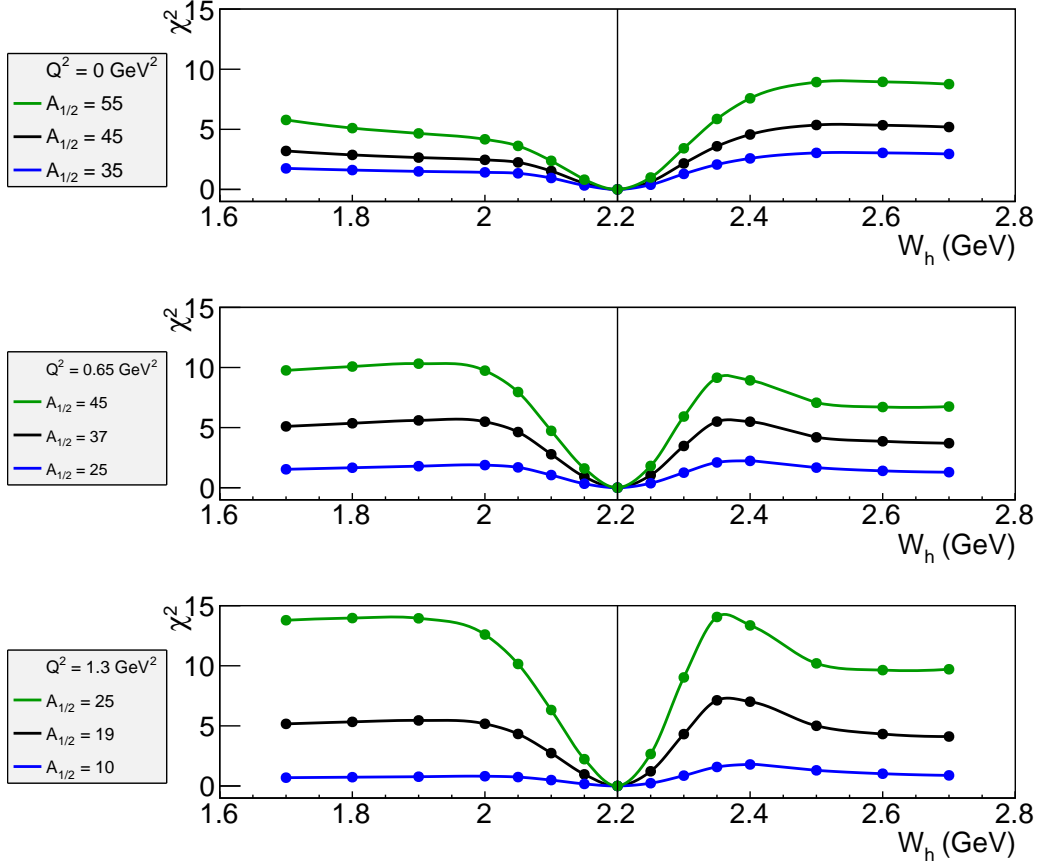


Figure 41: χ^2 versus W_h distributions for three Q^2 values obtained from JM model.

8 Beamtime estimate

The complete hybrid baryon program will require 2 beam energies, 6.6 GeV, 8.8 GeV to cover with high statistics the lowest Q^2 range where the scattered electron is detected in the angle range from $2.5^\circ \leq \theta_e \leq 4.5^\circ$. We request new beam time of 60 days that are divided into 30 days at 6.6 GeV and 30 days at 8.8 GeV.

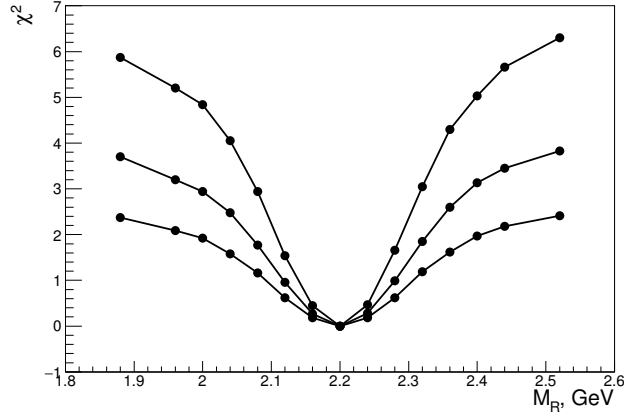


Figure 42: The χ^2 between two model cross sections. One cross section was calculated with the hybrid mass equal to 2.2 GeV. The other cross section was calculated with the variable hybrid mass (M_R). The χ^2 square was calculated as described in section ?? using the estimated statistical errors. Three lines from bottom to top correspond to the three values of A_{12} : 15, 19 and 25 in the units of $10^{-3} \text{ GeV}^{-1/2}$. The value 19 is the minimal A_{12} from the table 7 for the spin 1/2 resonance at $Q^2=0.5 \text{ GeV}^2$. Run condition are as in the same table.

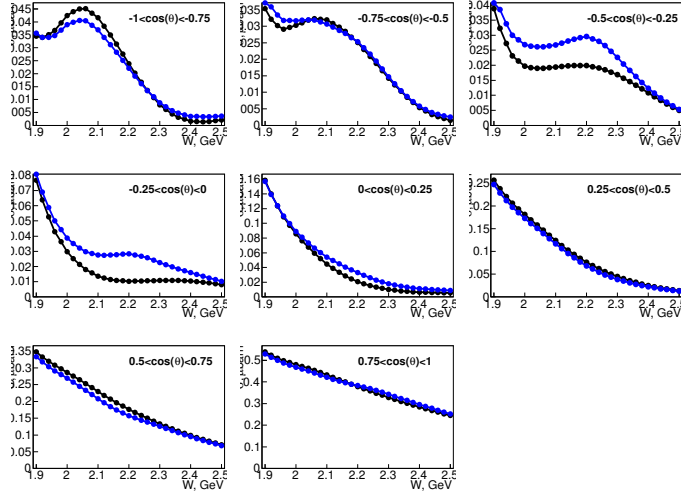


Figure 43: The integrated model cross section (in black) and model plus resonance ($A_{12}=40 \times 10^{-3} \text{ GeV}^{-1/2}$) cross section (in blue) at different $\cos(\theta_K)$ bins and at $Q^2=0.5 \text{ GeV}^2$. The pronounced structures at small $\cos(\theta_K)$ can be indications of a resonance.

9 Summary

In this Proposal we laid out an extensive program to study the excitation of nucleon resonances in meson electroproduction using electron beam energies of 6.6 and 8.8 GeV. The main focus is on the search for gluonic light-quark baryons in the mass range up to 3.0 GeV and in the Q^2 range from 0.05 to 2.0 GeV^2 . We have estimated the rates for two of the

channels we propose to study, $K^+\Lambda$ ($K^+\Sigma$) and $p\pi^+\pi^-$, but all other channels detected in CLAS12 will be subjected to analyses as well. The expected rates are very high, thanks to the very forward scattered electrons with a minimum Q^2 of 0.05 GeV² that are detected in the Forward Tagger. The data will be subjected to state-of-the-art partial wave analyses that were developed during the past years for baryon resonance analyses. Beyond the main focus of this Proposal on hybrid baryons, a wealth of data will be collected in many different channels that will put meson electroproduction data on par with real photoproduction in terms of production rates and will allow for a vast extension of the ongoing N^* electroexcitation program with CLAS at lower energies. It will complement the already approved program to study nucleon resonance excitations at the highest Q^2 achievable at 11 GeV beam energy, by the experiment E12-11-005.

A Appendix A - KY electroproduction

In the electroproduction of KY on the proton a beam of incoming electrons of energy E_e impinges on a fixed proton target of mass M_p , the scattered electrons emerging with energy $E_{e'}$ are detected at the the direction identified by the angles $(\theta_{e'}, \phi_{e'})$ and the kaons produced with momentum $\tilde{p}_k = (E_k, \vec{p}_k)$ are measured. The cross section is five-fold differential in the in the scattered electron energy and direction $dE_{e'}d\Omega_{e'}$ and kaon direction $d\Omega_K$. In the single photon exchange approximation, a virtual photon of momentum $\tilde{q} = \tilde{p}_e - \tilde{p}_{e'} = (\nu, \vec{q})$, is emitted by the scattered electron and absorbed by the proton. The cross section can be expressed by the product of an equivalent flux of virtual photons Γ and the virtual photo-production of the KY final state as:

$$\frac{d^5\sigma}{dE_{e'}d\Omega_{e'}d\Omega_K} = \Gamma \frac{d^2\sigma}{d\Omega_K^*} \quad (14)$$

where the virtual photoabsorbption cross section is expressed γ^*p or KY CM reference frame and the the photon flux Γ is given by the relation:

$$\Gamma = \frac{\alpha}{2\pi^2} \frac{E_{e'}}{E_e} \frac{W^2 - m_p^2}{Q^2} \frac{1}{1 - \epsilon} \quad (15)$$

and it depends on the electron scattering process only, in terms of the variables $Q^2 = -\tilde{q}^2$, the photon virtuality, $W = \sqrt{M_p^2 + 2M_p\nu - Q^2}$, the total energy in the γ^*p CM reference frame and the virtual photon polarization ϵ :

$$\epsilon = \frac{4E_e E_{e'} - Q^2}{2(E_e^2 + E_{e'}^2) + Q^2}. \quad (16)$$

The kinematic of the process is shown in Figure 44.

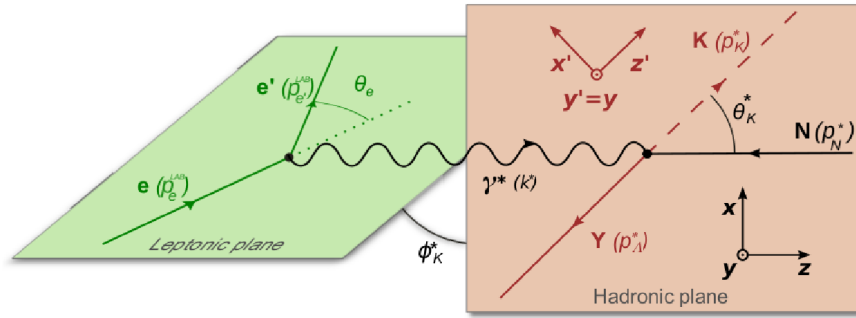


Figure 44: Kinematics of the KY photoproduction. The quantities in the leptonic plane are expressed in the laboratory frame. The quantities in the hadronic plane are expressed in the center of mass of the γ^*p or KY system.

After integrating after the azimuthal angle of the scattered electron, the photoabsorbption cross section can be expressed in terms of the variables Q^2 , W and the kaon scattering

angles in the KY CMS θ_k^* and ϕ_k . Introducing the appropriate Jacobian, the form of the cross section may be rewritten as:

$$\frac{d^4\sigma}{2\pi dW dQ^2 d\Omega_k^*} = \Gamma_v \frac{d^2\sigma_v}{d\Omega_k^*} \quad (17)$$

where

$$\Gamma_v = \frac{\alpha}{4\pi} \frac{W}{E^2} \frac{W^2 - m_P^2}{Q^2(1 - \epsilon)} \frac{1}{m_P^2} \quad (18)$$

is the corresponding flux of virtual photons.

For the case of an unpolarized electron beam, with no target or recoil polarizations, the virtual photon absorbtion cross section can be written as:

$$\frac{d^2\sigma}{d\Omega_k^*} = \frac{d^2\sigma_T}{d\Omega_k^*} + \epsilon_L \frac{d^2\sigma_L}{d\Omega_k^*} + \epsilon_T \frac{d^2\sigma_{TT}}{d\Omega_k^*} \cos 2\phi_K + \sqrt{2\epsilon_L(1 + \epsilon_T)} \frac{d^2\sigma_{TL}}{d\Omega_k^*} \cos \phi_K. \quad (19)$$

where the $\frac{d^2\sigma_i}{d\Omega_k^*}$ are the structure functions that measure the response of the hadronic system. $i = T, L, TT$ and LT represent the transverse, longitudinal and interference structure functions and depend on the variables W, Q^2 and θ_k^* only.

In the formalism used in the Gent model [9] the cross section may be related to the reaction amplitude:

$$M_{\lambda_\gamma}^{\lambda_p \lambda_f} = \langle \lambda_f | T_r | \lambda_\gamma \lambda_p \rangle \quad (20)$$

in term of the nine helicity dependent bilinear functions:

$$H_{\lambda\lambda'} = \sum_{\lambda_N \lambda_Y} M_{\lambda}^{\lambda_N \lambda_Y} (M_{\lambda'}^{\lambda_N \lambda_Y})^\dagger \quad (21)$$

where λ and λ' assume all possible values of the virtual photon helicity, $0, \pm 1$.

The transverse, longitudinal and interference structure functions are defined as:

$$\begin{aligned} \frac{d^2\sigma_L}{d\Omega_K^*} &= 2\chi \frac{1}{(4\pi)^2} H_{0,0} \\ \frac{d^2\sigma_T}{d\Omega_K^*} &= \chi \frac{1}{(4\pi)^2} (H_{1,1} + H_{-1,-1}) \\ \frac{d^2\sigma_{TT}}{d\Omega_K^*} &= -\chi \frac{1}{(4\pi)^2} (H_{1,-1} + H_{-1,1}) \\ \frac{d^2\sigma_{LT}}{d\Omega_K^*} &= -\chi \frac{1}{(4\pi)^2} (H_{0,1} + H_{1,0} - H_{-1,0} - H_{0,-1}) \end{aligned} \quad (22)$$

where the normalization factor χ assumes the form:

$$\chi = \frac{1}{16W m_P} \frac{\sqrt{W^4 + (m_K^2 - m_\Lambda^2)^2 - 2W^2(m_K^2 + m_\Lambda^2)}}{2W} \frac{2m_P}{W^2 - m_P^2}. \quad (23)$$

The hybrid resonance amplitudes $M_{\lambda}^{\lambda_N \lambda_Y}$ described in Appendix B and reported in Tables 8 and 9 for spin $\frac{1}{2}$ and $\frac{3}{2}$ resonances, respectively have been added to the $\mathcal{M}_{\lambda}^{\lambda_N \lambda_Y}$ reaction amplitudes from [9] (KY model A) to form a set of total amplitudes:

$$M'_{\lambda}^{\lambda_N \lambda_Y} = M_{\lambda}^{\lambda_N \lambda_Y} + \mathcal{M}_{\lambda}^{\lambda_N \lambda_Y}. \quad (24)$$

The resulting calculated cross sections from Eq. 23 have been used as KY model B to study the sensitivity of the proposed experiment to the hybrid baryons electrocouplings.

B Appendix B - Hybrid Baryon excitation Amplitude

The excitation of a single hybrid resonance in the helicity representation $\langle \lambda_f | T_r | \lambda_\gamma \lambda_p \rangle$ may be expressed using a relativistic Breit-Wigner (BW) ansatz:

$$M_{\lambda_\gamma}^{\lambda_p \lambda_f} = \langle \lambda_f | T_r | \lambda_\gamma \lambda_p \rangle = \frac{\langle \lambda_f | T_{dec} | \lambda_R \rangle \langle \lambda_R | T_{em} | \lambda_\gamma \lambda_p \rangle}{M_r^2 - W^2 - i\Gamma_r M_r}, \quad (25)$$

where M_r and Γ_r are the resonance mass and total width, respectively; we assumed both total and partial decay widths to be energy independent.

The matrix elements $\langle \lambda_R | T_{em} | \lambda_\gamma \lambda_p \rangle$ and $\langle \lambda_f | T_{dec} | \lambda_R \rangle$ are the electromagnetic production and hadronic decay amplitudes of the N^* with helicity $\lambda_R = \lambda_\gamma - \lambda_p$, in which λ_γ and λ_p stand for the helicities of the photon and proton in the initial state, and λ_f represents the helicity of final-state hadron in the N^* decays.

In the case of KY final state, the hadronic decay amplitudes $\langle \lambda_f | T_{dec} | \lambda_R \rangle$ are related to the Γ_{λ_f} partial hadronic decay widths of the N^* to KY final states f of helicity $\lambda_f = \lambda_Y$ by:

$$\langle \lambda_f | T_{dec} | \lambda_R \rangle = \langle \lambda_f | T_{dec}^{J_r} | \lambda_R \rangle d_{\mu\nu}^{J_r}(\cos \theta_K) e^{i\mu\phi_K}, \quad (26)$$

with $\mu = \lambda_R$ and $\nu = -\lambda_Y$, and

$$\langle \lambda_f | T_{dec}^{J_r} | \lambda_R \rangle = \frac{2\sqrt{2\pi}\sqrt{2J_r+1}M_r\sqrt{\Gamma_{\lambda_f}}}{\sqrt{p_i^r}} \sqrt{\frac{p^r}{p}}. \quad (27)$$

p^r and p are the magnitudes of the three-momenta of the final state K for the $N^* \rightarrow KY$ decay evaluated at $W = M_r$ and at the running W , respectively. The variables θ_K , ϕ_K are the CMS polar and azimuthal angles for the final kaon, and J_r stands for the N^* spin.

The final state Λ or Σ baryons can only be in the helicity states $\lambda_f = \pm\frac{1}{2}$. The hadronic decay amplitudes $\langle \lambda_f | T_{dec}^{J_r} | \lambda_R \rangle$ with $\lambda_f = \pm\frac{1}{2}$ are related by P-invariance, which imposes the absolute values for both amplitudes to be the same. Therefore, the hybrid state partial decay widths to the $K\Lambda$ and $K\Sigma$ final states Γ_{λ_f} can be estimated as:

$$\Gamma_{\lambda_f} = \frac{1}{2}\Gamma_r 0.03, \quad (28)$$

where the factor 0.03 reflects the adopted 3% BF for hybrid baryon decays to the KY final state.

The following relationships between the transition amplitudes $\langle \lambda_R | T_{em} | \lambda_\gamma \lambda_p \rangle$ and the $\gamma_v NN^*$ electrocouplings from [52] have been used:

$$\begin{aligned} \langle \lambda_R | T_{em} | \lambda_\gamma \lambda_p \rangle &= \frac{W}{M_r} \sqrt{\frac{8M_N M_r q_{\gamma_r}}{4\pi\alpha}} \sqrt{\frac{q_{\gamma_r}}{q_\gamma}} A_{1/2,3/2}(Q^2), \\ \text{with } |\lambda_\gamma - \lambda_p| &= \frac{1}{2}, \frac{3}{2} \text{ for transverse photons, and} \\ \langle \lambda_R | T_{em} | \lambda_\gamma \lambda_p \rangle &= \frac{W}{M_r} \sqrt{\frac{16M_N M_r q_{\gamma_r}}{4\pi\alpha}} \sqrt{\frac{q_{\gamma_r}}{q_\gamma}} S_{1/2}(Q^2), \\ &\text{for longitudinal photons,} \end{aligned} \quad (29)$$

where q_γ is the absolute value of the initial photon three-momentum of virtuality $Q^2 > 0$ with $q_\gamma = \sqrt{Q^2 + E_\gamma^2}$ and E_γ the photon energy in the CMS frame at the running W

$$E_\gamma = \frac{W^2 - Q^2 - M_N^2}{2W}. \quad (30)$$

The $q_{\gamma,r}$ value is then computed from (30) with $W=M_r$.

We have investigated the effect of adding contributions to the KY and $\pi^+\pi^-p$ reaction amplitudes from hybrid baryon states with spin-parities $J^P = \frac{1}{2}^+$ and $\frac{3}{2}^+$. Electroexcitation of the former state can be described by two electrocouplings $A_{1/2}$ and $S_{1/2}$, while the latter should be described by three electrocouplings, $A_{1/2}$, $S_{1/2}$ and $A_{3/2}$. Information on the expected Q^2 -evolution of the aforementioned electrocouplings for hybrid states is, to the best of our knowledge, currently not available. Therefore we have varied the hybrid baryon electrocouplings to determine their minimal absolute values above which the signal from the hybrid baryon can be observed, in the difference between the angular distributions with and without hybrid baryon contributions. These studies have independently been done at fixed values of Q^2 , for different bins in the range proposed by this proposal. It may be noted that, at the very high Q^2 regime, the following relations for the hybrid baryon electrocouplings $A_{1/2}$, $S_{1/2}$ and $A_{3/2}$ have been used in literature [17], to model the hybrid baryon signatures:

$$\begin{aligned} A_{1/2} &= A, \\ S_{1/2} &= AQ, \\ A_{3/2} &= A/Q^2, \end{aligned} \quad (31)$$

where $Q = \sqrt{Q^2}$ and A is a common term. However in the low Q^2 regime these relations are not valid and we have considered fixed independent values for all three electrocouplings.

Substituting Eq. 26 and Eq. 29 in Eq. 25, one obtains:

$$\begin{aligned} M_{\lambda_\gamma}^{\lambda_p \lambda_f} &= \langle \lambda_f | T_r | \lambda_\gamma \lambda_p \rangle = \frac{\langle \lambda_f | T_{dec} | \lambda_\gamma \lambda_R \rangle \langle \lambda_R | T_{em} | \lambda_\gamma \lambda_p \rangle}{M_r^2 - W^2 - i\Gamma_r M_r} = \\ &= \frac{\langle \lambda_f | T_{dec}^{J_r} | \lambda_R \rangle}{M_r^2 - W^2 - i\Gamma_r M_r} d_{\mu\nu}^{J_r}(\cos\theta_K^*) e^{i\mu\phi_K^*} \frac{W}{M_r} \sqrt{\frac{cM_N M_r q_{\gamma r}}{4\pi\alpha}} \sqrt{\frac{q_{\gamma r}}{q_\gamma}} \begin{cases} A_{1/2,3/2}(Q^2), c = 8 \\ S_{1/2}(Q^2), c = 16 \end{cases} \end{aligned} \quad (32)$$

and substituting also Eq. 27 the following expression is obtained:

$$= \frac{2\sqrt{2\pi}\sqrt{2J_r+1}M_r\sqrt{\Gamma_{\lambda_f}}}{M_r^2 - W^2 - i\Gamma_r M_r} d_{\mu\nu}^{J_r}(\cos\theta_K^*) e^{i\mu\phi_K^*} \frac{W}{M_r\sqrt{p_i}} \sqrt{\frac{cM_N M_r q_{\gamma r}}{4\pi\alpha}} \sqrt{\frac{q_{\gamma r}}{q_\gamma}} \begin{cases} A_{1/2,3/2}(Q^2), c = 8 \\ S_{1/2}(Q^2), c = 16. \end{cases} \quad (33)$$

At this point it is possible to express the $M_{\lambda_\gamma}^{\lambda_p \lambda_Y}$ in terms of a factor that doesn't depend on the λ_p , λ_Y and λ_γ helicities:

$$F_{J_r} = \frac{2\sqrt{2\pi}\sqrt{2J_r+1}M_r\sqrt{\Gamma_{\lambda_f}}}{M_r^2 - W^2 - i\Gamma_r M_r} \frac{W}{M_r\sqrt{p_i}} \sqrt{\frac{cM_N M_r q_{\gamma r}}{4\pi\alpha}} \sqrt{\frac{q_{\gamma r}}{q_\gamma}} \begin{cases} A_{1/2}(Q^2) = A, c = 8 \\ S_{1/2}(Q^2) = AQ, c = 16 \end{cases} \quad (34)$$

which is multiplied by the terms that introduce the angular dependence upon the K angles in the CMS:

$$M_{\lambda_\gamma}^{\lambda_p \lambda_f} = \langle \lambda_f | T_r | \lambda_\gamma \lambda_p \rangle = F_{J_r} d_{\mu\nu}^{J_r}(\cos\theta_K^*) e^{i\mu\phi_K^*} \quad (35)$$

with $\mu = \lambda_R$ and $\nu = -\lambda_Y$. In the formalism used by the Gent RPP-2011[9] model, the expressions F_{J_r} must be multiplied by a factor $\sqrt{4\pi\alpha}$.

The $d_{\mu\nu}^{J_r}(\cos\theta_K^*)$ coefficients are the Wigner rotation matrix elements, for which the relationship $d_{m',m}^J = (-1)^{m-m'} d_{m,m'}^J = d_{-m,-m'}^J$ is valid.

For $J = \frac{1}{2}$ they present the following explicit form:

$$\begin{aligned} d_{1/2 \ 1/2}^{1/2}(\cos\theta_K^*) &= \cos\theta_K^*/2 \\ d_{1/2 \ -1/2}^{1/2}(\cos\theta_K^*) &= -\sin\theta_K^*/2 \\ d_{-1/2 \ -1/2}^{1/2}(\cos\theta_K^*) &= d_{1/2 \ 1/2}^{1/2}(\cos\theta_K^*) = \cos\theta_K^*/2 \\ -d_{-1/2 \ 1/2}^{1/2}(\cos\theta_K^*) &= d_{1/2 \ -1/2}^{1/2}(\cos\theta_K^*) = -\sin\theta_K^*/2 \end{aligned} \quad (36)$$

while for $J = \frac{3}{2}$ one has:

$$\begin{aligned} d_{3/2 \ 3/2}^{3/2}(\cos\theta_K^*) &= \frac{1 + \cos\theta_K^*}{2} \cos\theta_K^*/2 = d_{-3/2 \ -3/2}^{3/2}(\cos\theta_K^*) \\ d_{3/2 \ 1/2}^{3/2}(\cos\theta_K^*) &= -\sqrt{3} \frac{1 + \cos\theta_K^*}{2} \sin\theta_K^*/2 = -d_{-3/2 \ -1/2}^{3/2}(\cos\theta_K^*) \\ d_{3/2 \ -1/2}^{3/2}(\cos\theta_K^*) &= \sqrt{3} \frac{1 - \cos\theta_K^*}{2} \cos\theta_K^*/2 = (-1)^{-3/2-1/2} d_{-3/2 \ 1/2}^{3/2}(\cos\theta_K^*) = d_{-3/2 \ 1/2}^{3/2}(\cos\theta_K^*) \\ d_{3/2 \ -3/2}^{3/2}(\cos\theta_K^*) &= -\frac{1 - \cos\theta_K^*}{2} \sin\theta_K^*/2 \\ d_{1/2 \ 1/2}^{3/2}(\cos\theta_K^*) &= \frac{3\cos\theta_K^* - 1}{2} \cos\theta_K^*/2 = d_{-1/2 \ -1/2}^{3/2}(\cos\theta_K^*) \\ d_{1/2 \ -1/2}^{3/2}(\cos\theta_K^*) &= -\frac{3\cos\theta_K^* + 1}{2} \sin\theta_K^*/2 = -d_{-1/2 \ 1/2}^{3/2}(\cos\theta_K^*) \end{aligned} \quad (37)$$

The final expressions for the hybrid baryon excitation amplitudes $M_{\lambda_\gamma}^{\lambda_p \lambda_f}$, are given in Table 8 and Table 9, for $J = \frac{1}{2}$ and $J = \frac{3}{2}$, respectively. No explicit dependence on the ϕ_K angle is introduced.

λ_γ	$\lambda_p = 1/2$ $\lambda_Y = 1/2$	$\lambda_p = 1/2$ $\lambda_Y = -1/2$	$\lambda_p = -1/2$ $\lambda_Y = 1/2$	$\lambda_p = -1/2$ $\lambda_Y = -1/2$
1	$F_{1/2}A_{1/2}(-\sin\theta_K^*/2)$	$F_{1/2}A_{1/2}(\cos\theta_K^*/2)$	0	0
0	$F_{1/2}S_{1/2}(\cos\theta_K^*/2)$	$F_{1/2}S_{1/2}(\sin\theta_K^*/2)$	$F_{1/2}S_{1/2}(-\sin\theta_K^*/2)$	$F_{1/2}S_{1/2}(\cos\theta_K^*/2)$
-1	0	0	$F_{1/2}A_{1/2}(\cos\theta_K^*/2)$	$F_{1/2}A_{1/2}(\sin\theta_K^*/2)$

Table 8: Expressions for $M_{\lambda_\gamma}^{\lambda_p\lambda_Y}$ for $J^P = \frac{1}{2}^+$ for all possible values of λ_P , λ_Y and λ_γ . The Wigner rotation matrix elements have been inserted.

λ_γ	$\lambda_p = 1/2$ $\lambda_Y = 1/2$	$\lambda_p = 1/2$ $\lambda_Y = -1/2$	$\lambda_p = -1/2$ $\lambda_Y = 1/2$	$\lambda_p = -1/2$ $\lambda_Y = -1/2$
1	$F_{3/2}A_{1/2}d_{1/2\ -1/2}^{3/2}$	$F_{3/2}A_{1/2}d_{1/2\ 1/2}^{3/2}$	$F_{3/2}A_{3/2}d_{3/2\ -1/2}^{3/2}$	$F_{3/2}A_{3/2}d_{3/2\ 1/2}^{3/2}$
0	$F_{3/2}S_{1/2}d_{-1/2\ -1/2}^{3/2}$	$F_{3/2}S_{1/2}d_{-1/2\ 1/2}^{3/2}$	$F_{3/2}S_{1/2}d_{1/2\ -1/2}^{3/2}$	$F_{3/2}S_{1/2}d_{1/2\ 1/2}^{3/2}$
-1	$F_{3/2}A_{3/2}d_{-3/2\ -1/2}^{3/2}$	$F_{3/2}A_{3/2}d_{-3/2\ 1/2}^{3/2}$	$F_{3/2}A_{1/2}d_{-1/2\ -1/2}^{3/2}$	$F_{3/2}A_{1/2}d_{-1/2\ 1/2}^{3/2}$

Table 9: Values of $M_{\lambda_\gamma}^{\lambda_p\lambda_Y}$ for $J^P = \frac{3}{2}^+$ for all the possible values of λ_P , λ_Y and λ_γ . Note that now the terms with $\mu = 3/2$ are non-zero.

References

- [1] K. A. Olive *et al.* [Particle Data Group Collaboration], Chin. Phys. C **38**, 090001 (2014)
- [2] I. G. Aznauryan and V. D. Burkert, Prog. Part. Nucl. Phys. **67**, 1 (2012).
- [3] I.G. Aznauryan *et al.*, Int. J. Mod. Phys. E **22**, 1330015 (2013).
- [4] I. G. Aznauryan *et al.* [CLAS Collaboration], Phys. Rev. C **78**, 045209 (2008).
- [5] T. Barnes and F. E. Close, Phys. Lett. B **123**, 89 (1983); E. Golowich, E. Haqq, and G. Karl, Phys. Rev. D **28**, 160 (1983); C.E. Carlson and T.H. Hansson, Phys. Lett. B **128**, 95 (1983); I. Duck and E. Umland, Phys. Lett. B **128** (1983) 221.
- [6] I. G. Aznauryan *et al.* [CLAS Collaboration], Phys. Rev. C **80**, 055203 (2009).
- [7] J. J. Dudek and R. G. Edwards, Phys. Rev. D **85**, 054016 (2012).
- [8] V. I. Mokeev, V. D. Burkert, T. S. H. Lee, L. Elouadrhiri, G. V. Fedotov and B. S. Ishkhanov, Phys. Rev. C **80**, 045212 (2009).
- [9] L. De Cruz, J. Ryckebusch, T. Vrancx and P. Vancraeyveld, Phys. Rev. C **86**, 015212 (2012).
- [10] A. Anisovich *et al.*, Eur. Phys. J. A **48**, 15 (2012).
- [11] D. Ronchen *et al.*, Eur. Phys. J. A **50**, 101 (2014).
- [12] A.P. Szczepaniak and M.R. Pennington, Phys. Lett. B **737**, 283 (2014).
- [13] See <http://pdg.lbl.gov/2015/reviews/rpp2015-rev-n-delta-resonances.pdf>
- [14] S. Capstick and P. R. Page, Phys. Rev. C **66**, 065204 (2002); Phys. Rev. D **60**, 111501 (1999).
- [15] P. R. Page, Int. J. Mod. Phys. A **20**, 1791 (2005).
- [16] C. K. Chow, D. Pirjol and T. M. Yan, Phys. Rev. D **59**, 056002 (1999).
- [17] C. E. Carlson and N. C. Mukhopadhyay, Phys. Rev. Lett. **67**, 3745 (1991).
- [18] T. T. Takahashi and H. Suganuma, Phys. Rev. Lett. **90**, 182001 (2003).
- [19] E. Kou, Phys. Rev. D **63**, 054027 (2001).
- [20] Z. P. Li, Phys. Rev. D **44**, 2841 (1991).
- [21] Z. P. Li, V. Burkert and Z. J. Li, Phys. Rev. D **46**, 70 (1992).
- [22] T. Vrancx, J. Ryckebusch and J. Nys, Phys. Rev. C **89**, no. 6, 065202 (2014)
- [23] The StrangeCalc web-site <http://rprmodel.ugent.be/calc/>

- [24] I. V. Anikin, V. M. Braun, and N. Offen, Phys. Rev. D **92**, 074044 (2015).
- [25] J. Segovia , B. El-Bennich, E. Rojas, et al., Phys. Rev. Lett. **115**, 015203 (2015).
- [26] V. I. Mokeev et al., Phys. Rev. C **93**, 054016 (2016).
- [27] M. Dugger et al., (CLAS Collaboration), Phys. Rev. C **79**, 065206 (2009).
- [28] K. Park et al., (CLAS Collaboration), Phys. Rev. C **91**, 045203 (2015).
- [29] V. I. Mokeev et al., Eur. Phys. J. Web Conf. **113**, 01013 (2016).
- [30] A. V. Anisovich et al., Eur. Phys. J. A **48**, 15 (2012).
- [31] A. V. Anisovich et al., Eur. Phys. J. A **48**, 88 (2012).
- [32] A. V. Anisovich et al., Eur. Phys. J. A **49**, 158 (2013).
- [33] J. W. C. McNabb et al. (CLAS Collaboration), Phys. Rev. C **69**, 042201 (2004).
- [34] R. Bradford et al. (CLAS Collaboration), Phys. Rev. C **73**, 035202 (2006).
- [35] R. Bradford et al. (CLAS Collaboration), Phys. Rev. C **75**, 035205 (2007).
- [36] M. E. McCracken et al. (CLAS Collaboration), Phys. Rev. C **81**, 025201 (2010).
- [37] K. H. Glander et al. (SAPHIR Collaboration), Eur. Phys. J. A **19**, 251 (2004).
- [38] T. C. Jude et al. (Crystal Ball Collaboration), Phys. Lett. B **735**, 035205 (2014).
- [39] A. Lleres et al. (GRAAL Collaboration), Eur. Phys. J. A **31**, 79 (2007).
- [40] A. Lleres et al. (GRAAL Collaboration), Eur. Phys. J. A **39**, 149 (2009).
- [41] A. Sarantsev, "The BoGa Amplitude Analysis Methods and its Extension to High W and to Electroproduction", the invited talk at the Workshop "Nucleon Resonances: From Photoproduction to High Photon Virtualities", ECT*, Trento, October 12-16 2015, http://boson.physics.sc.edu/gothe/ect*-15program.html
- [42] H. Kamano, S. X. Nakamura, T-S. H. Lee, T. Sato, Phys. Rev. C **88**, 035209 (2013).
- [43] H. Kamano, T-S. H. Lee, AIP Conf. Proc. **1432**, 74 (2012).
- [44] N. Suzuki, T. Sato, and T-S. H. Lee, Phys. Rev. C **82**, 045206 (2010).
- [45] J. Nys, "Hunting the Resonances in $p(\gamma, K^+)\Lambda$ Reactions: (Over)Complete Measurements and Partial-Wave Analyses", the invited talk at the Workshop "Nucleon Resonances: From Photoproduction to High Photon Virtualities", ECT*, Trento, October 12-16 2015, http://boson.physics.sc.edu/gothe/ect*-15program.html
- [46] D. Carman et al. (CLAS Collaboration), Phys Rev C **87**, 025204 (2013).

- [47] M. Ripani, V. Mokeev, M. Anghinolfi, M. Battaglieri, G. Fedotov, E. Golovach, B. Ishkhanov and M. Osipenko *et al.*, Nucl. Phys. A **672**, 220 (2000).
- [48] I. G. Aznauryan, V. D. Burkert, G. V. Fedotov, B. S. Ishkhanov and V. I. Mokeev, Phys. Rev. C **72**, 045201 (2005).
- [49] V. I. Mokeev *et al.*, in “Proc. of the Workshop on the Physics of Excited Nucleon. NSTAR2005”, ed. by S. Capstick, V. Crede, P. Eugenio, World Scientific Publishing Co., p. 47.
- [50] For details see: <https://www.jlab.org/Hall-B/clas12-web/>
- [51] M. Ripani *et al.* [CLAS Collaboration], Phys. Rev. Lett. **91**, 022002 (2003)
- [52] V. I. Mokeev *et al.* [CLAS Collaboration], Phys. Rev. C **86**, 035203 (2012)
- [53] G. V. Fedotov *et al.* [CLAS Collaboration], Phys. Rev. C **79**, 015204 (2009)
- [54] C. Wu, J. Barth, W. Braun, J. Ernst, K. H. Glander, J. Hannappel, N. Jopen and H. Kalinowsky *et al.*, Eur. Phys. J. A **23**, 317 (2005).
- [55] Aachen-Berlin-Bonn-Hamburg-Heidelberg-Munich Collaboration, Phys. Rev. **175**, 1669-1696 (1968).
- [56] E. Golovach *et al.*, $\gamma p \rightarrow p\pi^+\pi^-$ cross sections from g11a experiment, CLAS ANALYSIS NOTE (in preparation).
- [57] Mo, Luke W. and Tsai, Yung-Su Rev. Mod. Phys. **41**, 205-235 (1969).
- [58] T. Corthals, D. G. Ireland, T. Van Cauteren and J. Ryckebusch, Phys. Rev. C **75**, 045204 (2007).
- [59] A. Afanasev, I. Akushevich, V. Burkert and K. Joo, Phys. Rev. D **66**, 074004 (2002).
- [60] K. Park *et al.* [CLAS Collaboration], Phys. Rev. C **91**, 045203 (2015).
- [61] V. I. Mokeev *et al.*, Phys. Rev. C **80**, 022002 (2009).
- [62] D. Luke and P. Soding, Multiple Pion Photoproduction in the s Channel Resonance Region, Springer Tracts in Modern Physics 59 (1971).
- [63] E. Amaldi, S. Fubini and G. Furlan, Pion Electroproduction. Springer Tracts in Modern Physics **83**, ed. by G. Hohler (Springer Verlag, Berlin 1979).